

Source of Acquisition
CASI Acquired

Chas. J. McCarty
THIS DOCUMENT AND EACH AND EVERY
PAGE HEREIN IS HEREBY RECLASSIFIED

FROM *Conf* TO *Unclass*

AS PER LETTER DATED *NACA Liaison*

NACA Liaison
CHANCE VUGHT CORPORATION LIBRARY

NATIONAL ADVISORY COMMITTEE FOR AERONAUTICS

SPECIAL REPORT No. 95

WIND-TUNNEL INVESTIGATION OF AIR INLET

AND OUTLET OPENINGS FOR AIRCRAFT

By Francis M. Rogallo and William E. Gauvain
Langley Memorial Aeronautical Laboratory

SR-95

October 1938

WIND-TUNNEL INVESTIGATION OF AIR INLET
AND OUTLET OPENINGS FOR AIRCRAFT

By Francis M. Rogallo and William E. Gauvain

SUMMARY

An investigation was made in the N.A.C.A. 5-foot vertical wind tunnel of a large variety of duct inlets and outlets to obtain information relative to their design for the cooling or the ventilation systems on aircraft. Most of the tests were of openings in a flat plate but, in order to determine the best locations and the effects of interference, a few tests were made of openings in an airfoil.

The best inlet location for a system not including a blower was found to be at the forward stagnation point; for one including a blower, the best location was found to be in the region of lowest total head, probably in the boundary layer near the trailing edge.

Design recommendations are given, and it is shown that correct design demands a knowledge of the external flow and of the internal requirements in addition to that obtained from the results of the wind-tunnel tests.

INTRODUCTION

Scoops and vents of many types are in general use on every airplane for purposes of utilizing air flow, such as: ducted cooling; cabin ventilation; carburetor intake; engine exhaust; and battery, gas tank, and float vents. Information necessary for the determination of the most efficient shapes and locations and for the design of particular installations has, however, been lacking. To meet this need, the N.A.C.A. undertook an experimental investigation of the openings of induced-flow systems.

In this investigation, a great number of openings in a flat plate and a few in an N.A.C.A. 0018 wing section were tested. The test conditions and the models were systematically varied so that the results would indicate the effects of: wind velocity; size, shape, and location of openings; length and angle of ducts; interference between an opening and a body, and between inlet and outlet openings in the same body.

Theoretical characteristics of inlet and outlet openings have previously been determined and are useful as an indication of trends and as an aid in the correlation and explanation of experimental data. Because of the necessity of simplifying assumptions, however, theoretical results are often insufficient as design information and must be supplemented by empirical data. In 1936 Rokus and Troller (reference 1) published the results of a few tests of openings in a flat plate. Some of the published drag curves, particularly those for the conventional-type scoops with and without fairing, do not agree very well with theory or with N.A.C.A. test results. Reasons for the disagreement have not been determined.

APPARATUS

Wind Tunnel

All the tests were made in the 5-foot vertical wind tunnel of the N.A.C.A., which is described in reference 2. As shown in figure 1, a flat panel was placed upright between the entrance and the exit cones, projecting about 12 inches beyond the stream on each side. The front face of the panel was vertical 12 inches from the edge of the exit cone and was smoothly faired into the entrance cone at the top. No attempt was made to fair the downstream edge of the panel into the exit cone, but the opening behind the panel was blocked off to prevent stray air currents from affecting the drag readings.

Static and dynamic-pressure surveys were made in the modified jet and the tunnel calibration for all tests was based on the results of these surveys. Addition of the plane had little effect upon either the static-pressure gradient or the velocity gradient, except in the region near the plane. The variation of velocity over the mounting plate out to a distance of more than 12 inches was only 1.0 percent of the average velocity, excepting the boundary layer, which is separately treated.

The center line of openings for the wing model was 18 inches from the plane, a region little affected by the plane. The normal vertical static-pressure and velocity variations of this small tunnel over a 3-foot length (the chord of the wing used) were about 6 percent and 3 percent, respectively, of the average values.

Induced-Flow System

In order to represent the condition of flow through an opening into or out of a large chamber, such as the interior of a wing or a fuselage, the set-up comprised a box whose inside dimensions were 16 by 16 by 20 inches and whose front face was the floating mounting plate shown in figure 1. The duct connecting this box with the blower and the flowmeter was attached to its rear face, as shown in figure 2. If the unobstructed jet from this duct had been allowed to impinge upon the front inside face of the box during outlet tests, the resulting flow would not have represented the desired condition of uniform approach velocity. A section of 14-mesh screen was therefore placed about 2 inches from the rear end of the box and arranged in such a manner that the flow out of the box with the front face removed was fairly uniform. During tests, the static pressure in the box was measured by a flush tap in the center of the top face.

In order to represent the condition of flow into or out of an opening attached to a straight duct with uniform cross section of area about equal to that of the opening, as, for example, a carburetor scoop or an engine-exhaust system, a short length of duct with a bellmouth entry was used. (See figs. 2 and 3.) Had a continuous duct been used, it would have increased the model-installation difficulties, especially with ducts at an angle of less than 90° to the front face. Several flush taps were installed in the duct (see fig. 3) to obtain static-pressure data. The circular duct and bellmouth shown in figure 3 were detachable and were used in all the tests with circular ducts. A rectangular duct and bellmouth were used in all the tests of recess-type inlets and outlets. Use of the bellmouth entries prevented entrance conditions from affecting the flow pattern at the outlet end during tests of outlet openings.

The centrifugal blower (see figs. 2 and 4) was driven by a variable-speed direct-current motor and was capable of developing a pressure rise of 20 inches of water at a flow rate of 500 cubic feet per minute. The case was airtight, shaft clearance being sealed by an oil reservoir between two retainers.

The orifice drum (figs. 2 and 4) was made of an oil drum approximately 23 inches in diameter and 35 inches high, and the six sharp-edge orifices of diameters from 1

to 4 inches were bored in brass plates 10 inches square and 1/8-inch thick. The orifices were calibrated over a pressure range of 0 to 40 pounds per square foot against orifices obtained from the National Bureau of Standards; the orifice coefficient determined for all orifices with flow in either direction was 0.59.

Balance System

The balance system is shown in figure 2. The floating mounting plate and the attached box formed one side of a parallelogram whose opposite side was a rigid steel pipe attached to a concrete pillar extending up from the floor of the building. This pipe acted as a duct, being connected to the floating chamber through two flexible joints, as shown in the figure. Ball bearings were used at all four joints of the parallelogram. The floating chamber and the attached structure were counterweighted, and the drag scale was attached by a wire as shown. Sufficient counterweight was applied to assure tension in the balance wire at all times.

The scale was of the beam type, automatically operated by a motor and electric contacts at the end of the beam. Oil dash pots were used for damping the lateral and the vertical oscillations of the floating mounting plate, and clearance between the plate and the surrounding metal frame was assured by a system of indicating lights.

The ball-bearing jointed parallelogram and flexibly coupled duct were arranged in such a manner as to reduce to a minimum the drag correction resulting from pressure and flow in the system. The plate opening was stopped up and drag tests were run through the complete range of positive and negative pressures; the correction due to pressure was found to be negligible. With tunnel velocity zero and the plain circular holes centrally located in the floating plate, the corrections for flow in both directions were determined. The correction for flow in the inlet direction amounts to a maximum of about 5 percent of the drag. The correction for flow in the outlet direction is of opposite sign and about one-half as great as that for the inlet direction at any given rate of flow.

MODELS

A pictorial index of the general arrangements investigated is given by tables I and II; the numbers under the sketches refer to the figures that give the complete details. Photographs of models are shown in figures 1 and 5 and drawings are included with the characteristic curves of figures 11 to 59 and 62 to 66. The flat plate and all the hinged flaps tested on it and on the N.A.C.A. 0018 wing model were of 1/16-inch steel plate. The flap surfaces were plane and the edges sharp. The circular pipe used for ducts and models in flat-plate tests was 3-inch seamless steel tubing of about 0.080-inch wall thickness. The external scoop-type inlets and outlets were formed from sheet copper about 1/32 inch thick; and the recess-type inlets and outlets were made of galvanized iron, also 1/32 inch thick.

It may be noticed that slight differences exist between the tabulated areas of openings and the areas that may be computed from the dimensions on the drawings. The linear and the angular dimensions given are approximately correct, but the tabulated areas are the result of careful measurements of the openings as tested. The tabulated areas were used in the reduction of the data to coefficient form.

All the guide vanes were of thin sheet brass, shaped as recommended in reference 3. The set of vanes used in the recess-type openings was adjusted so as to divide the bend into four nearly equal parts with either the 10° or the 15° recess. The three vanes, as a unit, were shifted when necessary.

The 36- by 36-inch N.A.C.A. 0018 wing model shown in figure 5 was wood, partly covered by 1/8-inch-thick pressed-wood board. Two ribs divided the interior into three nearly equal compartments, the central one having a clear width of 12 inches.

When the wing was mounted in the tunnel, the steel plate at its end was fastened to the floating chamber as though the complete wing were an opening being tested on the flat mounting plate. The wing extended 16 inches above and 20 inches below the horizontal center line of the mounting plate. Because the trailing edge would have been only 3 inches above the lower edge of the plane shown in figure 1, the plane was extended another 2 feet into

the exit cone (see fig. 2) before the wing was installed. Openings in the two sides of the wing were, insofar as possible, made exactly alike and the angle of attack was maintained at zero throughout the tests.

RESULTS

Symbols and Coefficients

The symbols and coefficients used herein are defined as follows:

A, mouth area of opening, unless otherwise defined.

A_d , duct area at location of pressure tap.

D, drag.

p , static pressure relative to that of free stream.

q , dynamic pressure of free stream, unless qualified.

q'' , dynamic pressure at edge of boundary layer.

ρ , mass density of air.

Q, volume of flow per unit time.

H, total head.

$V = \sqrt{2q/\rho}$, velocity of free stream.

V' , velocity at any point.

V'' , velocity at any point at edge of boundary layer.

Q/AV , coefficient of flow.

p/q , coefficient of static pressure.

$\Delta p/q = (p/q)_i - (p/q)_o$

$H/q = p/q + (A/A_d)^2 (Q/AV)^2$, coefficient of total pressure.

D/qA , coefficient of drag.

C_{PL} , coefficient of power loss.

$$\eta = \left(\frac{\Delta p}{q} / \frac{D}{qA} \right) (Q/AV)$$

V_i/V , theoretical velocity ratio at inlet.

V_o/V , theoretical velocity ratio at outlet.

$$C = \frac{Q/A}{\sqrt{2p/\rho}}, \text{ orifice coefficient.}$$

Subscripts:

i, inlet.

o, outlet.

r, radiator.

f, flowmeter.

A standard form of presentation of test results has been adopted, all the variables being expressed as dimensionless coefficients. The flow coefficient Q/AV is the ratio of the average velocity through the area A to the velocity of the free stream, where A is usually taken as the minimum cross-sectional area of the opening. The drag coefficient D/qA is always based on the same area as the flow coefficient, and D is the total drag minus the tare drag of the plain flat plate, or of the plate and the wing. The static-pressure coefficient p/q is the ratio of local static pressure to free-stream dynamic pressure. Locations of the reference-pressure taps for ducted openings are given on the drawings. When no duct was used, the static pressure was determined at the center of the top face of the floating chamber.

The power-loss coefficient C_{PL} is a criterion of merit, which may be expressed as follows:

$$C_{PLi} = \frac{DV - (HQ + qQ)}{qQ} \quad (1)$$

$$C_{PLo} = \frac{DV + (HQ + qQ)}{qQ} \quad (2)$$

where DV is the drag power; HQ , the pressure power; and qQ , the kinetic power of the induced flow. For inlets, $(HQ + qQ)$ represents available power whereas, for outlets, it represents expended power; hence the difference in signs in the right-hand members of equations (1) and (2). These coefficients, which are more fully described in reference 4, may also be expressed as functions of the drag, the flow, and the total-pressure coefficients, as follows:

$$C_{PL_i} = \frac{D/qA}{Q/AV} - (H/q + 1) \quad (3)$$

$$C_{PL_o} = \frac{D/qA}{Q/AV} + (H/q + 1) \quad (4)$$

External Conditions

The external conditions at the locations of the openings, with the openings sealed or removed, are given in the following table.

Location on wing	p/q	q''/q	v''/v	Boundary layer
0.000c	1.00	0	0	0
.175c	-.66	1.66	1.29	negligible
.800c	-.08	1.04	1.02	figure 8
flat plate	-.02	1.00	1.00	figure 7

Velocity distributions in the boundary layer of the flat plate and at the wing were determined by means of a survey comb (fig. 6) and a multiple-tube manometer. These results were corrected for total-pressure gradient (see reference 5) and are plotted in figures 7 and 8. The curves of figure 8 extend above unity because the ratio of point to free-stream velocity, rather than the ratio of point to potential-flow velocity, was plotted. These curves show that the boundary layer was of about the same thickness at corresponding points on the two sides of the wing and that it was considerably thicker at the center

of the span than 10 inches inboard or outboard of that location. The thickening at the center was caused by the installation of flaps at 0.175c, even though the flaps were closed and sealed during the boundary-layer determinations. No additional surveys were made after the adjustable flaps were replaced by preformed plates, but comparison of drag tests showed that the boundary-layer thickening shown in figure 8 corresponded to more than 7 percent of the wing drag, even though the span of the flaps was less than 30 percent that of the wing.

Duct Pressure Gradients

Flat-plate tests.— Pressure gradients were measured in the circular and rectangular ducts by flush pressure taps in the duct walls. Inlet gradients for the flush, circular-opening, 90° duct (model 3P30-90, fig. 23) at four rates of flow are given in figure 9, together with average gradients for the same duct with elbow (model 2P336, fig. 27) and with conventional scoops (models 5P3-PB and 5P3-PC, fig. 28). Average gradients are given for the scoops and the elbow because the variation with flow coefficient over a wide range was very small and showed no definite trend.

The rising pressure gradients shown in figure 9 are a well-known property of elbows in ducts and of sharp-edge entrances. (See reference 3.) They are the result of break-away from the inside surface behind the bend, or entrance, and subsequent return of the flow to the surface farther downstream. After the velocity has returned to a fairly uniform distribution, the gradient changes sign and starts to follow the regular pipe-loss curve. The duct length used was too short to allow return of the gradient to that for pure pipe loss, the tap farthest downstream being very near the maximum static-pressure point for the greater part of the tests with the circular duct and being even farther upstream with the rectangular duct. It is obvious that the bend affects the velocity distribution for some distance along the duct, and this interference should be considered in the design of a system. It will be of little use to expand a duct that is already flowing only half full; moreover, a bend or other change of cross section very near the opening cannot be assumed to have the same characteristics as it would have behind a long duct.

The flow coefficient Q/AV would be expected to have little effect upon the pressure gradient behind a scoop or elbow because it does not affect the ratio of average velocities on the two sides of the bend. This expectation was satisfied by the tests of models 2P336, 5P3-PB, and 5P3-PC, for which average curves are given in figure 9. On the other hand, the large effect of flow coefficient upon the gradient of model 3P30-90 is seen to be the result of a change in the ratio of velocities on the two sides of the bend, the bend being the region of the opening even though the duct itself is straight. The variation may also be thought of as the result of a change in the angle of bend.

The outlet-duct pressure measurements gave the following results: The pressure drop from box into bellmouth for circular and rectangular ducts, respectively, was $1.13q$ and $1.17q$ in the duct, corresponding entrance losses being $0.13q$ and $0.17q$. The gradients in the ducts were nearly straight lines, the pressure dropping at $0.15q$ and $0.20q$ of the duct per foot for circular and rectangular sections, respectively; these slopes were merely pipe-loss gradients and were not affected by either the shape of the outlet opening or the flow past it except within about one diameter of the end of the uniform section.

These results show that both the entrance and the pipe losses for the rectangular duct were higher than for the circular duct. The entrance losses may have been affected by the nearness of the screen, for they are higher than expected from results of hydraulic tests (reference 6, p. 206). The pipe losses, too, are higher than expected, but the low accuracy with which pipe-loss determinations can be made on such short specimens would not lead one to expect very close agreement with other tests. Pipe losses are usually of secondary importance, however, relative to losses at the outlet opening.

Wing tests.— In the determination of the duct pressure gradients shown in figure 10, which also serve as wing flowmeter calibrations, the static-pressure tubes were connected to a multiple-tube manometer and the pressures were observed over a wide range of flow conditions. In these tests, the air was taken into the wing at the front or the rear and was then passed through the flowmeter (see the appendix), through holes in the wing ribs into the chamber behind the mounting plate, and thence through the regular system. The air was metered by the orifice drum.

The positive static-pressure gradients in the downstream direction are the result of a partial conversion of dynamic to static pressure, the static-pressure increases downstream of the flowmeter being in fair agreement with Borda's formula (reference 6, pp. 207-210).

Characteristics of Openings in the Flat Plate

The conditions under which the openings were tested will probably never be reproduced in practice. Even if the openings themselves were built exactly like the models tested, the flow around the bodies in which they are placed would be such as to cause differences in the time and the space variations of pressure and velocity, which might have a large effect upon the aerodynamic characteristics of the openings. Relative to the accuracy with which these effects may be estimated in any practical application, the results presented may be considered exact for the particular conditions prevailing. That is, in the use of the results of one of these tests for design purposes, the probable error in them is negligible in comparison with that involved in the estimation of the effects of boundary-layer conditions and interference differing from those of the original test. Thus, the absolute precision is not of great importance, and small errors that remained constant during all tests may be neglected.

It should be noted that the power-loss coefficient is usually the difference between two numbers of the same order of magnitude, and consequently its percentage accuracy is below that of the other coefficients. Thus, errors in the other coefficients will show up greatly magnified in the power-loss coefficient, especially errors in drag at low rates of flow. In general, the lower the power-loss coefficient, the lower its percentage accuracy. The remarkable smoothness of most of the curves of C_{PL} and the infrequency of erratic points, in spite of the tendency of this coefficient to magnify errors, indicate that the relative precision of measurements was high.

All the original tests of openings in a flat plate were made at a tunnel velocity of approximately 40 miles per hour, but many of these tests were repeated at about 80 miles per hour to determine the effects of stream velocity and to serve as checks on the results at the lower speed. The tunnel dynamic pressures were maintained at

constant heights of alcohol representing 40 and 80 miles per hour in standard air at a manometer temperature of 88° F., which was a little above the average temperature for all tests made. The dynamic pressures were corrected for variations in temperature of the manometer alcohol. Keeping the heights of alcohol, rather than the actual pressures, constant made temperature corrections unnecessary for orifice-drum and duct-pressure manometers. The actual velocities both in the tunnel and in the induced-flow system were not determined during these tests because they were not required, all results being given as ratios independent of small variations in velocity within the accuracy of the measurements made.

Results of tests of openings in the flat plate are given in figures 11 to 59. Comparison of the results of tests run at both 40 and 80 miles per hour shows very little variation of characteristics with velocity for most of the devices tested, and the small variations that are apparent can usually be accounted for by the difference in boundary-layer thickness at the two velocities. Tests of the 3- and 4-inch-diameter pipes, the 2- and 3-inch-diameter holes, and the $1\frac{1}{2}$ - and $2\frac{3}{4}$ -inch chord flaps showed that outlet characteristics are little affected by the size of the device and that inlet characteristics are little affected when the opening is outside the boundary layer of the plate. When the opening, or a part of it, lies within the boundary layer of the plate, however, any variation of opening size that results in a variation of the ratio of opening height to boundary-layer thickness has a large effect upon the inlet characteristics. This boundary-layer effect is evident not only from the comparison of tests of similar models but also from tests of a single flap adjusted to different angles so that the openings are of different heights. (See figs. 14 and 17.)

The test results show the beneficial effects of properly fairing the rear portions of conventional scoops, pipes, and elbows that project into the air stream and of necking down the openings for both the inlet and the outlet. Thickening and rounding the leading edges of scoops did not show any definite improvement as compared with a necked-down sharp-edge entrance, but these tests did not cover a sufficient range of shapes to constitute the basis for a general conclusion.

The internal flap openings and the recess-type inlets and outlets with ducts did not provide much pressure for

maintaining the flow but exhibited very low power-loss coefficients for blower-induced flow. Recess inlets with no surfaces projecting above the plane, nevertheless, produced built-up static pressures as high as one-third of the free-stream dynamic pressure. (See fig. 34.)

Figures 28 and 55 show that a hood-covered duct at 45° with the surface had less bend loss than one at 90° with the surface, as would be expected. Tests of the recess-type inlets and outlets (figs. 34-36, 58, and 59) showed that, for sharp 90° bends, guide vanes were beneficial and square corners were slightly better than rounded ones, these results being in agreement with those of reference 3. The effects of guide vanes are also shown in figures 32 and 57.

Cross-Wind Orifice Coefficients

From the pressure characteristics of figures 11 and 38, orifice coefficients C may be computed and compared with orifice coefficients derived from tests in still air. Because such a comparison seemed to be of fundamental value, the curves of figures 60 and 61 were prepared from the original data corresponding to figures 11 and 38 and from additional tests of the same openings with zero tunnel velocity.

Figure 60 shows the coefficients plotted against the orifice pressure. Figure 61 shows the same coefficients plotted against the ratio of orifice to cross-wind pressures. On this basis, the tunnel zero velocity points are at infinity, and the cross-wind curves would be expected to approach the cross-wind zero-velocity orifice coefficients as the pressure ratio is increased.

Variations of orifice diameter and tunnel velocity had little effect upon inlet coefficients but considerable effect upon outlet coefficients for the arrangements and conditions investigated (fig. 61).

Characteristics of Openings in an N.A.C.A. 0018 Wing

Separate sets of openings.- The results of tests of separate sets of openings in the N.A.C.A. 0018 wing are given in figures 62 to 66. All tests were made at an air-stream velocity of approximately 80 miles per hour, and the test procedure was the same as for flat-plate tests.

Tare drag of the wing with adjustable flaps was determined with the flaps installed, but closed and sealed. Tare drag was therefore higher, and the boundary layer at the rear flaps was thicker than for a smooth wing. Tare drag of the wing with fixed openings was determined before the nose openings were installed, a drag test being made with all flaps removed and replaced by smooth, preformed plates, carefully faired into the wing contour. The tare drag and thickness of boundary layer were, consequently, less than for the adjustable-flap tests. Because of these differences, the fixed openings relative to the adjustable ones are actually better than shown in the figures.

In the determination of the static-pressure data of figures 62 to 66, the pressure taps used were the ones nearest the wing flowmeter on the same side as the openings being tested. (See fig. 10.) A study of the pressure gradients of figure 10 shows that the static pressures at the outlet openings were somewhat greater than those just behind the flowmeter, as has already been discussed.

The power-loss coefficients were computed in the same manner as for the flat-plate tests. Assuming that the dynamic pressure in the duct was equal to $\frac{1}{2} \rho (Q/A_d)^2$ involved little error in the reduction of flat-plate-test data because the duct velocities were fairly uniform at the static-pressure taps, but the same assumption in the computation of power-loss coefficients of outlets in the wing makes those coefficients erroneously low. From the data of figure 10, it appears that the error in C_{PL} is about $0.2 (Q/AV)^2$ for the 0.0347 square foot outlets and one-fourth as much for the 0.0174 square foot outlets. No correction was made for this error because it is consistent and therefore does not affect the value of the results; it does account, however, for the negative C_{PL} shown in figure 66.

The wing tests were made chiefly to check the applicability of flat-plate data to the design of openings in typical aerodynamic bodies. The locations chosen were, therefore, the practical extremes of static-pressure, velocity, and boundary-layer thickness available on the model used.

The inlet and outlet characteristics of the internal flap at 10° with the surface as tested on the flat plate

and on the wing are given in figures 67 and 68. The characteristics of the wing-nose inlet are also given in figure 67.

Flat-plate data would not be expected to apply to openings at the front stagnation point, and figures 67 and 68 show that such data are not applicable either there or in the high-velocity region, which, in this case, is the 0.175c location. The drag coefficient with the nose inlet is in good agreement with the value that would be expected from tests of a flush opening in a flat plate with zero boundary layer, but the pressure coefficient is much higher because no bend loss is involved.

Agreement of flat-plate coefficients with those determined for the 0.175c location is poor, principally because of the high interference drag caused by a departure from smooth flow at that location.

Agreement of flat-plate and wing data at the 0.800c location is fair because the boundary layers are of about the same relative thickness and the effects of interference are small. The presence of some interference drag, however, could account for the small and nearly constant difference between the drag curves for the outlet condition; the curves are nearly coincident for the inlet condition. Static-pressure coefficients of both inlet and outlet on the wing are less than on the plate over the full range of flow; the difference may be ascribed chiefly to the different internal arrangements and to the small negative static pressure naturally occurring at the 0.800c location.

Combinations of inlet and outlet openings.— Nine combinations of inlet and outlet openings in the wing were tested and the results are given in table III together with characteristics computed from figures 62 to 66.

All combination tests were made at an air-stream velocity of 80 miles per hour, tare drags were the same as for the corresponding tests of individual sets of openings, and static pressures were measured on the two sides of the flowmeter at the pressure taps nearest the flowmeter. The rate of flow was computed from the measured pressure drop through the flowmeter and from the data of figure 10.

The drag of the openings in combination is, in general, less than that of the openings individually, a tendency an-

anticipated inasmuch as the drag of openings at the 0.800c location is reduced by the boundary-layer thickening that results from openings in the nose or at the 0.175c location. The power-loss coefficients and the efficiencies are correspondingly affected.

DISCUSSION

The Ducted System as a Complete Unit

In reference 4, the ideal, or theoretical, efficiencies and the power-loss coefficients are derived for the generalized induced-flow system and for the important special case of zero angularity of inlet and outlet flow relative to the free stream. For this case

$$C_{PL_{i+o}} = (V_o/V - 1)^2 - (V_i/V - 1)^2 \quad (5)$$

where V_i/V and V_o/V are the hypothetical velocity ratios at inlet and outlet, respectively; that is, the velocity ratios that would exist at a great distance from the induced-flow system if there were no mixing or loss of total head.

From equation (5) it may be seen that, for minimum C_{PL} of the complete system, $V_o/V = 1$ and V_i/V is as far from unity as possible in either a positive or a negative direction. If a pressure drop occurs in the system, as is usually the case, $V_o/V < V_i/V$ and vice versa. Therefore, in order that $V_o/V = 1$, V_i/V must be greater than unity in a pressure-drop system and less than unity in a pressure-rise system. These relationships divide induced-flow systems into two distinct types, one in which the flow is induced by the external pressure difference at the openings, and the other in which flow is induced by a pump or blower within the system. The first type will be called an externally induced-flow system, and the second type will be called a blower-induced-flow system. There should be no borderline case, since it has been shown that V_i/V should be as far from unity as possible.

Maintaining ideal outlet conditions in an externally induced-flow system will usually be impossible because the

pressure drop through the system will be greater than the maximum pressure rise in the propeller slipstream, the optimum location for the inlet of such a system.

In a blower-induced-flow system, however, it should always be possible to operate at the desired condition. Furthermore, such a system could be made to provide adequate cooling or ventilation at all times, even though designed for maximum efficiency at one particular flight condition, because it would be relatively independent of the velocity or attitude of the aircraft.

In the design of a system, the required flow and the pressure drop must be determined, particularly for an externally induced-flow system for which the available pressure drop is limited. The flow requirement will usually be known or assumed at the outset but can be determined experimentally by a blower and metering equipment such as those used in the present investigation. Such equipment could, moreover, be used to determine the pressure drop through an experimental induced-flow system and to determine the effects of changes in the system, thereby allowing a cut-and-try method of approaching the best possible duct arrangement in an actual installation. An experimental attack on the problem of duct design is recommended because of the irregular shapes of ducts used in aircraft and the frequency of bends, expansions, contractions, and other changes of cross section; an analytical solution would not be dependable except for a few simple arrangements for which adequate test results are available.

The Inlet Opening

Ideal characteristics.- From reference 4, the ideal characteristics of an inlet opening for the special case of zero angle of approach are as follows:

$$C_D = D/qA = 2(Q/AV) V_i/V \quad (6)$$

$$p/q = (V_i/V)^2 - (A/A_d)^2 (Q/AV)^2 \quad (7)$$

$$C_{PL_i} = - (V_i/V - 1)^2 \quad (8)$$

These equations, which are plotted in figure 69, clearly illustrate the effects of V_i/V and Q/AV upon the characteristics of an inlet opening.

Inlet design for externally induced-flow systems.-

Theory indicates that the inlet opening of an externally induced-flow system should be in the region of maximum total head; that is, the region in the propeller slipstream corresponding to about the 0.75 radius. Tests indicate, moreover, that the opening should be at the forward stagnation point on a typical aerodynamic body. If so located, the characteristics of the opening may be computed from the theory, the accuracy of such a computation being shown by the comparison in figure 67 for the special case of $V_i/V = 1.0$. If desired, an allowance may be made for the small discrepancies shown.

Figure 67 shows that the actual characteristics of the nose inlet tested are very nearly ideal. It must be remembered, however, that the test installation, with openings on the chord line of a symmetrical wing at zero lift, is not likely to be reproduced in practice. Movement of the stagnation point with change in lift coefficient will make it impossible to maintain the opening at the stagnation point over the full flight range unless some practical method is devised for varying the inlet location. Even a small displacement of the inlet relative to the stagnation point would be expected to increase the drag and decrease the available pressure, but the magnitude of those losses cannot be predicted from the results of the present investigation. Another loss that will generally be encountered in practical installations of wing-nose inlets is a bend loss just inside the opening. Such a loss was not present in the test installation because of the symmetry of the model and of the flow relative to the chord line.

Computed characteristics of a well-shaped and properly located opening at the nose of a fuselage may be more reliable than for a wing-nose inlet on account of the smaller relative movement of the stagnation point.

Because of practical considerations, it will often be found desirable to locate the inlet opening of an externally induced-flow system back of the forward positive-pressure region. In such installations it is recommended that the inlet be located as near the trailing edge as possible in order to reduce interference drag and to take advantage of the natural static-pressure rise. The opening should be outside the boundary layer, and the scoop should be necked down at the front and properly faired at the rear. If a short radius bend is required, it should be fitted with guide vanes as prescribed in reference 3.

Inlet design for blower-induced-flow systems.- Both theory and test results show that the inlet opening of a blower-induced-flow system should be as near the rear stagnation point as practicable in order to reduce the interference drag and to take maximum advantage of the boundary layer and the positive static pressure. The rearward limiting position of the opening will be determined by necessary duct space and by the construction of the wing or fuselage, especially where movable surfaces are employed, such as high-lift or control devices.

Tests of both the flat plate and the wing showed that the external flap has a higher loss than the internal type and that the pressure recovery is improved by the use of an expanding section inside the opening, such as was used in the case of the overlapping flaps. The opening WRIB (fig. 64) was the best of those tested, and the characteristics of this type of opening would be expected to improve as the ratio of opening gap to boundary-layer thickness is decreased; i.e., a long narrow opening should be better than a short wide one of the same area because it will take in air of a lower average total head.

The drag of a well-shaped opening near the trailing edge may be easily computed with satisfactory accuracy from equation (6) if the velocity distribution in the boundary layer is known. The results of such computations are given in table IV, together with test results, and it may be seen that the computed drags are very near the measured drags except for the external flaps, which naturally experience an additional form drag. In the computations, flow coefficients near the point of minimum C_{pL} were chosen.

Table IV also shows that, for the openings tested, the measured static pressures are less than the computed total heads by roughly 1.5 times the dynamic pressure of the air flowing through the gap, except for the internal flaps at relatively high angles. These pressure drops were anticipated from previous knowledge of flow through a small opening into a large chamber. (See fig. 10.) For design purposes, an error in the computation of the pressure characteristics is not so serious for the blower-induced-flow system as for the externally induced-flow system because the flow may be regulated by the blower.

The Outlet Opening

Ideal characteristics.— From reference 4, the ideal characteristics of outlet openings are as follows:

$$C_D = D/qA = - 2(Q/AV) (V_o/V) \cos \theta \quad (9)$$

$$H/q = (V_o/V)^2 \quad (10)$$

$$C_{PL_o} = - 2 V_o/V \cos \theta + (V_o/V)^2 + 1 \quad (11)$$

in which θ is the hypothetical angle of the exhaust jet relative to that of the free stream.

In figure 70 these equations are plotted at three values of θ for the special case of an outlet either on a flat plate or on a body at such a location that the local velocity is equal to the free-stream velocity; i.e., $V_o/V = Q/AV$.

Outlet openings in aerodynamic bodies will cause interference drag, the amount depending upon the shape and location of the openings. Even flush openings on flat plates, however, will not exhibit ideal characteristics because of interaction of the issuing jet and the external stream, as shown by a comparison of figures 51 and 70, and because discharge coefficients, particularly for sharp-edge openings, are not unity, as shown by figures 60 and 61. If the effective areas, rather than the actual areas had been used in the reduction of test data, the agreement between figures 38 and 70 would have been much better, as would the agreement between the theory and the flat-plate curves of figure 68.

Density corrections.— In the development of the theory, ideal fluid was assumed and, in the tests, the density variation was negligible; but, in many applications, particularly to engine-exhaust systems, the density of the issuing jet will be widely different from that of the surrounding stream. In all such cases corrections must be applied, depending upon the characteristics of the particular device being used and its location on the body. If external interference effects are negligible, as for a flush opening at the rear of a body, substitution of the density of the issuing jet in the ideal equations or empirical coefficients will give ideal or actual characteristics, respectively.

If, on the other hand, the characteristics are almost completely determined by the external flow, as for an external-hood-type outlet at low flow coefficients, the density of the external stream would be used in computing drag and static pressure.

If the installation does not fall into either of the foregoing classifications but is somewhere between, it will be necessary to estimate the separate contributions of internal and external flows to the over-all characteristics and to correct accordingly.

Outlet design for externally induced-flow systems.-

Theory indicates and tests prove the high drag cost of maintaining at the outlet opening a total head which is low relative to that of the free stream. It is therefore recommended that the outlet velocity be maintained as near the ideal as practicable and that the opening be located in a low-velocity region, preferably at the rear of the body, in order to reduce interference drag. It seems hardly necessary to state that the jet direction should be as near that of the potential flow as practicable.

With a given inlet condition, the total head at the outlet opening is determined by the pressure drop in the system. The importance of reducing internal losses cannot therefore be overemphasized because such losses are accompanied by external losses, which appear as energy left in the wake. This external loss, which occurs only in systems having motion relative to the surrounding fluid, makes duct design so important for aircraft using externally induced-flow systems. Present practice, particularly in regard to the cooling of air-cooled engines, indicates that these basic principles have not heretofore been fully appreciated.

Outlet design for blower-induced-flow systems.- The ideal outlet conditions for a blower-induced-flow system are the same as for an externally induced-flow system but, whereas it is almost impossible in the externally induced-flow system to realize them, the outlet conditions for the blower-induced-flow system are fully controllable. Exhausting at free-stream total head is the ideal optimum, but the practical optimum will depend upon the characteristics of the blower and the ducts used and must, therefore, be determined for each particular installation. It seems reasonable to expect, however, that the practical optimum will seldom be far from the ideal.

Sample Problem

Example: A flow of 6.13 cubic feet per second is required for a radiator with the pressure characteristics of the wing flowmeter shown in figure 10 when the airplane speed is 352.2 feet per second (240 m.p.h.). The cooler is to be installed in a wing in the same manner as the flowmeter, and openings WNI (fig. 64) and WREA (fig. 66) are to be used. It is assumed that the characteristics given in figures 64 and 66 are applicable.

From figure 10, $\Delta p/q_r = 1.36$ and $A_r = 0.033$ sq. ft.

$$q_r/q = \left(\frac{6.13}{0.033 \times 352.2} \right)^2 = 0.2785$$

$$\Delta p/q = (\Delta p/q_r) (q_r/q) = 0.38$$

From the curves of C_{PL} against p/q of figures 64 and 66 and the requirement that the difference in p/q for inlet and outlet must equal 0.38, as just computed, the pressure coefficient for each opening is determined for the condition of minimum total C_{PL} . Then from the curves of p/q and C_{PL} against Q/AV , the flow coefficients are determined, from which the sizes of the openings may be calculated. The values so determined are tabulated as follows:

	p/q	C_{PL}	Q/AV	A (sq. ft.)
Inlet	0.82	0.36	0.35	0.0497
Outlet	.44	-.02	.67	.0260

The table gives the optimum sizes of the openings for the conditions assumed. If any other sizes are used, the C_{PL} will be higher, even though the required flow and pressure characteristics are obtained. The total C_{PL} calculated for the same arrangement and nearly the same $\Delta p/q$, but for openings of the areas tested rather than the optimums, is given in table III as 0.51. It is thus evident that, even though the proper shapes and locations of openings are used, the system will be inefficient if the openings are not of the proper size.

CONCLUSIONS

1. The use of wind-tunnel results for designing an opening at a particular location on an aircraft demands a knowledge of the external flow at that location and of the internal flow and the pressure requirements of the system.

2. Drag and pressure characteristics of openings in aerodynamic bodies may be computed from the results of tests on flat plates if interference effects are known.

3. The aerodynamically best location for the inlet opening of an externally induced-flow system is at the front stagnation point of the body and in the maximum total-head region of the propeller slipstream.

4. The aerodynamically best location for the inlet opening of a blower-induced-flow system is in the region of lowest total head, probably at the base of the boundary layer near the trailing edge of the body.

5. For minimum power loss of an outlet opening, the velocity and the direction of the jet should be maintained approximately the same as that of the potential flow at the location of the opening.

Langley Memorial Aeronautical Laboratory,
National Advisory Committee for Aeronautics,
Langley Field, Va., August 31, 1938.

APPENDIX

Duct Flowmeter

Need often arises for a simple type of duct flowmeter, the calibration of which is independent of disturbances in the stream either in front of or behind it. Previous tests seemed to indicate that such a flowmeter could be built as shown in figure 71. It consists of a number of circular holes of unit length-diameter ratio with small impact and static-pressure tubes installed one-quarter tube length from the outlet side, as shown in the figure. Such a meter was built and tested in the set-up shown in figure 72.

This set-up included a rectangular duct with bellmouth entrance and static-pressure taps installed flush with the inside duct surface at the locations shown in the figure. The flowmeter was mounted in the center of the duct, and obstructions were placed in the stream 1 foot on either side of it. Each of these obstructions blocked off approximately one-half the duct area, as shown in the figure. By means of the blower and the orifice drum previously described, known quantities of air were drawn through the duct over a flow range corresponding to a flowmeter pressure drop of from 1 to 8 inches of alcohol. Flowmeter pressures and duct static pressures were measured with a multiple-tube manometer with each of the obstructions separately in place, with no obstructions, and with the two end holes of the flowmeter stopped up.

Very little scale effect was noticed over the range of tests for any given obstruction. Flowmeter calibration was little affected by the obstructions placed behind the meter, but those placed ahead of it had a large effect, as may be seen in figure 71. In fact, the flowmeter pressures appeared to give a much less satisfactory calibration than the duct static pressures on the two sides of the meter. These duct static pressures were much steadier at any given condition of the duct and they did not show so much variation with change of obstruction as did the flowmeter pressures. It was therefore decided to use duct static pressures for flow determination in the subsequent wing-opening tests and it was also thought advisable to recalibrate the system for each condition of the inlet openings. That this decision was wise is evident from a study of the duct gra-

dient curves of figure 10 which show a much greater variation of calibration than is shown by the results given in figure 71.

From the results of these tests, it must be concluded that neither the flowmeter pressure taps nor the duct static-pressure taps yield a calibration inappreciably affected by flow changes in the duct ahead of the flowmeter.

REFERENCES

- ✓ 1. Rokus, F., and Troller, Th.: Tests on Ventilation Openings for Aircraft. Jour. Aero. Sci., vol. 3, no. 6, April 1936, pp. 203-208.
2. Wenzinger, Carl J., and Harris, Thomas A.: The Vertical Wind Tunnel of the National Advisory Committee for Aeronautics. T.R. No. 387, N.A.C.A., 1931.
3. Wirt, Loring: New Data for the Design of Elbows in Duct Systems. Gen. Elec. Rev., vol. 30, no. 6, June 1927, pp. 286-296.
4. Rogallo, Francis M.: Theoretical Investigation of Induced-Flow Systems. T.N. No. (to be published), N.A.C.A., 1938.
5. Young, A. D., and Maas, J. N.: The Behavior of a Pitot Tube in a Transverse Total-Pressure Gradient. R. & M. No. 1770, British A.R.C., 1937.
6. Schoder, Ernest W., and Dawson, Francis M.: Hydraulics. McGraw-Hill Book Co., Inc., 1927.

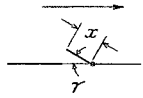
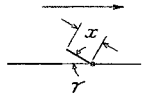
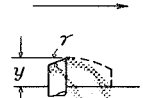
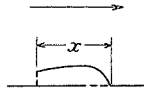
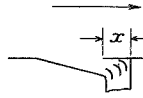
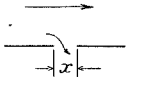
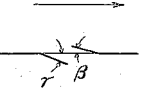
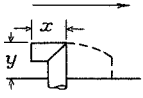
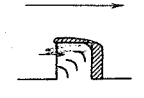
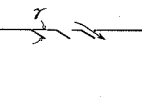
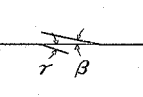
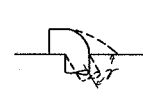
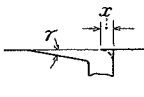
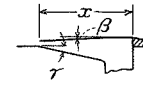
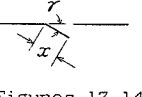
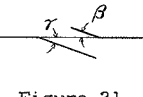
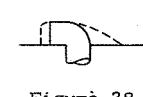
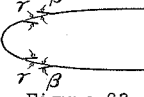
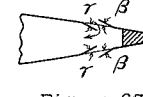
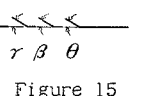
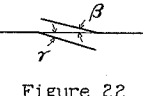
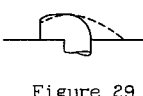
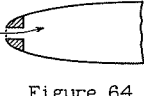
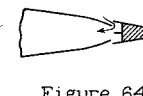
<p>Theory, figure 69 Comparison of results of theory and experiment, Figure 67</p> 	<p>Figures 16,17</p> 	<p>Figures 24,25</p> 	<p>Figures 30,31</p> 	<p>Figure 34</p> 
<p>Figure 11</p> 	<p>Figures 18,19</p> 	<p>Figures 26,27</p> 	<p>Figure 32</p> 	<p>Figures 35,36</p> 
<p>Figure 12</p> 	<p>Figure 20</p> 	<p>Figures 23,28</p> 	<p>Figure 33</p> 	<p>Figure 37</p> 
<p>Figures 13,14</p> 	<p>Figure 21</p> 	<p>Figure 28</p> 	<p>Figure 62</p> 	<p>Figure 63</p> 
<p>Figure 15</p> 	<p>Figure 22</p> 	<p>Figure 29</p> 	<p>Figure 64</p> 	<p>Figure 64</p> 

Table II.- General arrangements of outlet openings investigated.

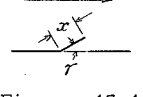
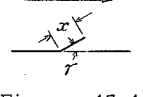
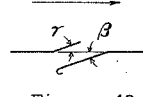
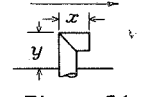
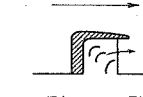
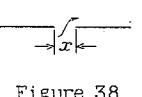
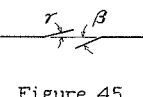
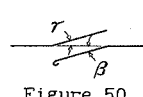
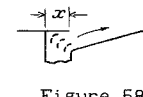
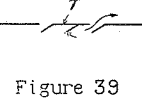
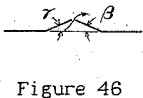
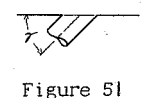
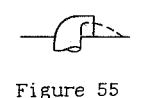
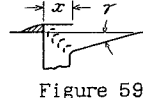
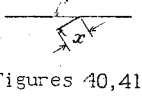
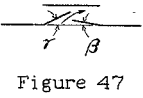
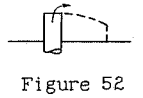
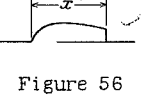
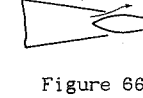
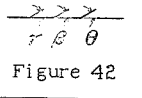
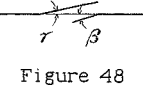
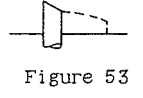
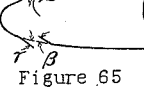
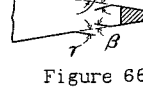
<p>Theory, figure 70 Comparison of results of theory and experiment, Figure 68</p> 	<p>Figures 43,44</p> 	<p>Figure 49</p> 	<p>Figure 54</p> 	<p>Figure 57</p> 
<p>Figure 38</p> 	<p>Figure 45</p> 	<p>Figure 50</p> 	<p>Figure 55</p> 	<p>Figure 58</p> 
<p>Figure 39</p> 	<p>Figure 46</p> 	<p>Figure 51</p> 	<p>Figure 55</p> 	<p>Figure 59</p> 
<p>Figures 40,41</p> 	<p>Figure 47</p> 	<p>Figure 52</p> 	<p>Figure 56</p> 	<p>Figure 66</p> 
<p>Figure 42</p> 	<p>Figure 48</p> 	<p>Figure 53</p> 	<p>Figure 65</p> 	<p>Figure 66</p> 

TABLE III. Characteristics of Combinations
of Inlet and Outlet Openings
in an N.A.C.A. 0018 Wing

^a Inlet opening	^b Outlet opening	$\frac{Q}{AV}$	Openings tested in combination				Openings tested individually (figs. 62-66)			
			$\frac{D}{qA}$	$\frac{\Delta p}{q}$	CPL	η (per-cent)	$\frac{D}{qA}$	$\frac{\Delta p}{q}$	CPL	η (per-cent)
WFI-10+0	WRE+5- 5	0.308	1.10	0.170	3.42	4.7	1.19	0.07	3.79	1.8
WFI-10+0	WRE+0-10	.279	.97	.140	3.34	4.0	1.09	.01	3.74	.3
WFI- 5+5	WRE+0-10	.312	1.25	.175	3.84	4.4	1.70	.19	5.15	3.5
WRI-10+0	WFE+0-10	.385	.39	.266	.74	26.3	.52	.25	1.04	18.5
WRI-10+0	WFE+5- 5	.443	.66	.352	1.14	23.7	.79	.32	1.43	17.9
WRI- 5+5	WFE+5- 5	.449	.75	.362	1.30	21.8	.97	.41	1.69	19.0
WRI- 5+5	WFE+0-10	.388	.50	.271	1.02	21.0	.70	.34	1.45	18.8
WNIS	WREA	^c .459	^c .48	.295	.74	28.4	^c .47	.18	.82	17.6
WNI	WREA	^c .501	^c .44	.385	.49	44.2	^c .47	.39	.51	41.6

^aSee figures 62, 63, and 64.

^bSee figures 65 and 66.

^cBased on outlet area.

TABLE IV. Comparison of Experimental and Theoretical Characteristics of Inlet Openings

(1)	(2)	(3)	(4)	(5)	(6)	(7)	(8)
^a Model	Q/AV Near minimum C _{PL}	Experimental		Theoretical		(3)-(5) (3)	(6)-(4) (2) ^a
		D/qA	p/q	D/qA	H/q		
7P-25+ 0	0.404	0.674	-0.036	0.650	0.655	0.036	4.24
7P-20+ 0	.397	.667	.093	.615	.608	.078	3.27
7P-15+ 0	.408	.677	.159	.608	.560	.102	2.41
7P-10+ 0	.499	.736	.138	.720	.528	.022	1.57
7P- 5+ 0	.497	.670	.081	.668	.455	.003	1.51
7P+ 0+ 5	.598	.967	-.101	.814	.465	.158	1.58
7P+ 0+10	.600	1.252	.020	.888	.552	.291	1.48
7P+ 0+15	.599	1.458	.092	.944	.629	.352	1.50
7P+ 0+20	.613	1.502	.089	1.015	.693	.324	1.61
7P+ 0+25	.617	1.541	.088	1.055	.740	.315	1.71
WRI-10+ 0	.400	.596	.064	.515	.415	.136	2.19
WRI- 5+ 0	.500	.763	-.060	.619	.382	.189	1.77
WRI- 5+ 5	.500	.853	.038	.658	.433	.229	1.58
WRI+ 0+ 5	.700	1.177	-.230	.892	.405	.242	1.30
WRI+ 0+10	.700	1.358	-.160	.947	.474	.302	1.29
WRI-B	.400	.564	.153	.515	.415	.087	1.64

^aSee figures 14, 17, 63, and 64.

FIGURE LEGENDS

- Figure 1.- Wind tunnel modifications. Note outlet opening on floating plate.
- Figure 2.- Induced-flow and balance systems.
- Figure 3.- Bellmouth on detachable duct at 45° with plate.
- Figure 4.- Orifice drum and blower.
- Figure 5.- N.A.C.A. 0018 wing model, showing adjustable flap openings at 0.175c and 0.800c locations.
- Figure 6.- Comb used for boundary-layer surveys.
- Figure 7.- Boundary-layer velocity distribution on vertical center line of mounting plate.
- Figure 8.- Boundary-layer velocity distribution at 0.800c location on N.A.C.A. wing, flap sealed; 80 m.p.h.
- Figure 9.- Duct pressure gradients. Inlet openings in flat plate. See figures 23, 27, and 28 for dimensions of models.
- Figure 10.- Section through central chamber of N.A.C.A. 0018 wing and internal pressure gradients.
- Figure 11.- Inlet characteristics of circular holes in thin plate, showing effects of hole diameter and tunnel velocity.
- Figure 12.- Inlet characteristics of $1\frac{1}{2}$ -inch-chord triple flaps, showing effects of flap angle.
- Figure 13.- Inlet characteristics of $1\frac{1}{2}$ -inch-chord internal flap, showing effects of flap angle.
- Figure 14.- Inlet characteristics of $2\frac{3}{4}$ -inch-chord internal flap, showing effects of flap angle.
- Figure 15.- Inlet characteristics of $1\frac{1}{2}$ -inch-chord external triple flaps, showing effects of flap angle and tunnel velocity.
- Figure 16.- Inlet characteristics of $1\frac{1}{2}$ -inch-chord external flap, showing effects of flap angle and tunnel velocity.

Figure 17.-- Inlet characteristics of $2\frac{3}{4}$ -inch-chord external flap, showing effects of flap angle.

Figure 18.-- Inlet characteristics of equal-chord opposed flaps, showing effects of β when γ is -15° .

Figure 19.-- Inlet characteristics of equal-chord opposed flaps, showing effects of flap angle.

Figure 20.-- Inlet characteristics of unequal-chord, overlapping, opposed flaps, with large flap external, showing effects of flap angle.

Figure 21.-- Inlet characteristics of unequal-chord, overlapping, opposed flaps, with small flap external, showing effects of flap angle.

Figure 22.-- Inlet characteristics of equal-chord, overlapping, opposed flaps, showing effects of flap angle.

Figure 23.-- Inlet characteristics of flush opening with circular duct, showing effects of duct angle and tunnel velocity.

Figure 24.-- Inlet characteristics of straight circular pipe projecting two diameters, showing effects of rake angle and tunnel velocity.

Figure 25.-- Inlet characteristics of straight circular pipe with 45° rake, showing effects of fairing and length of projection.

Figure 26.-- Inlet characteristics of circular pipe with elbow projecting two diameters, showing effects of fairing and tunnel velocity.

Figure 27.-- Inlet characteristics of circular pipe with elbow projecting one diameter, showing effects of fairing, elbow length, and tunnel velocity.

Figure 28.-- Inlet characteristics of external scoop with circular duct, showing effects of entrance shape, fairing, and duct angle.

Figure 29.-- Inlet characteristics of external scoop with circular duct, showing effects of fairing in front and rear.

Figure 30.-- Inlet characteristics of external scoop without duct, showing effects of length and area of mouth.

- Figure 31.- Inlet characteristics of external scoop without duct, showing effects of tunnel velocity, scoop shape, and location over circular hole. Also screens over mouth and throat.
- Figure 32.- Inlet characteristics of external scoop without duct, showing effects of guide vanes and scoop height.
- Figure 33.- Inlet characteristics of recess opening and duct, showing effects of recess angle and entrance shape.
- Figure 34.- Inlet characteristics of recess opening and duct, showing effects of cover length, guide vanes, and faired entrance.
- Figure 35.- Inlet characteristics of recess opening and duct with projecting scoop, showing effects of recess angle and internal fairing.
- Figure 36.- Inlet characteristics of recess opening and duct with projecting scoop, showing effects of bend treatment.
- Figure 37.- Inlet characteristics of external scoop with duct, showing effects of height of opening, throat expansion, and guide vanes.
- Figure 38.- Outlet characteristics of circular holes in thin plate, showing effects of hole diameter and tunnel velocity.
- Figure 39.- Outlet characteristics of $1\frac{1}{2}$ -inch-chord internal triple flaps, showing effects of flap angle.
- Figure 40.- Outlet characteristics of $1\frac{1}{2}$ -inch-chord internal flap, showing effects of flap angle.
- Figure 41.- Outlet characteristics of $2\frac{3}{4}$ -inch-chord internal flap, showing effects of flap angle.
- Figure 42.- Outlet characteristics of $1\frac{1}{2}$ -inch-chord external triple flaps, showing effects of flap angle and tunnel velocity.
- Figure 43.- Outlet characteristics of $1\frac{1}{2}$ -inch-chord external flap, showing effects of flap angle and tunnel velocity.
- Figure 44.- Outlet characteristics of $2\frac{3}{4}$ -inch-chord external flap, showing effects of flap angle.

- Figure 45.- Outlet characteristics of equal-chord, opposed flaps, showing effects of β when γ is 10° .
- Figure 46.- Outlet characteristics of equal-chord, opposed flaps, showing effects of β when γ is 20° .
- Figure 47.- Outlet characteristics of equal-chord, opposed flaps with cover plate, showing effects of flap angle and cover-plate clearance.
- Figure 48.- Outlet characteristics of unequal-chord, overlapping, opposed flaps, with large flap external, showing effects of flap angle and edge radius.
- Figure 49.- Outlet characteristics of unequal-chord, overlapping, opposed flaps, with small flap external, showing effects of flap angle.
- Figure 50.- Outlet characteristics of equal-chord, overlapping, opposed flaps, showing effects of flap angle.
- Figure 51.- Outlet characteristics of flush opening with circular duct, showing effects of duct angle and tunnel velocity.
- Figure 52.- Outlet characteristics of straight circular pipe with zero rake projecting two diameters, showing effects of fairing and tunnel velocity.
- Figure 53.- Outlet characteristics of straight circular pipe with 45° rake, showing effects of projection, fairing, and tunnel velocity.
- Figure 54.- Outlet characteristics of circular pipe with elbow, showing effects of elbow length and projection.
- Figure 55.- Outlet characteristics of flush circular ducts with and without hood covers, showing effects of hood, duct angle, and mouth obstruction.
- Figure 56.- Outlet characteristics of external hood without duct, showing effects of shape, length, and area of mouth.
- Figure 57.- Outlet characteristics of external hood without duct, showing effects of guide vanes and hood height.
- Figure 58.- Outlet characteristics of recess opening with 15° recess, showing effects of guide vanes and cover length.

Figure 59.- Outlet characteristics of recess opening, showing effects of hood length and projection, recess angle, and guide vanes.

Figure 60.- Variation of orifice coefficients with orifice pressure.

- (a) Inlet from cross wind.
- (b) Outlet into cross wind.

Figure 61.- Variation of orifice coefficients with ratio of orifice to cross-wind pressures.

- (a) Inlet from cross wind.
- (b) Outlet into cross wind.

Figure 62.- Inlet characteristics of 0.05c opposed flaps at 0.175c location on N.A.C.A. 0018 wing, showing effects of flap angle.

Figure 63.- Inlet characteristics of 0.05c opposed flaps at 0.800c location on N.A.C.A. 0018 wing, showing effects of flap angle.

Figure 64.- Inlet characteristics of faired openings at nose and 0.800c location on N.A.C.A. 0018 wing, showing effects of location and opening shapes.

Figure 65.- Outlet characteristics of 0.05c opposed flaps at 0.175c location on N.A.C.A. 0018 wing, showing effects of flap angle.

Figure 66.- Outlet characteristics of 0.05c opposed flaps and faired opening at 0.800c location on N.A.C.A. 0018 wing, showing effects of flap angle and opening shape.

Figure 67.- Inlet characteristics from wing tests, flat-plate tests, and theory, redrawn for comparison.

Figure 68.- Outlet characteristics from wing tests, flat-plate tests, and theory, redrawn for comparison.

Figure 69.- Theoretical aerodynamic characteristics of inlet openings, showing the effect of inlet-velocity ratio, V_1/V .

Figure 70.- Theoretical aerodynamic characteristics of outlet openings, showing the effect of duct angle.

Figure 71.- Duct flowmeter calibrations and duct pressure gradients, showing effect of obstructions.

Figure 72.- Duct flowmeter calibration set-up.

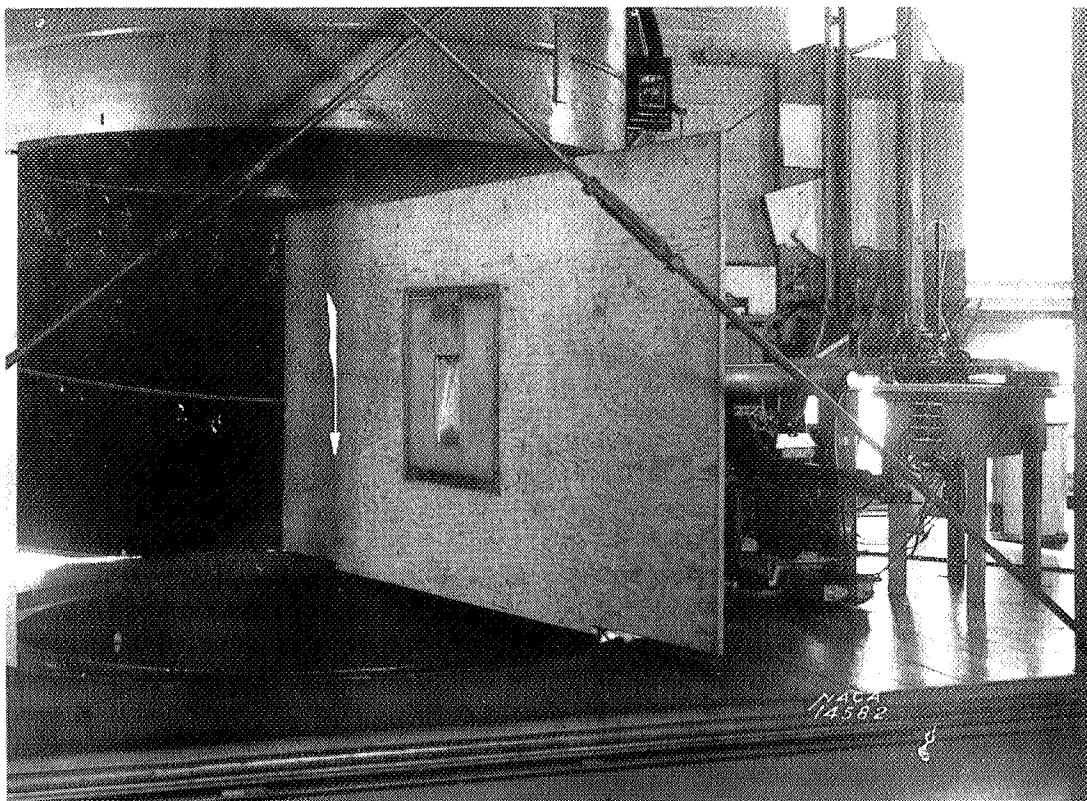


Figure 1

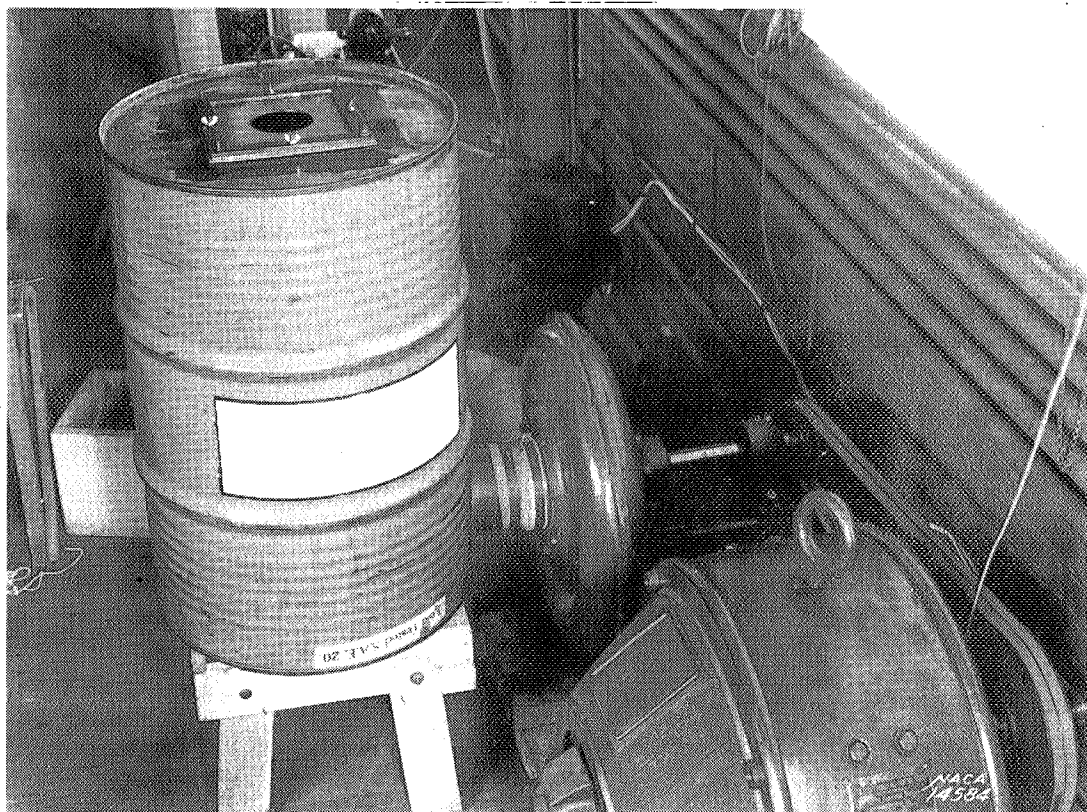


Figure 4

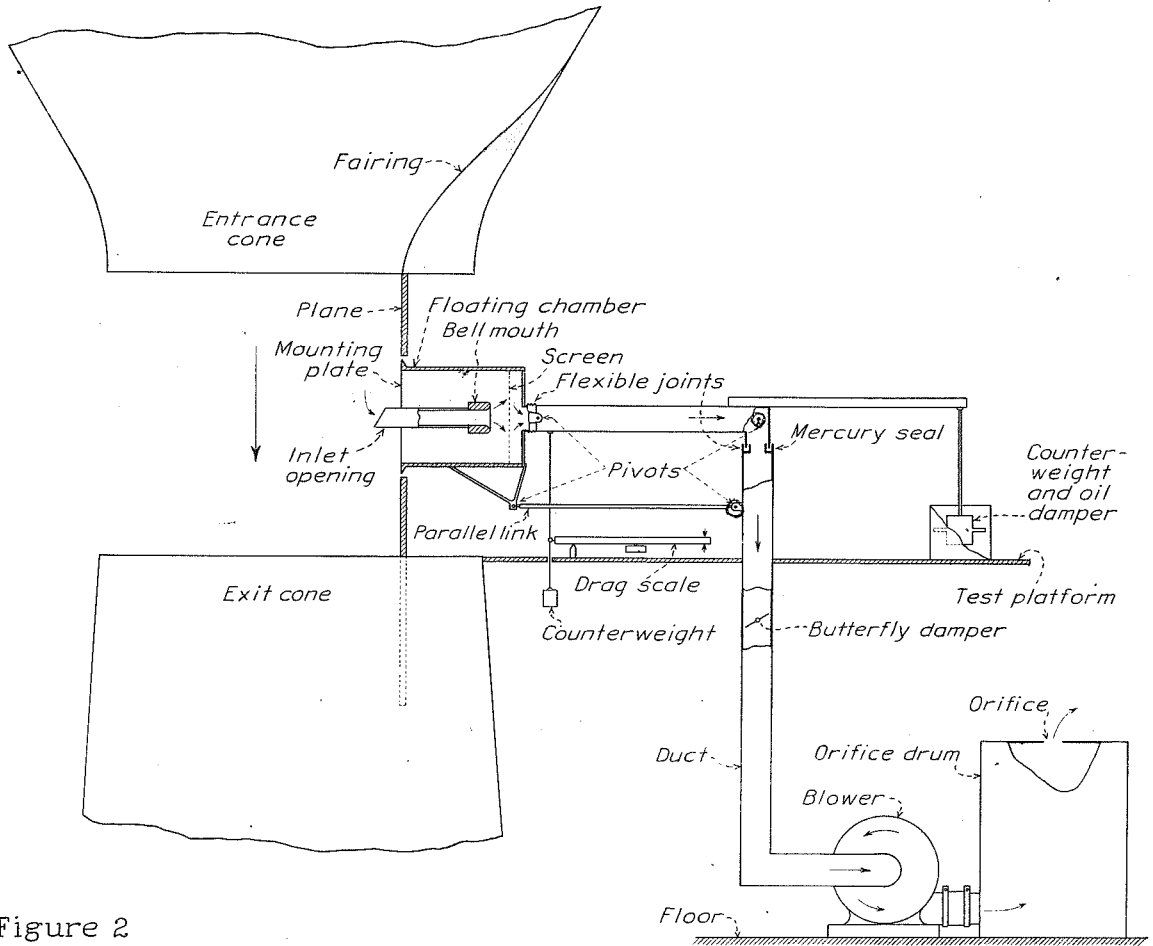


Figure 2

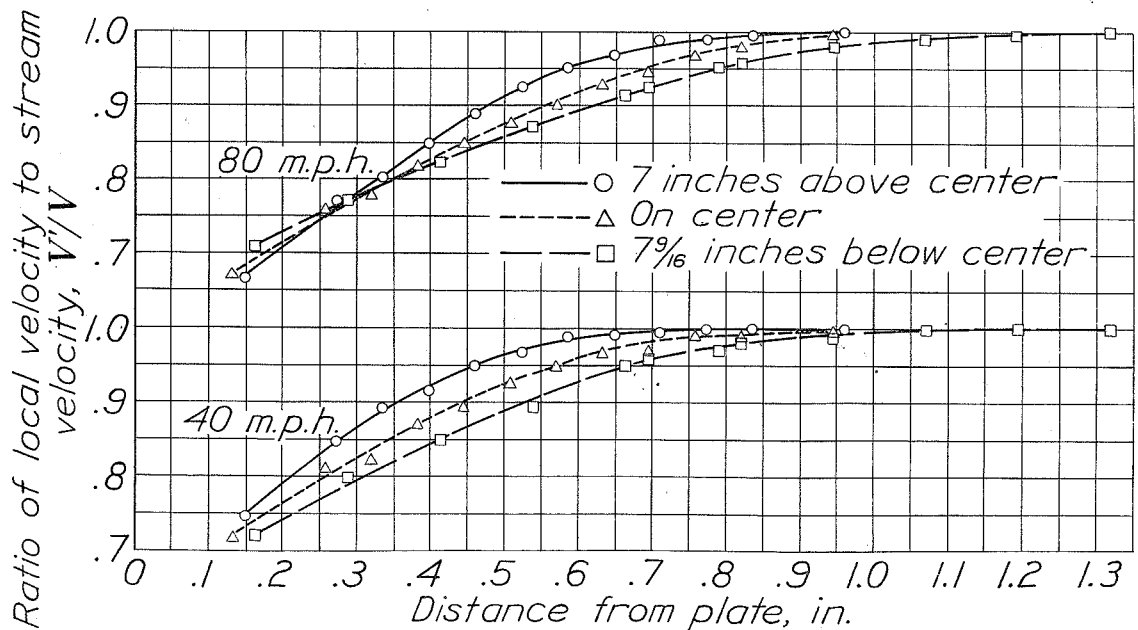


Figure 7

N.A.C.A.

Figs. 3,5,6

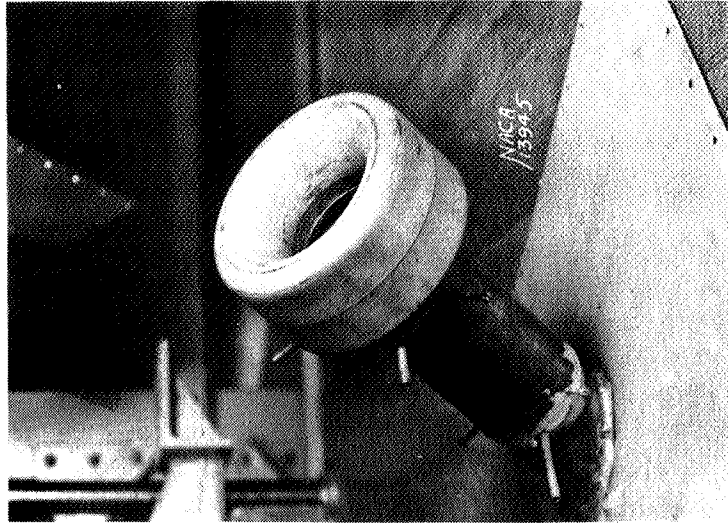


Figure 3

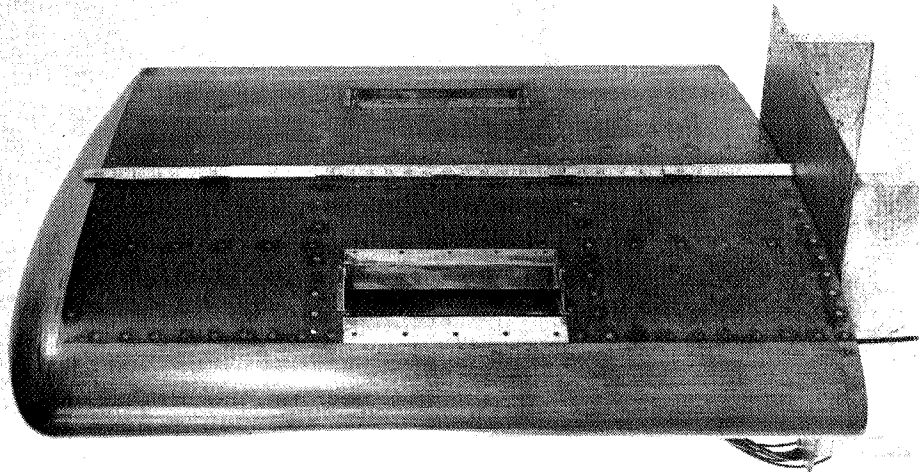


Figure 5

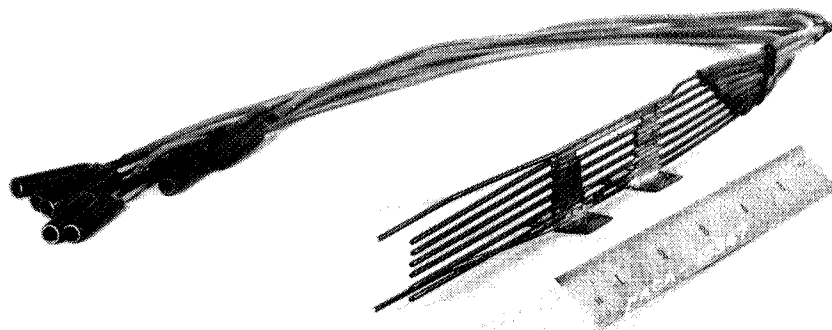


Figure 6

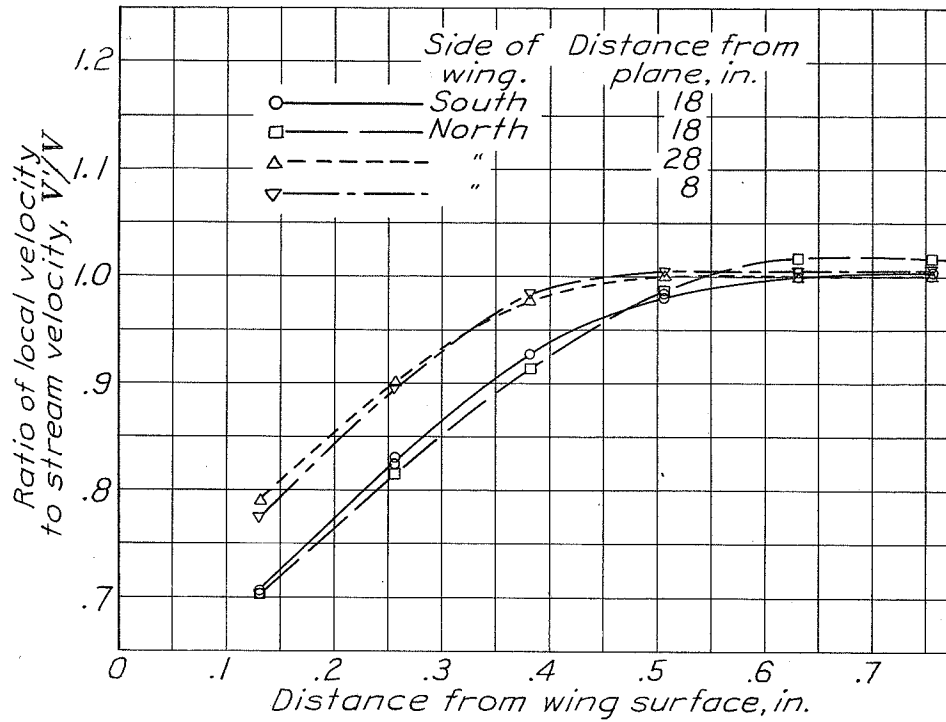


Figure 8

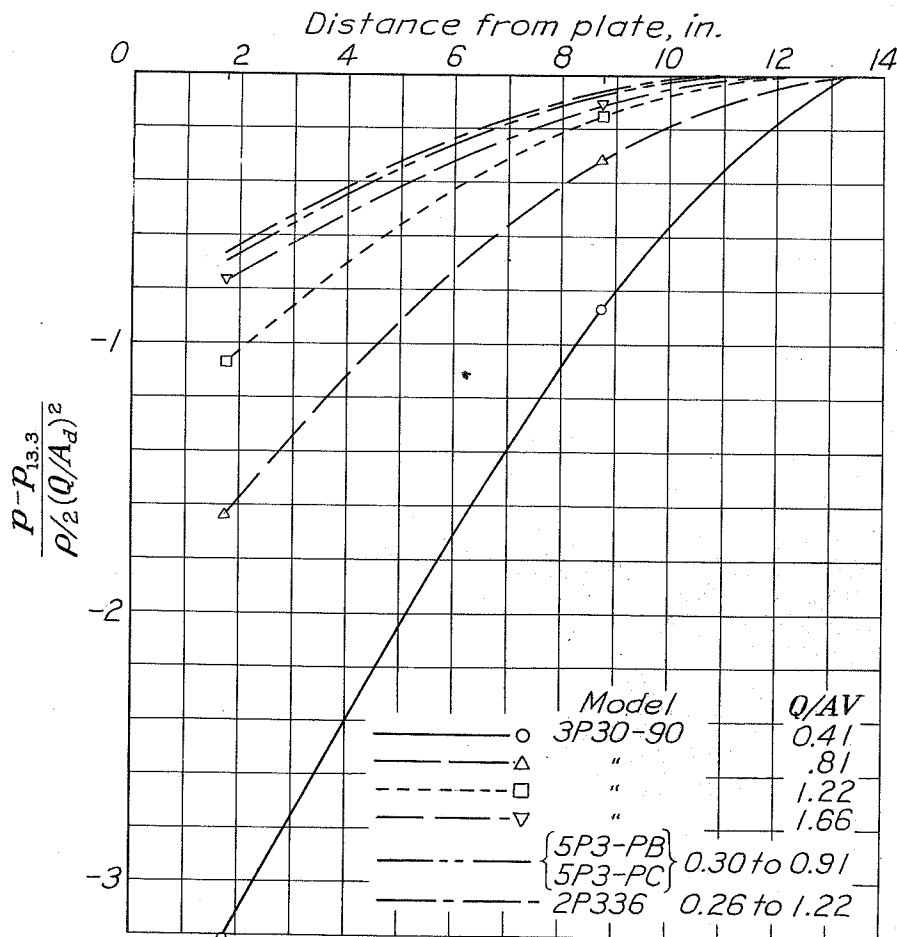


Figure 9

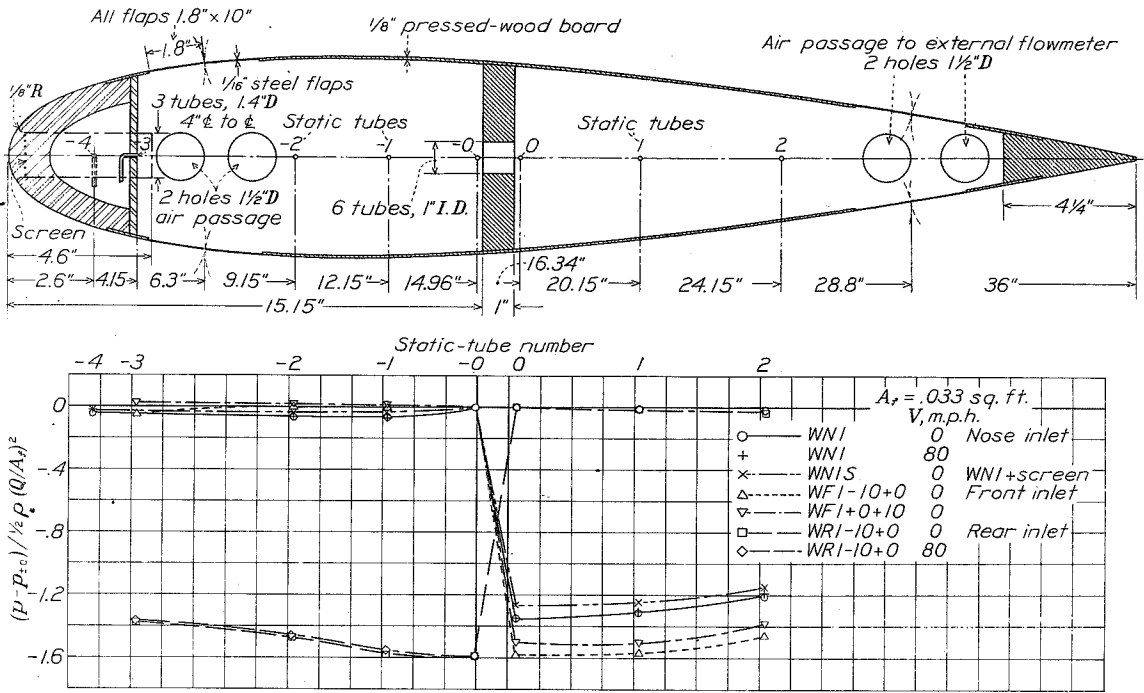


Figure 10

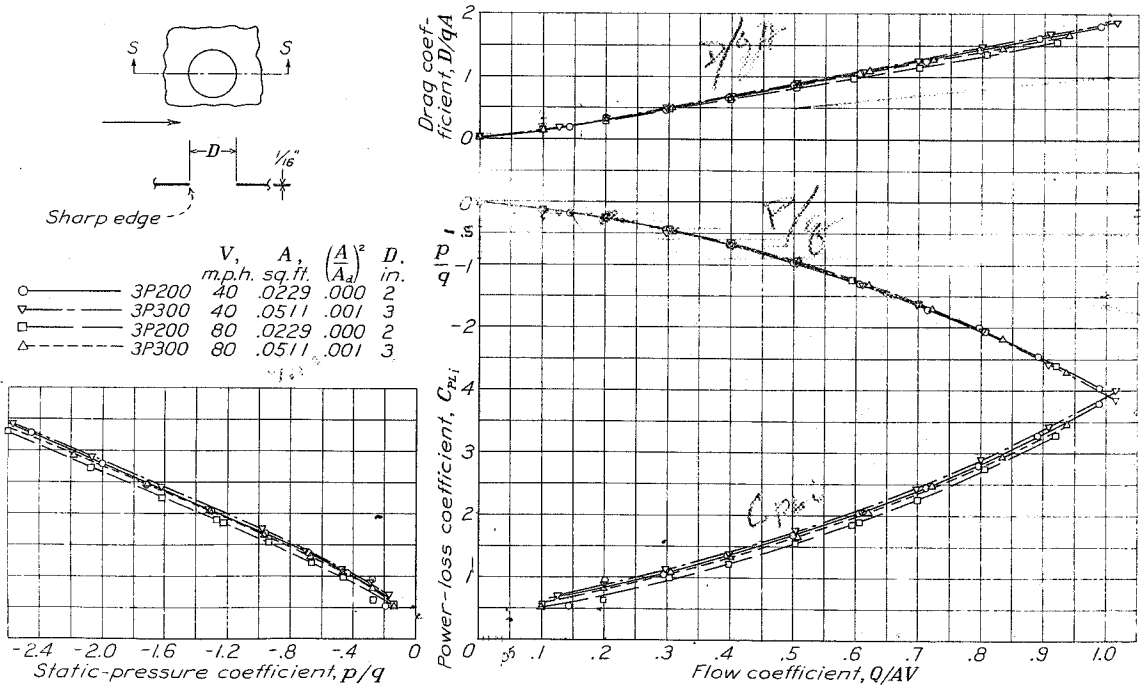


Figure 11.

Handwritten notes and signatures at the bottom of the page, including "35 AV" and "105 x 4000".

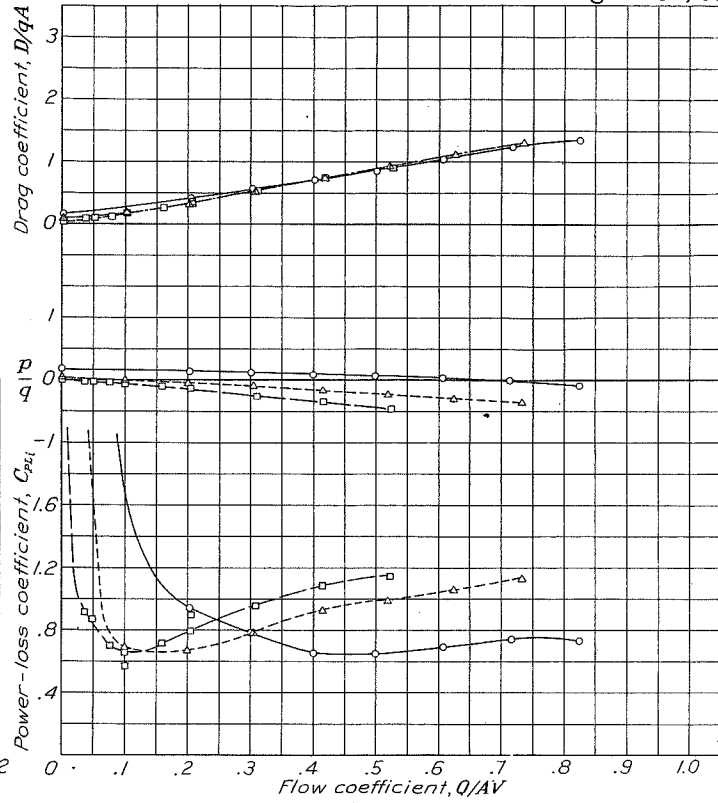
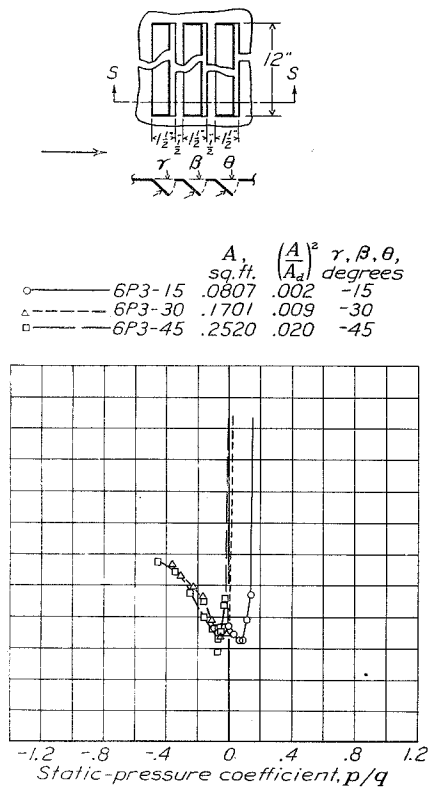


Figure 12

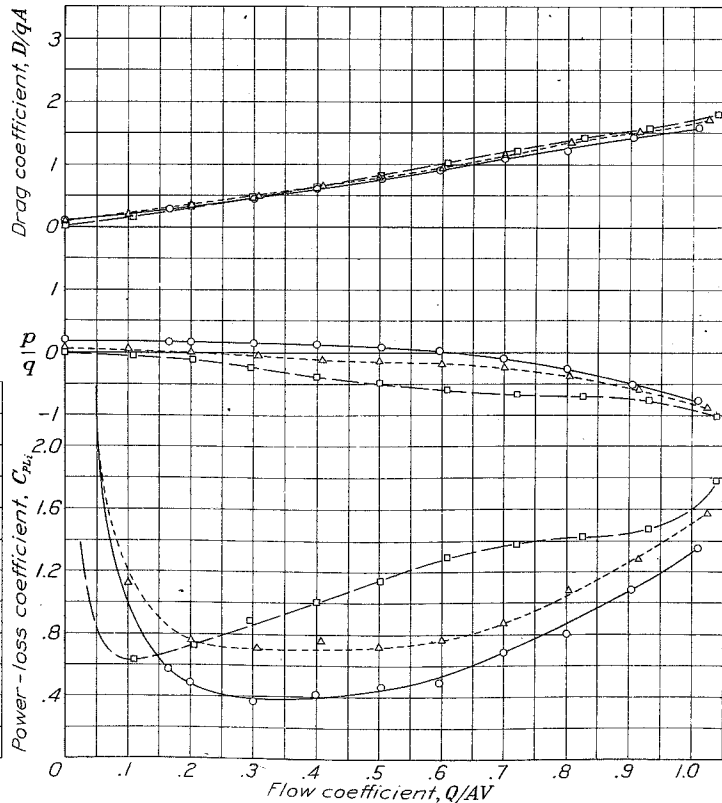
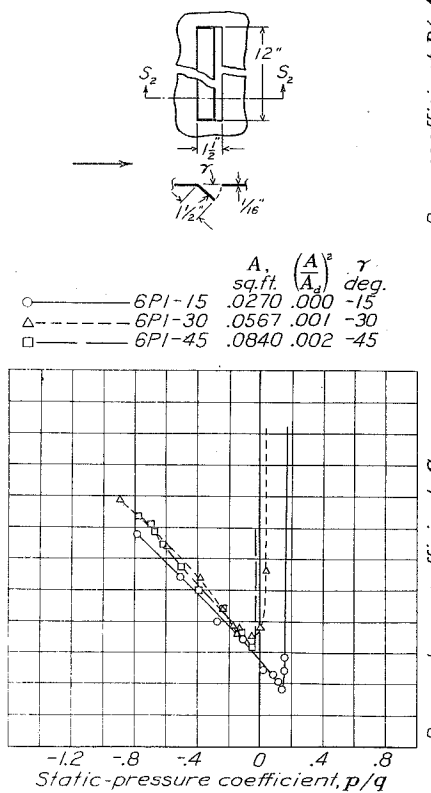


Figure 13

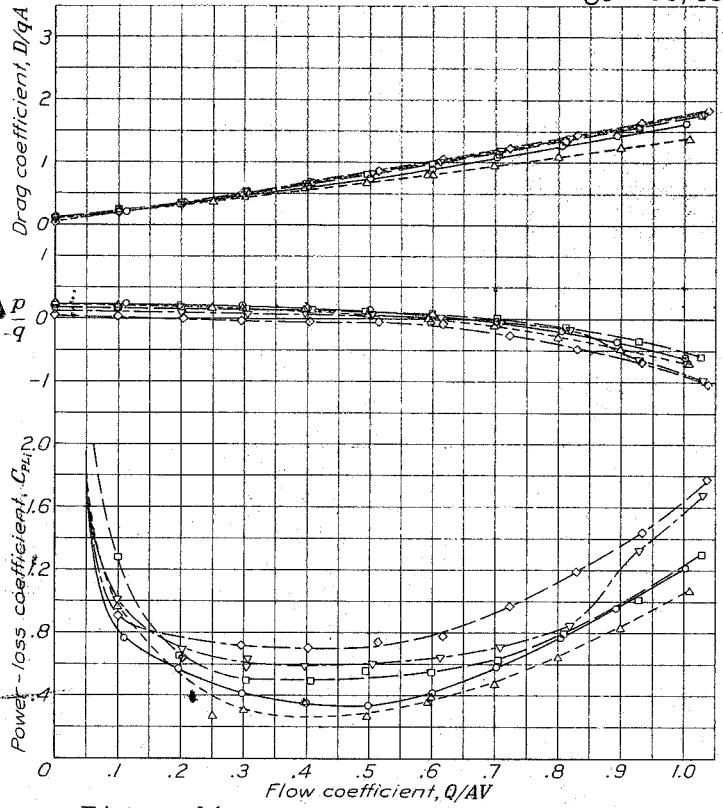
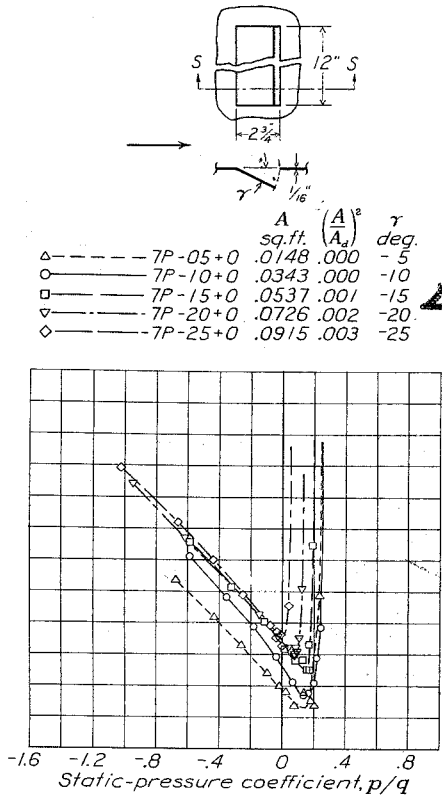


Figure 14

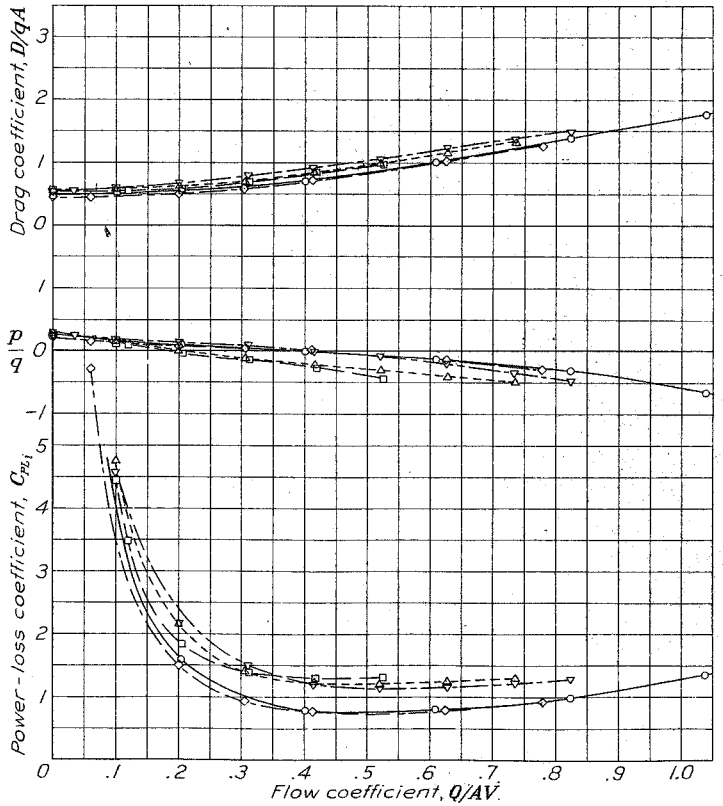
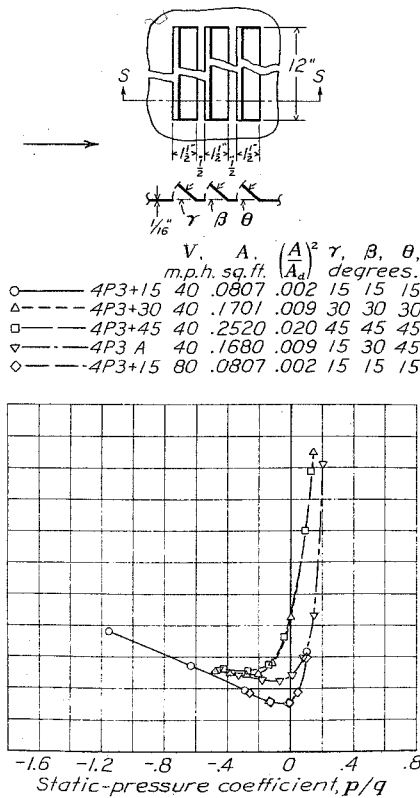


Figure 15

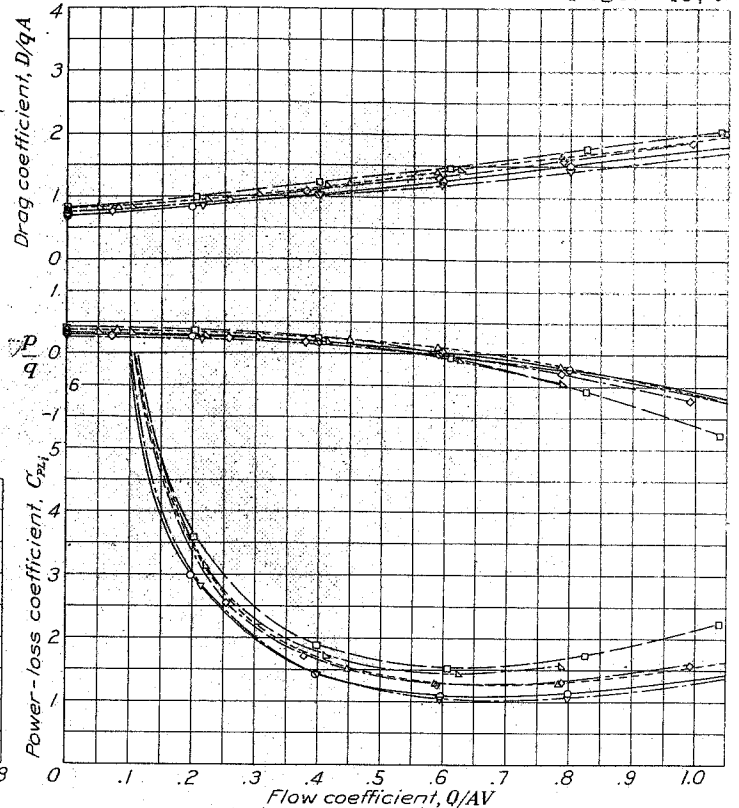
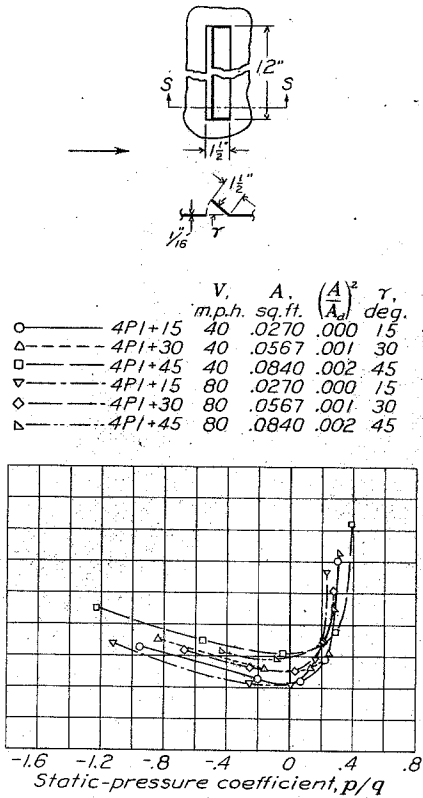


Figure 16

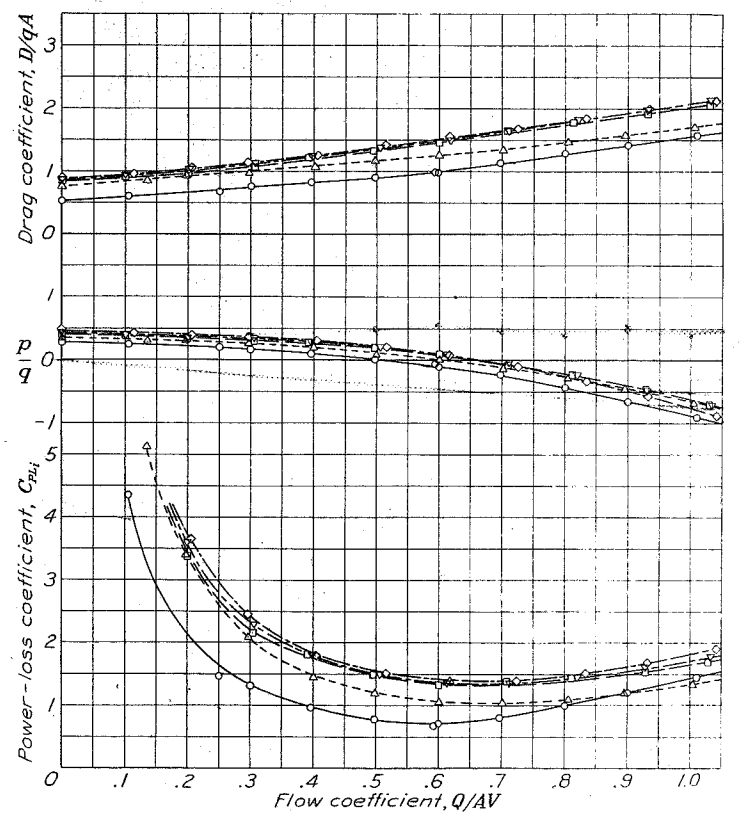
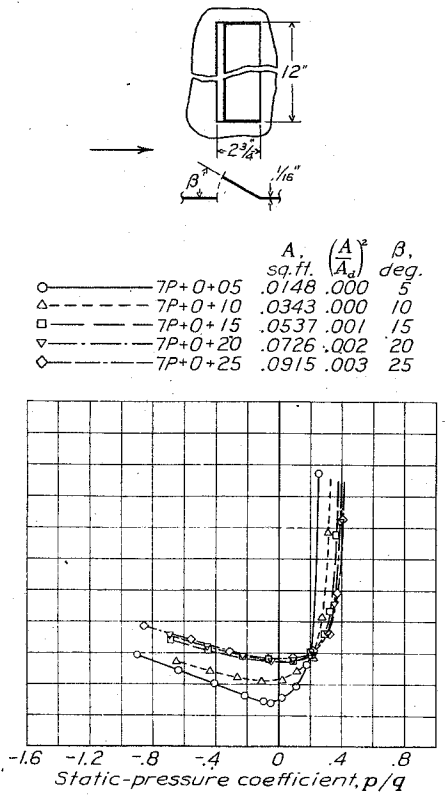


Figure 17

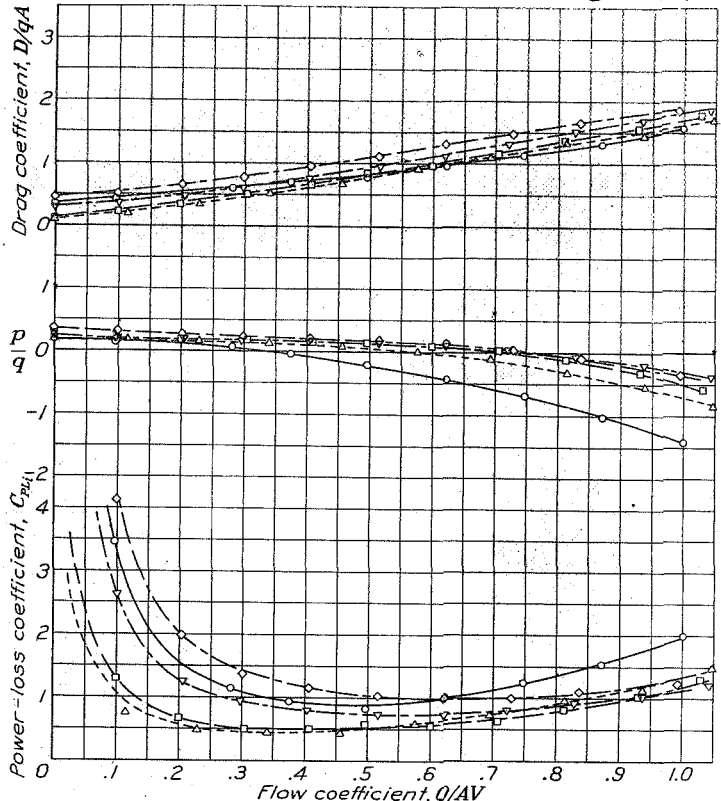
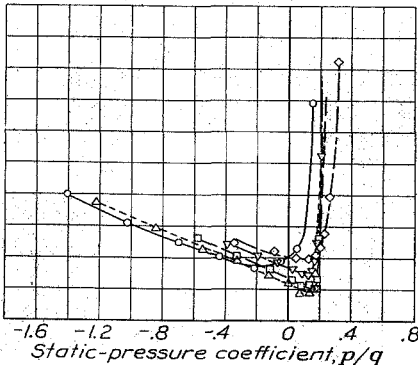
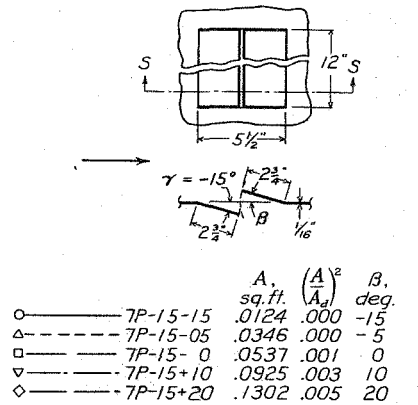


Figure 18

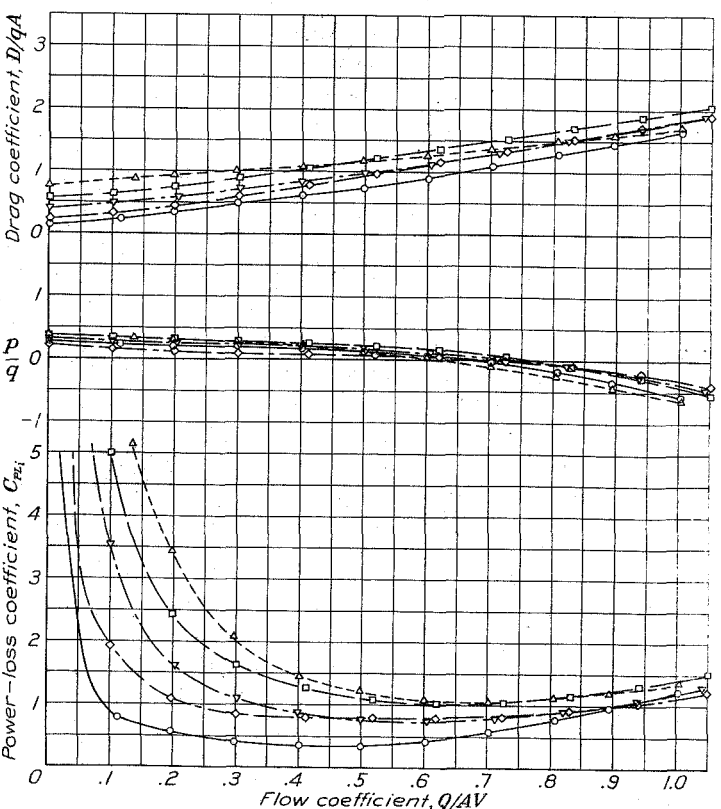
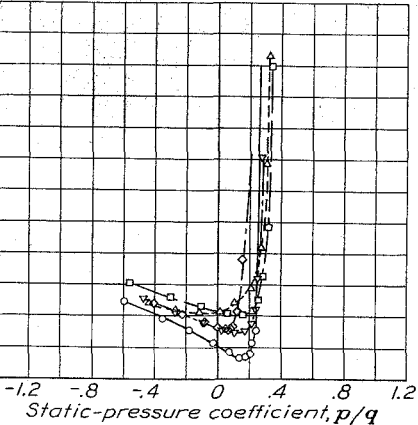
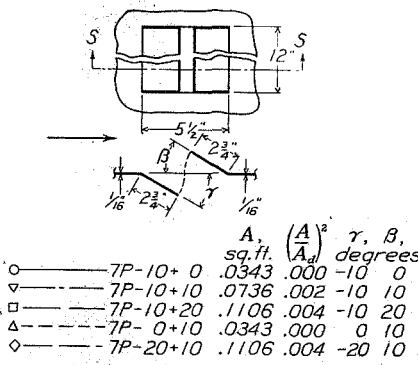
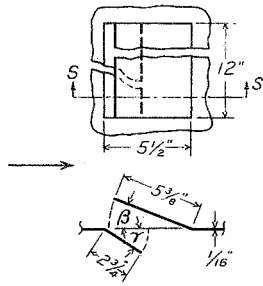


Figure 19

N.A.C.A.



	A	($\frac{A}{A_0}$) ²	γ, β
	sq.ft.		degrees
○	10P-20+05	.0272	.000 -20 5
△	10P-20+10	.0652	.001 -20 10

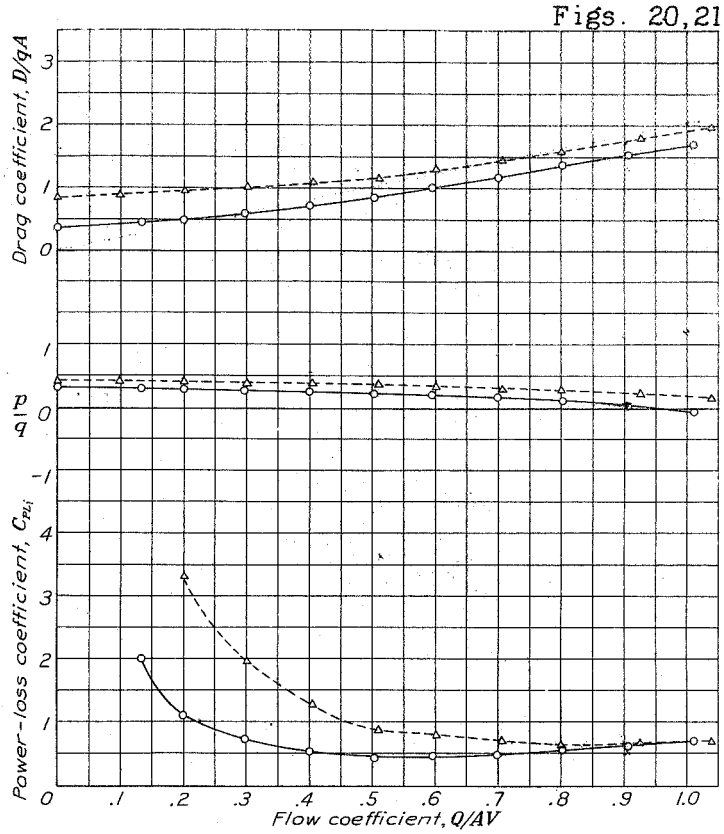
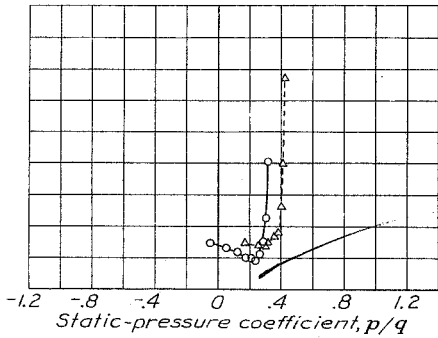
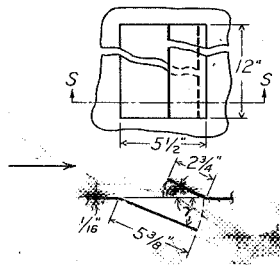


Figure 20



	A	($\frac{A}{A_0}$) ²	γ, β
	sq.ft.		degrees
○	9P-10+0	.0289	.000 -10 0
△	9P-15+0	.0478	.001 -15 0
□	9P-20+0	.0668	.001 -20 0
◇	9P-15+10	.0866	.002 -15 10
▽	9P-20+10	.1039	.003 -20 10
△	9P-20+20	.1435	.007 -20 20

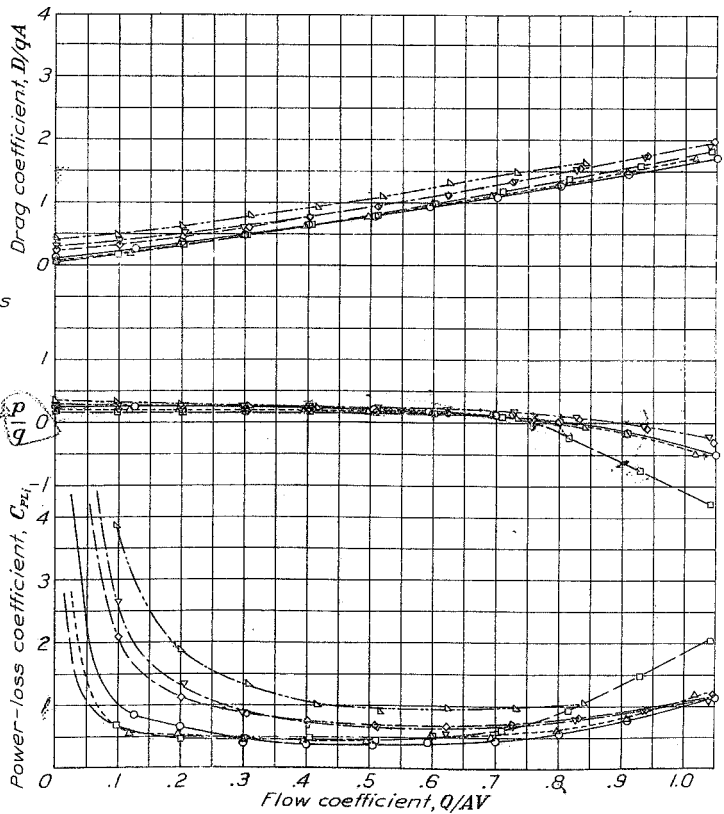
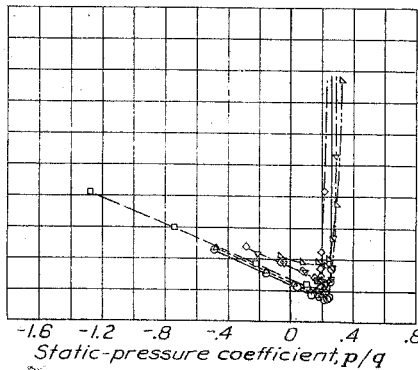
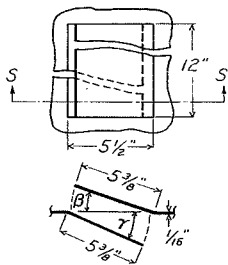


Figure 21



	A, sq. ft.	$\frac{A}{A_d}$	γ, β , degrees
○	11P-10+10	.0610	.001 -10 10
△	11P-20+05	.0264	.000 -20 5
▽	11P-20+10	.0643	.001 -20 10
□	11P-20+20	.1369	.006 -20 20
◇	11P-25+10	.0656	.001 -25 10
△	11P-30+10	.0660	.001 -30 10

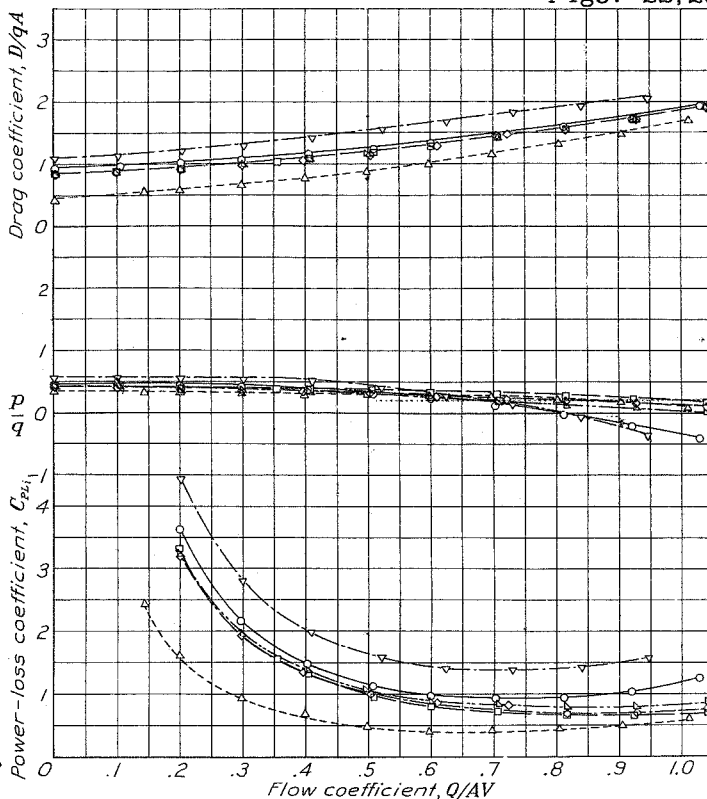
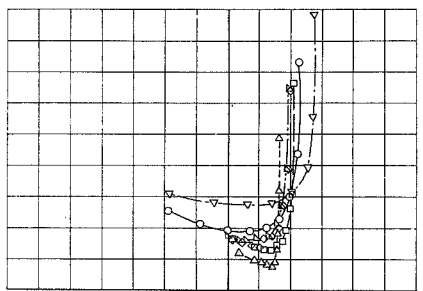
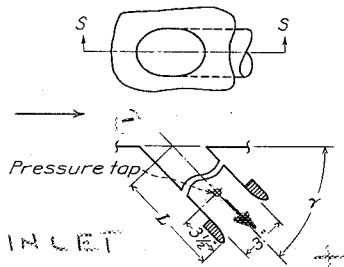


Figure 22



	V, m.p.h.	A, sq. ft.	$\frac{A}{A_d}$	L, in.	γ, β , deg.
○	3P30-90	40	.0441	1.000	16 3/4 90
△	3P30-60	40	.0441	1.000	13 1/2 60
□	3P30-45	40	.0441	1.000	13 45
▽	3P30-90	80	.0441	1.000	16 3/4 90

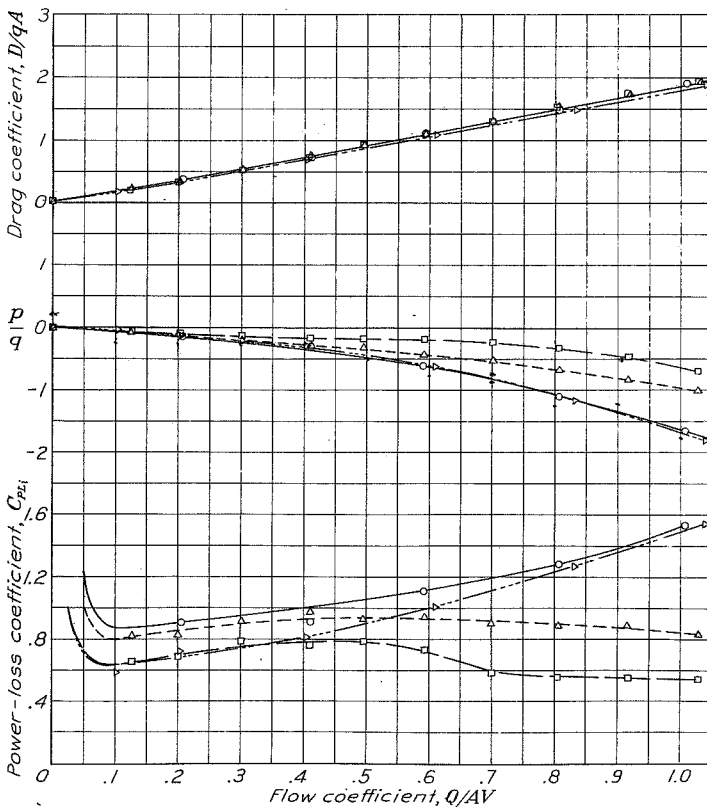
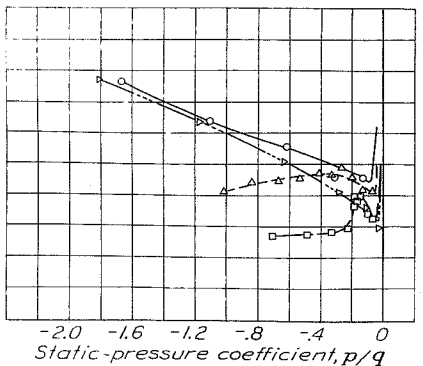
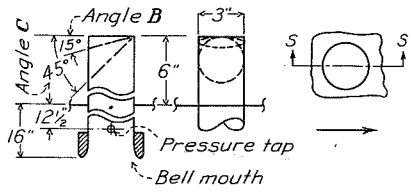


Figure 23

N.A.C.A.

Figs. 24,25



	V	A	(A) ²	De-
	m.p.h.	sq.ft.	(A _d)	tails
○	40	.0441	1.000	-
△	40	.0441	1.000	B
□	40	.0441	1.000	C
▽	80	.0441	1.000	-

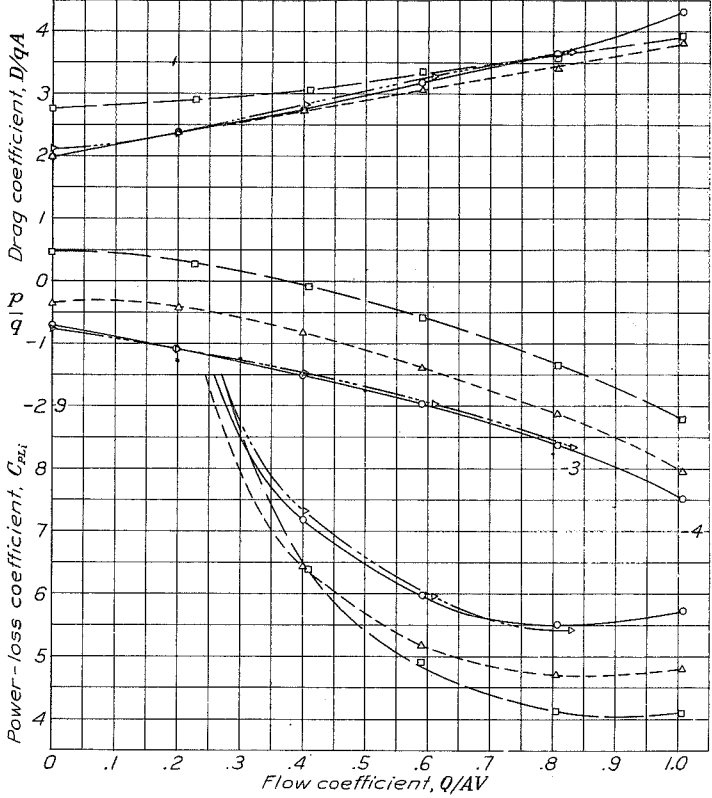
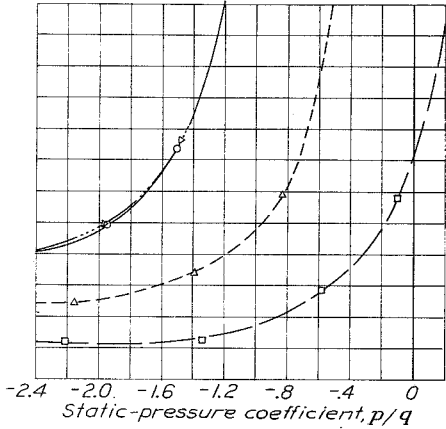
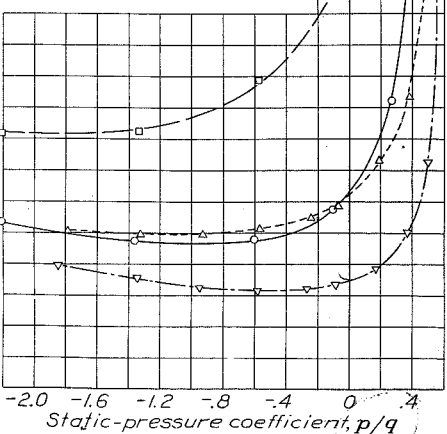
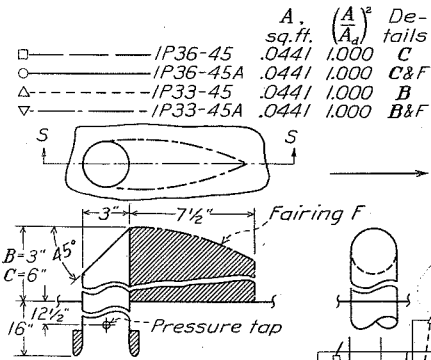


Figure 24



	A	(A) ²	De-
	sq.ft.	(A _d)	tails
□	.0441	1.000	C
○	.0441	1.000	C&F
△	.0441	1.000	B
▽	.0441	1.000	B&F

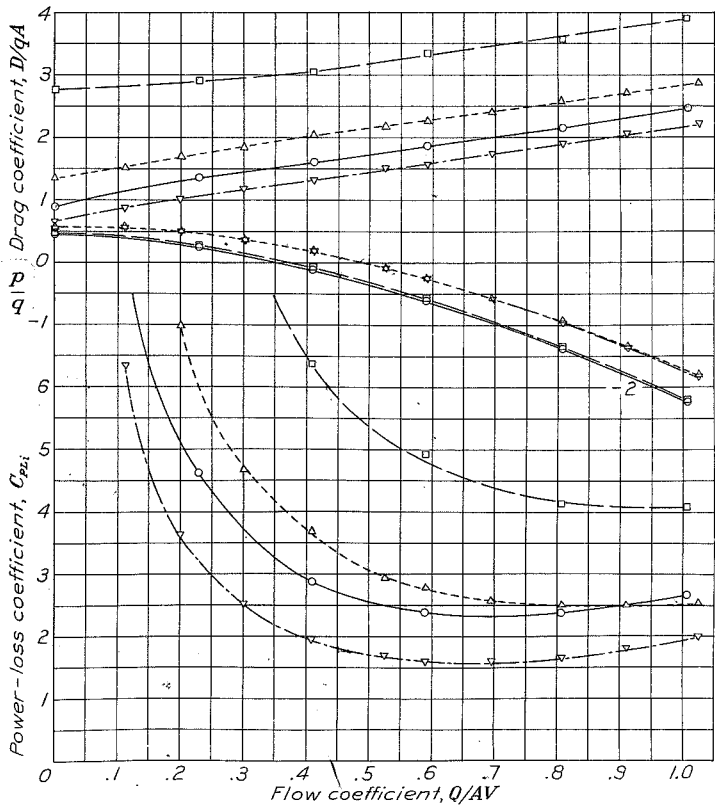


Figure 25

N.A.C.A.

Figs. 26,27

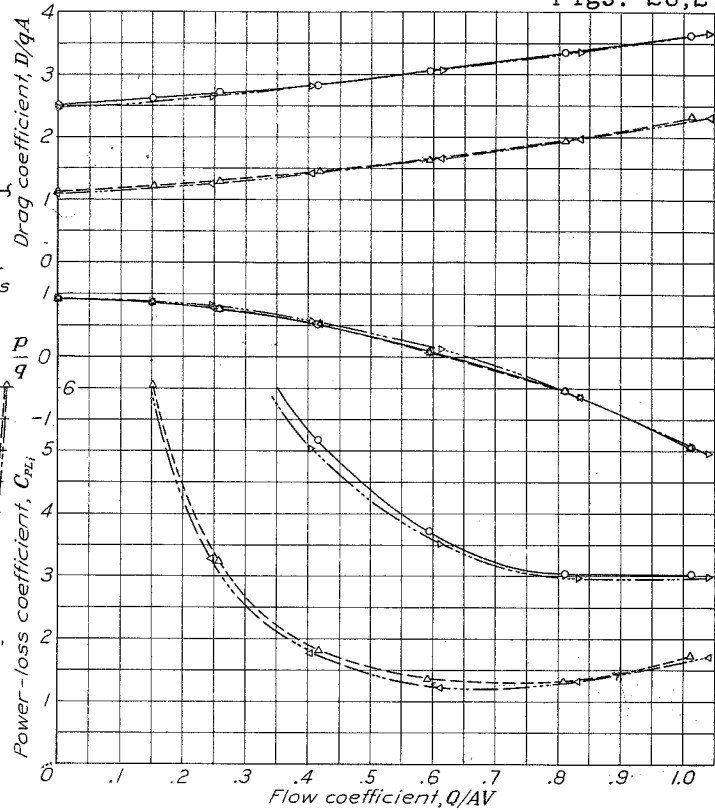
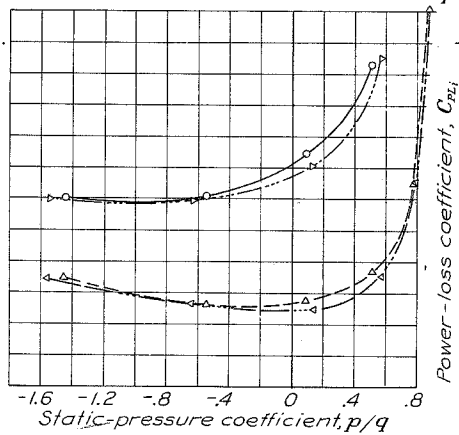
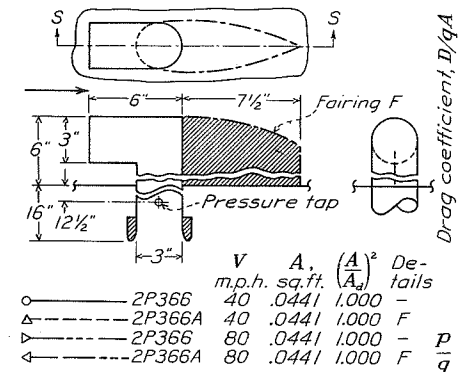


Figure 26

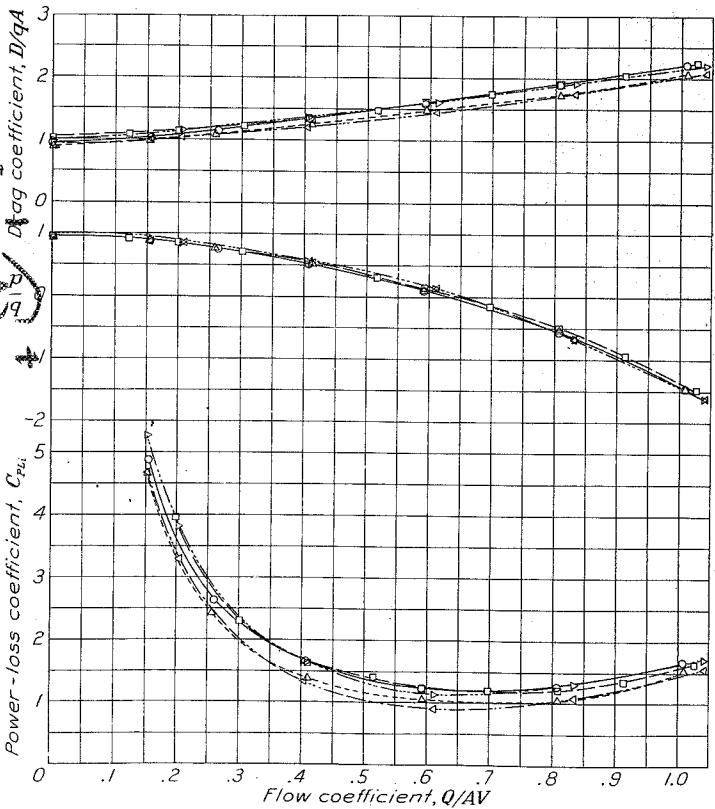
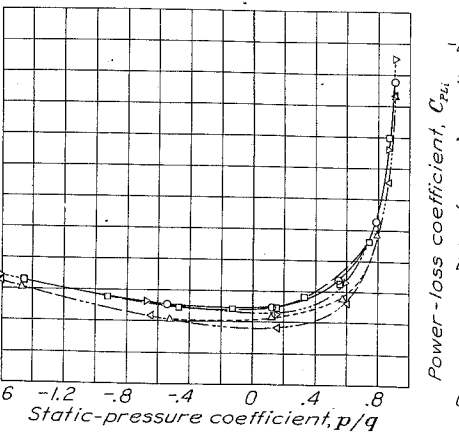
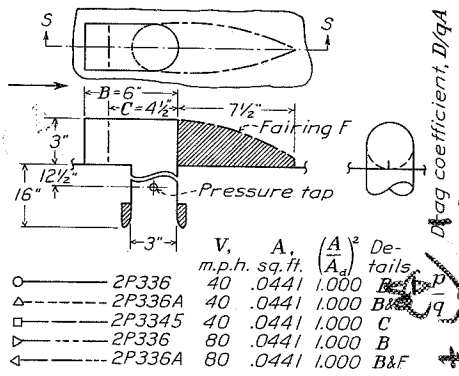
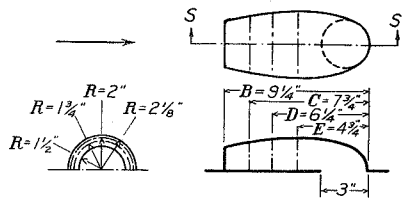


Figure 27

N.A.C.A.

Figs. 30, 31



	A	$(\frac{A}{A_0})^2$	De-
	sq. ft.		tails
○	13P475	.0514	.001 E
△	13P625	.0460	.001 D
□	13P775	.0365	.000 C
▽	13P925	.0257	.000 B

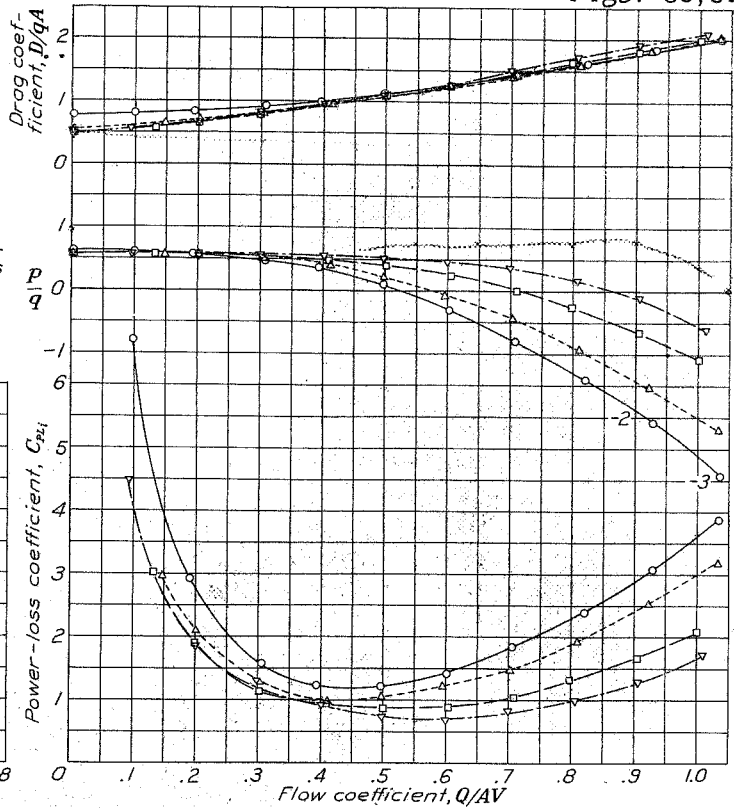
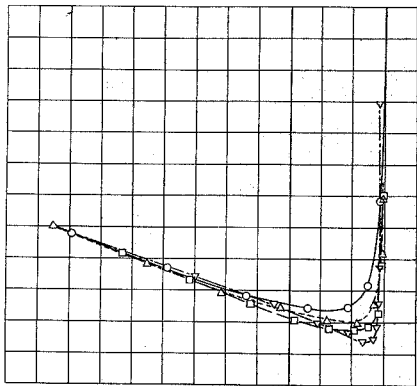
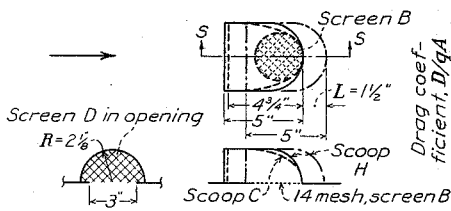


Figure 30



	V,	A,	$(\frac{A}{A_0})^2$	De-
	m.p.h.	sq. ft.		tails
□	5P3-1500	40	.0490	.001 H
△	5P3-300	40	.0490	.001 HL
○	13P475	40	.0514	.001 C
▽	13P475A	40	.0514	.001 C&B
◇	13P475B	40	.0514	.001 C&D
▷	5P3-1500	80	.0490	.001 H

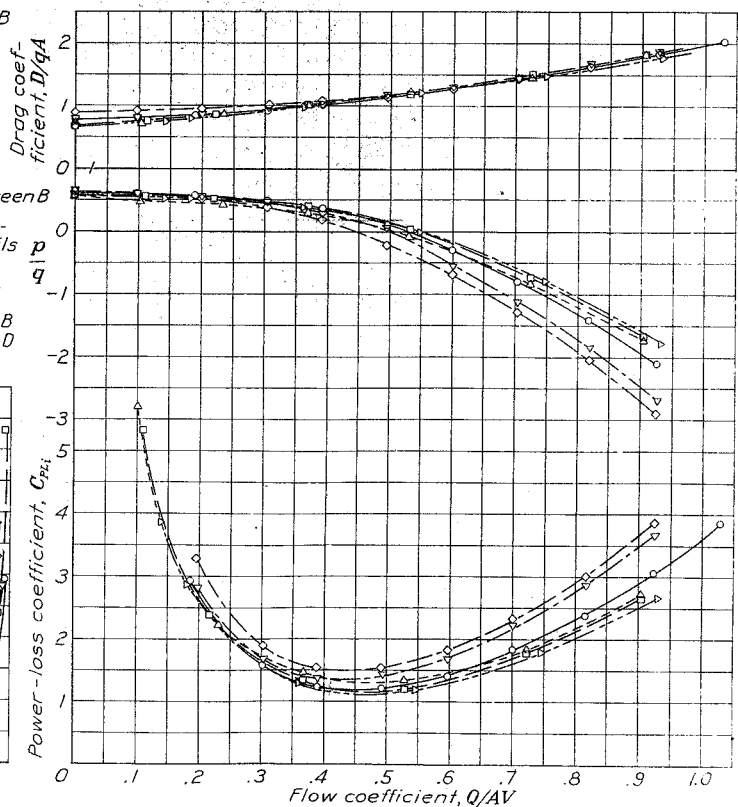
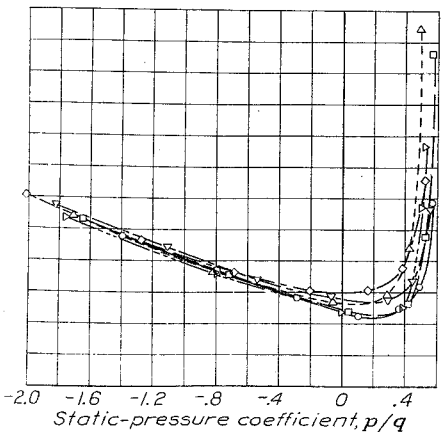


Figure 31

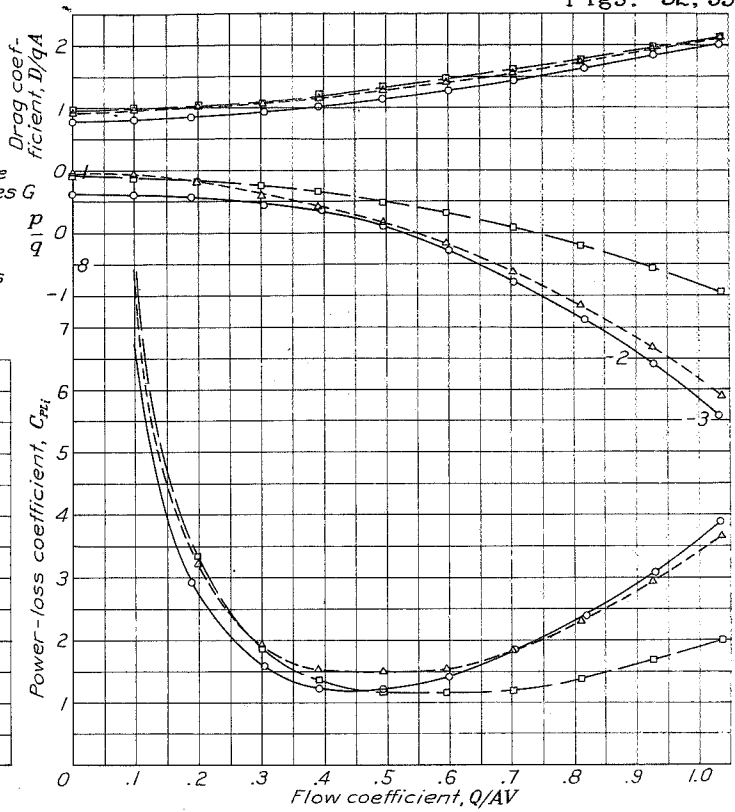
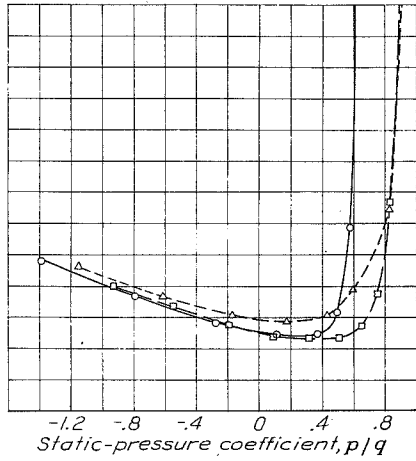
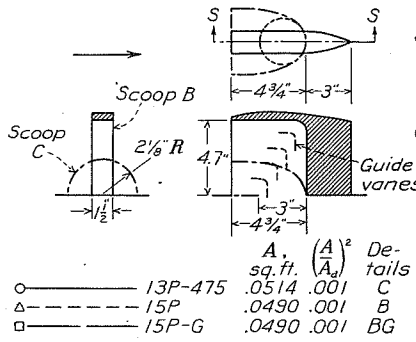
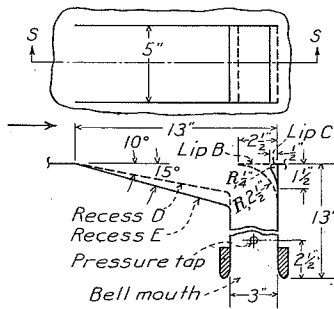


Figure 32



	A, sq. ft.	(A ₂) ²	De-tails
○	16P15-1	.1042	1.000 C&E
△	16P15-2	.0955	.840 B&E
□	16P10-1	.1042	1.000 C&D
▽	16P10-2	.0651	.391 B&D

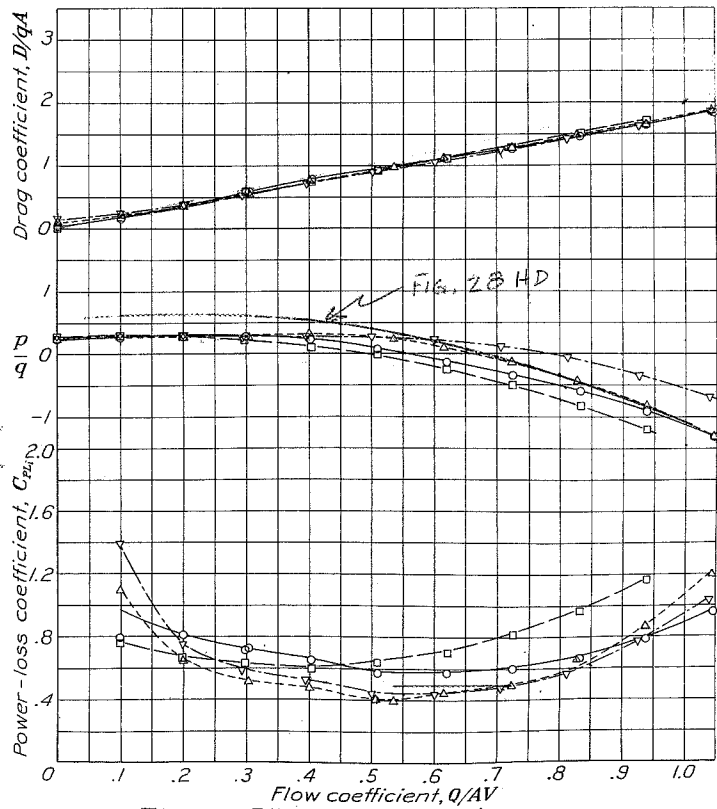
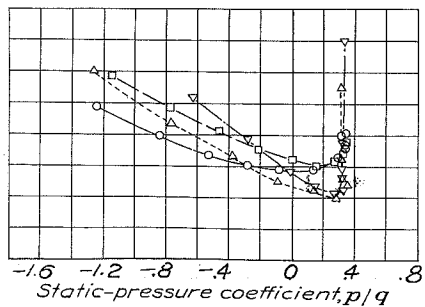
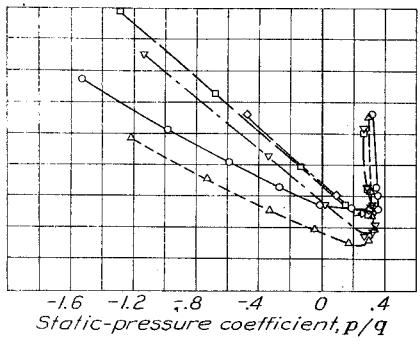
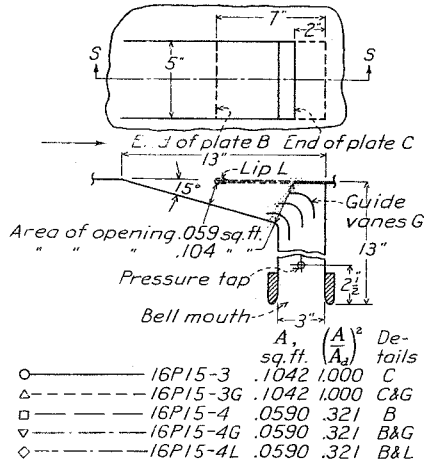


Figure 33



	A_1 sq. ft.	$(\frac{A_1}{A_2})^2$	De- tails
○	.1042	1.000	C
△	.1042	1.000	C&G
□	.0590	.321	B
▽	.0590	.321	B&G
◇	.0590	.321	B&L

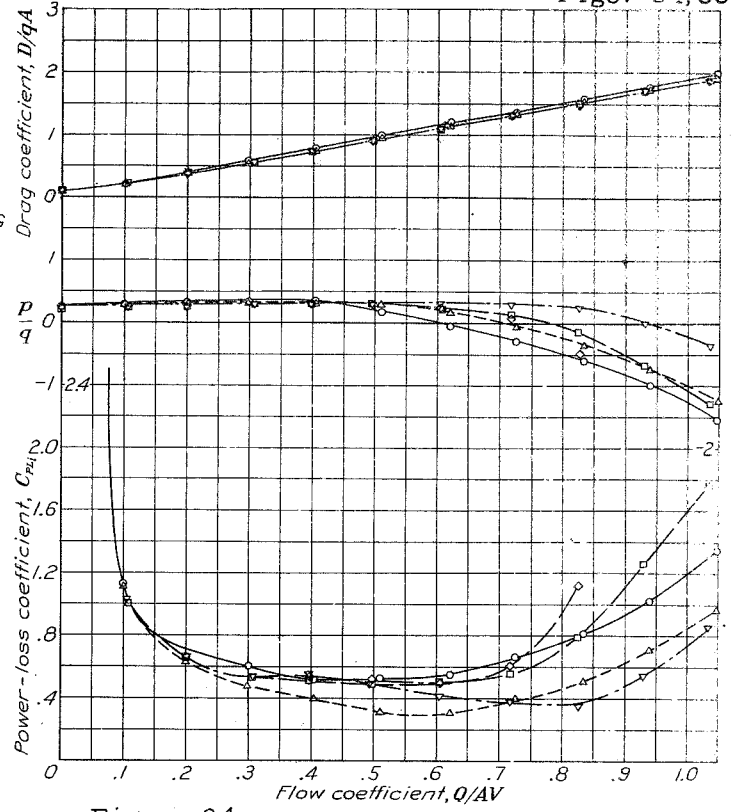
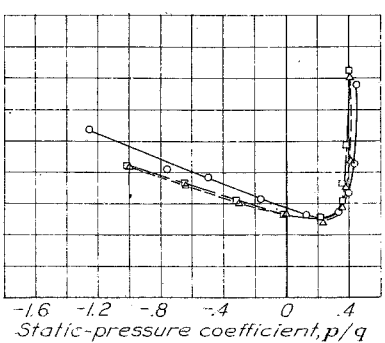
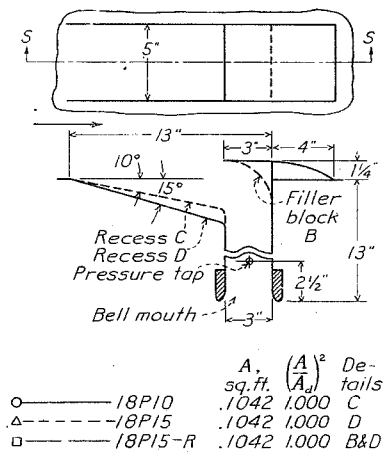


Figure 34



	A_1 sq. ft.	$(\frac{A_1}{A_2})^2$	De- tails
○	.1042	1.000	C
△	.1042	1.000	D
□	.1042	1.000	B&D

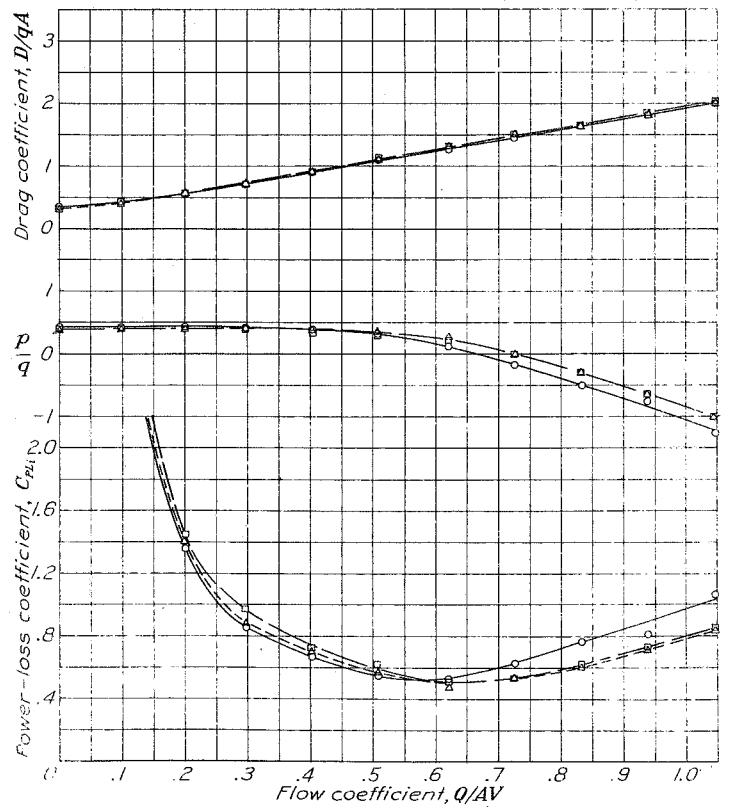


Figure 35

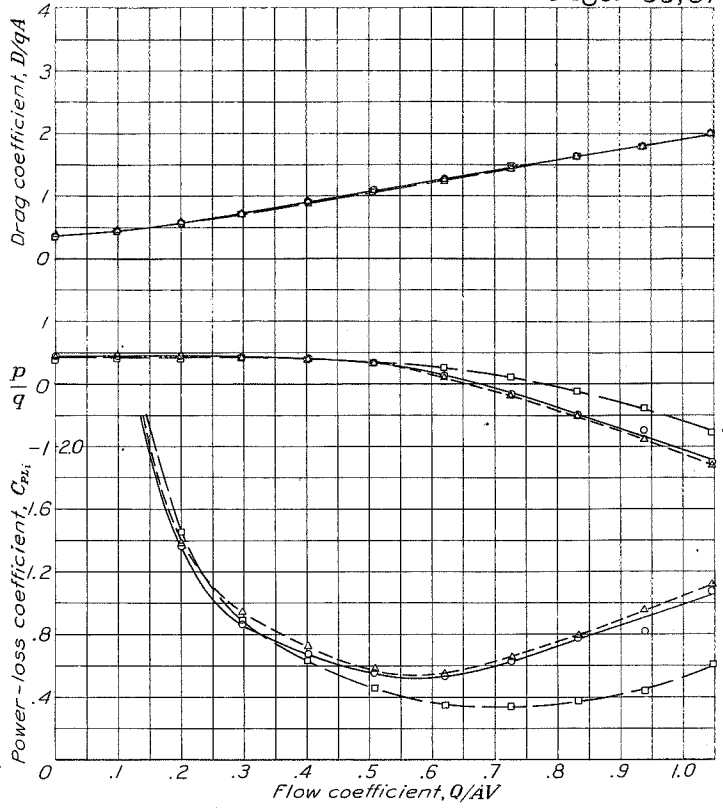
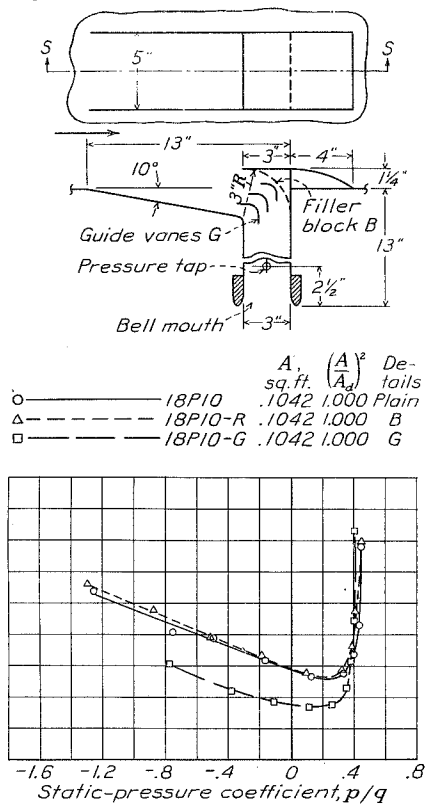


Figure 36

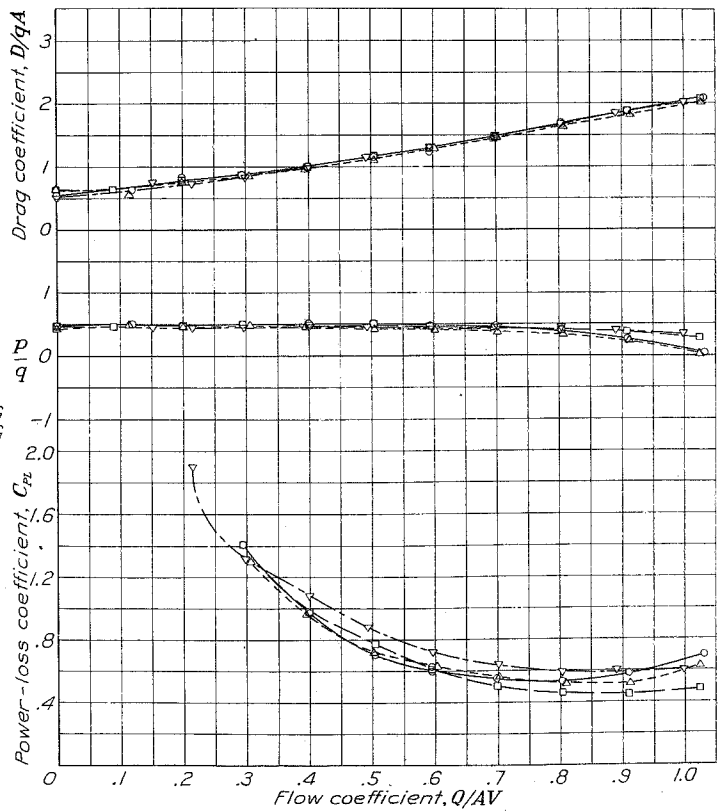
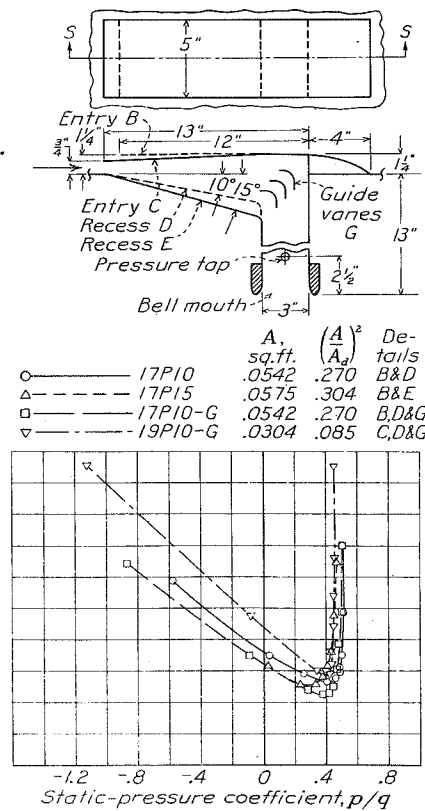
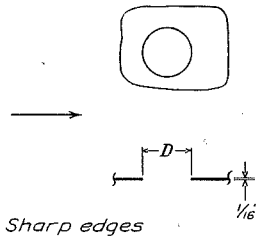
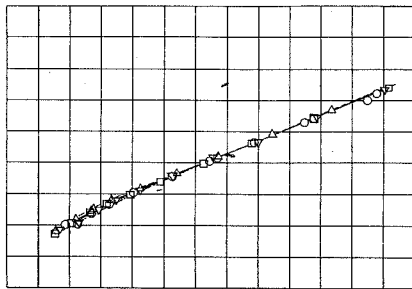


Figure 37

N.A.C.A.



	V , m.p.h.	A , sq. ft.	$\left(\frac{A}{A_0}\right)^2$	D , in.
○	35200	40	.0229	.000 2
▽	35300	40	.0511	.001 3
□	35200	80	.0229	.000 2
△	35300	80	.0511	.001 3



Static-pressure coefficient, p/q

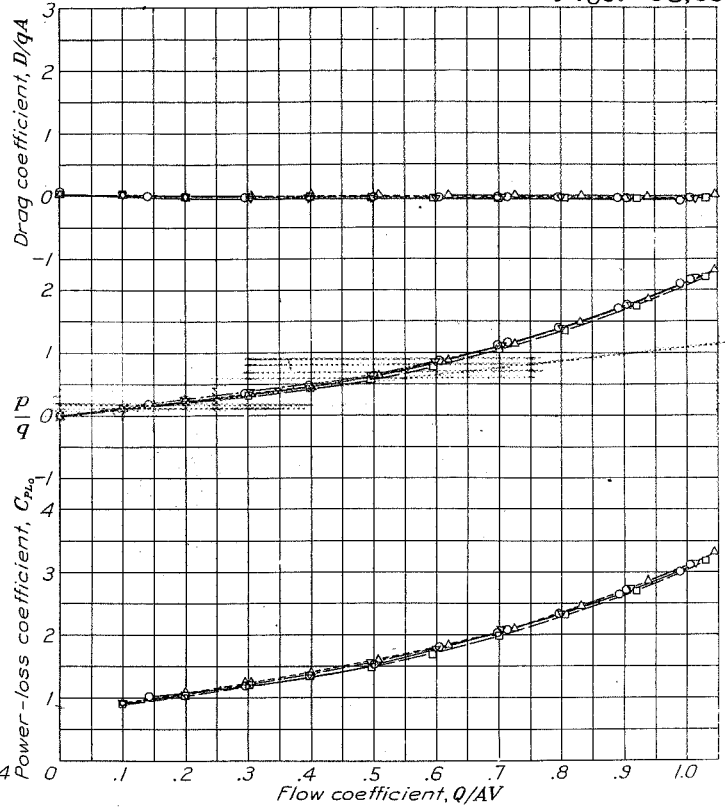
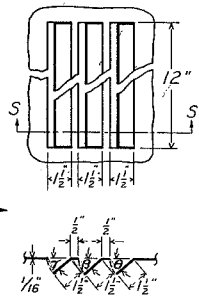
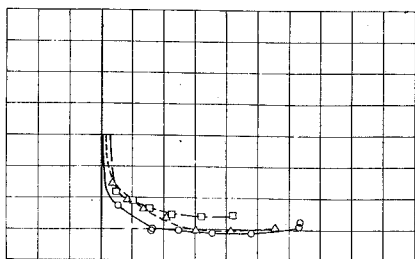


Figure 38



	A , sq. ft.	$\left(\frac{A}{A_0}\right)^2$	γ, β, θ , degrees
○	653-15	.0807	.002 -15
△	653-30	.1701	.009 -30
□	653-45	.2520	.020 -45



Static-pressure coefficient, p/q

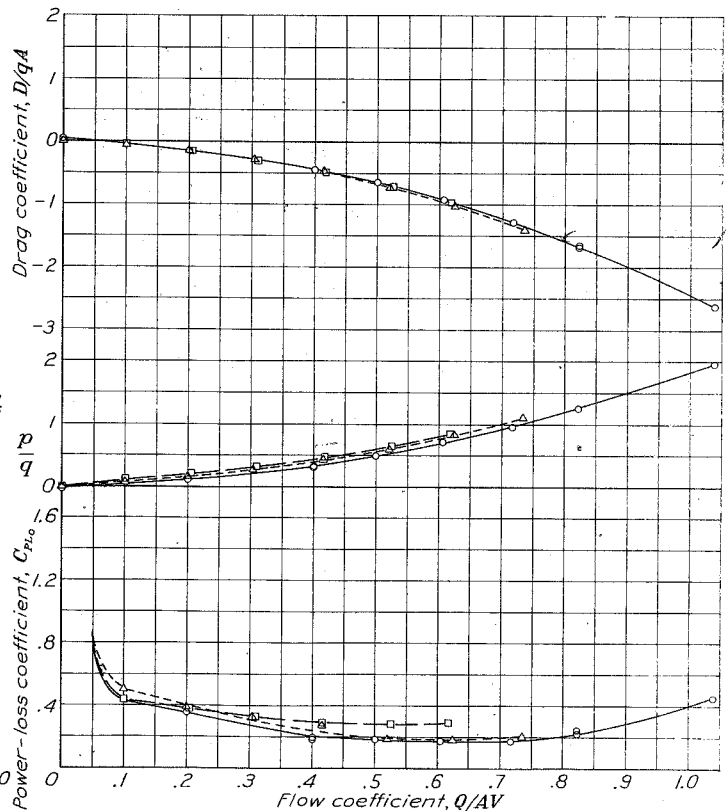
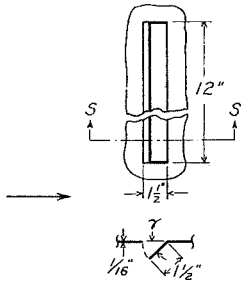


Figure 39

N.A.C.A.

Figs. 40,41



	$A, \left(\frac{A}{A_d}\right)^2$	$\gamma, \text{deg.}$
○ ———	6S1-15 .0270 .000 -15	
△ ———	6S1-30 .0567 .001 -30	
□ ———	6S1-45 .0840 .002 -45	

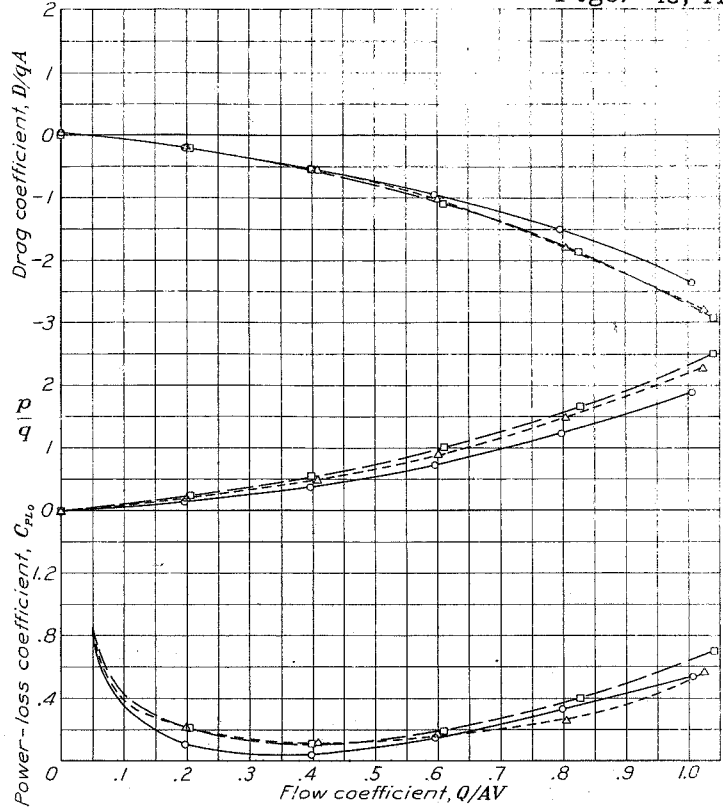
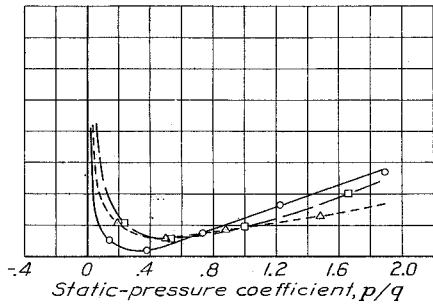
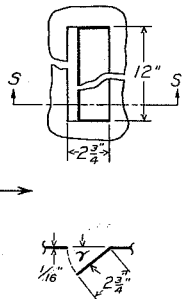


Figure 40



	$A, \left(\frac{A}{A_d}\right)^2$	$\gamma, \text{deg.}$
○ ———	7S-0-10 .0343 .000 -10	
△ ———	7S-0-20 .0726 .002 -20	
□ ———	7S-0-30 .1134 .004 -30	

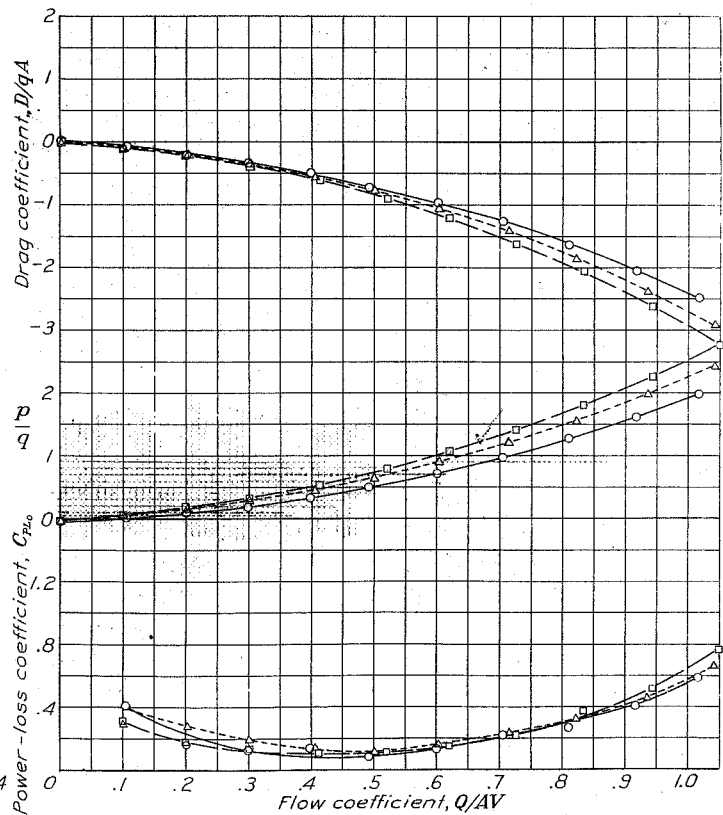
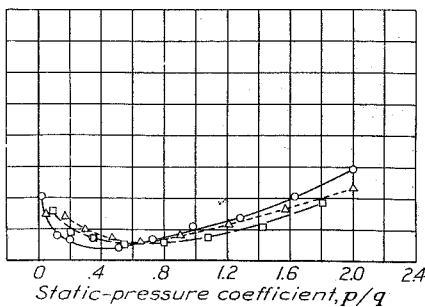
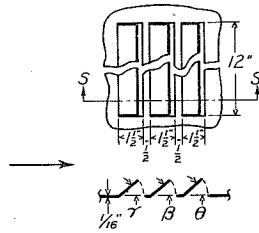


Figure 41



	V, m.p.h.	A, sq.ft.	$\left(\frac{A}{A_d}\right)^2$	τ , degrees	β , degrees	θ , degrees
○	453+15	40	.0807	.002	15	15
△	453+30	40	.1701	.009	30	30
□	453+45	40	.2520	.020	45	45
▽	453A	40	.1680	.009	15	30
◇	453B	40	.1680	.009	45	30
◇	453+30	80	.1701	.009	30	30

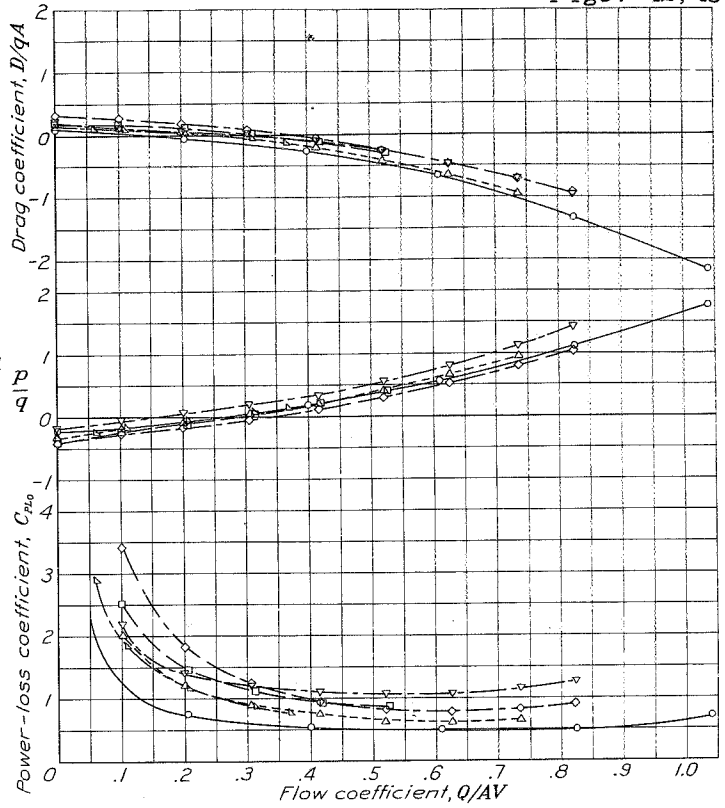
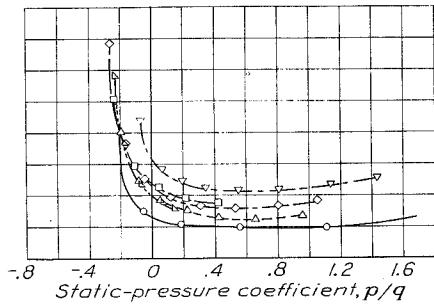
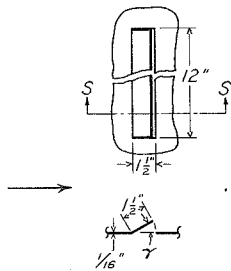


Figure 42



	V, m.p.h.	A, sq.ft.	$\left(\frac{A}{A_d}\right)^2$	τ , deg.
○	451+15	40	.0270	.000
△	451+30	40	.0567	.001
□	451+45	40	.0840	.002
▽	451+30	80	.0567	.001

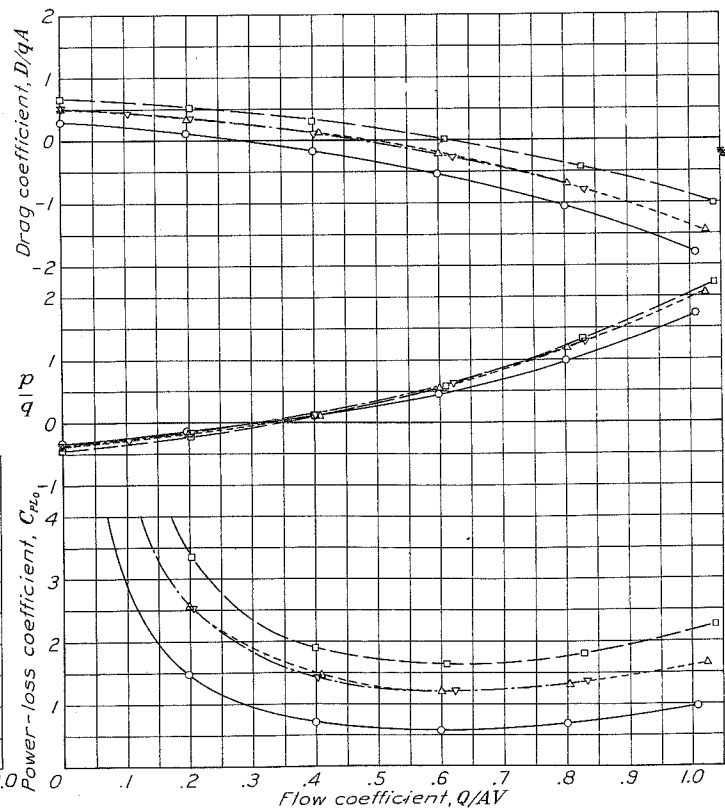
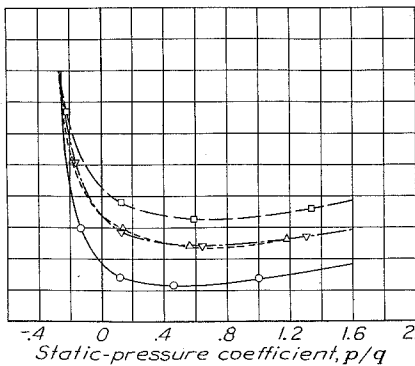
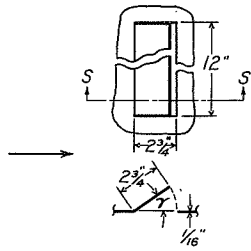


Figure 43

N.A.C.A.



	A , sq.ft.	$(\frac{A}{A_d})^2$	τ , deg.	
○	7S+10+0	.0343	.000	10
△	7S+20+0	.0726	.002	20
□	7S+30+0	.1134	.004	30

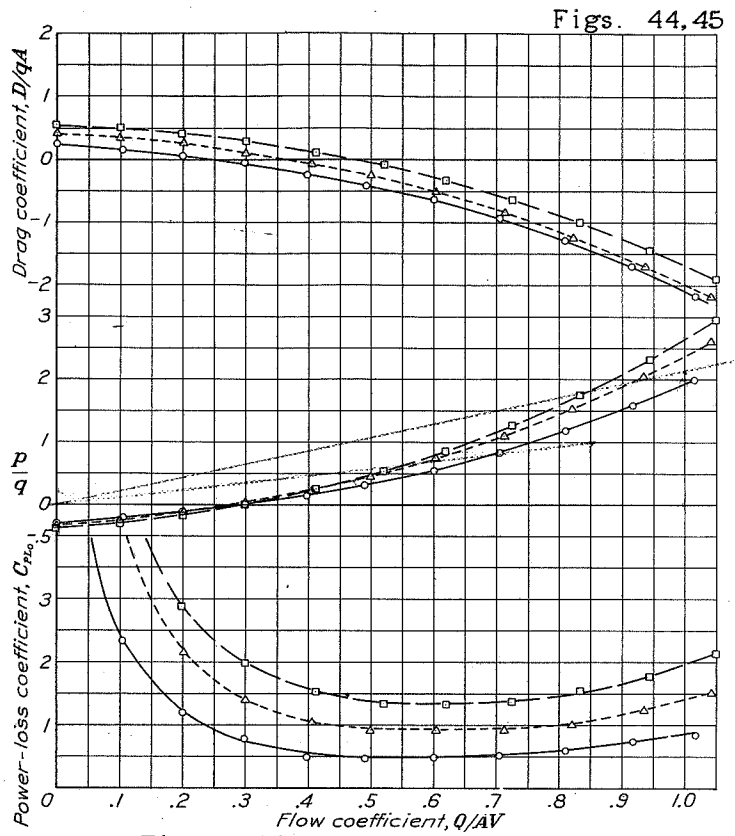
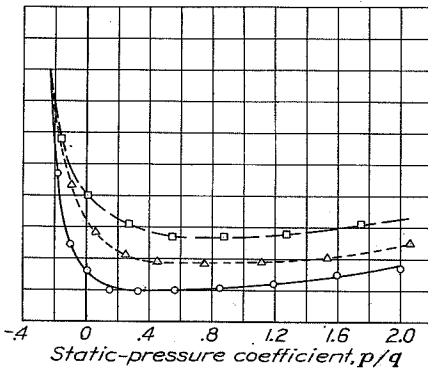
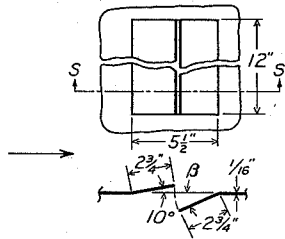


Figure 44



	A , sq.ft.	$(\frac{A}{A_d})^2$	β , deg.	
○	7S+10+0	.0343	.000	0
△	7S+10-10	.0736	.002	-10
□	7S+10-20	.1106	.004	-20
▽	7S+10-30	.1441	.007	-30

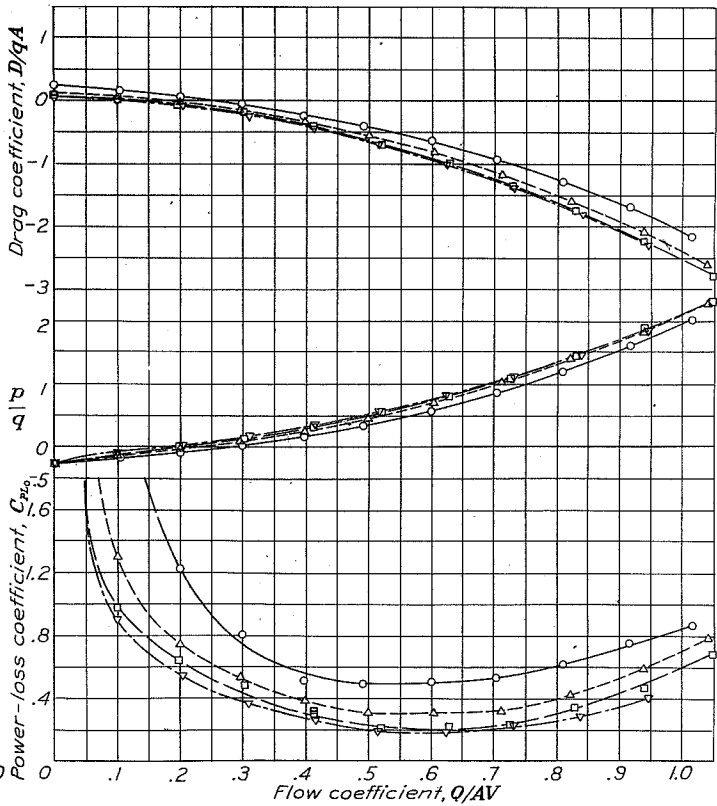
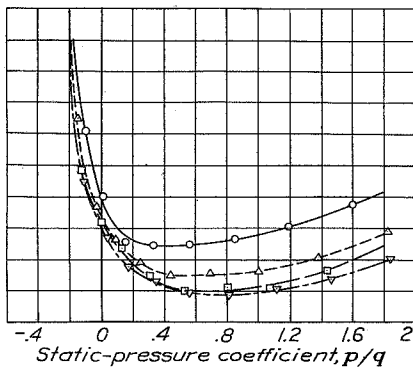
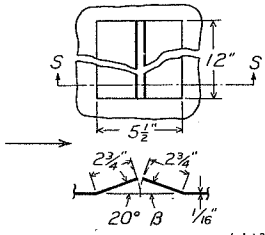


Figure 45

N.A.C.A.



	A_1	$(\frac{A_1}{A_2})^2$	β
	sq.ft.		deg.
△	7S+20+0	.0726	.002 0
○	7S+20+10	.0368	.000 10
□	7S+20+20	.0266	.000 20

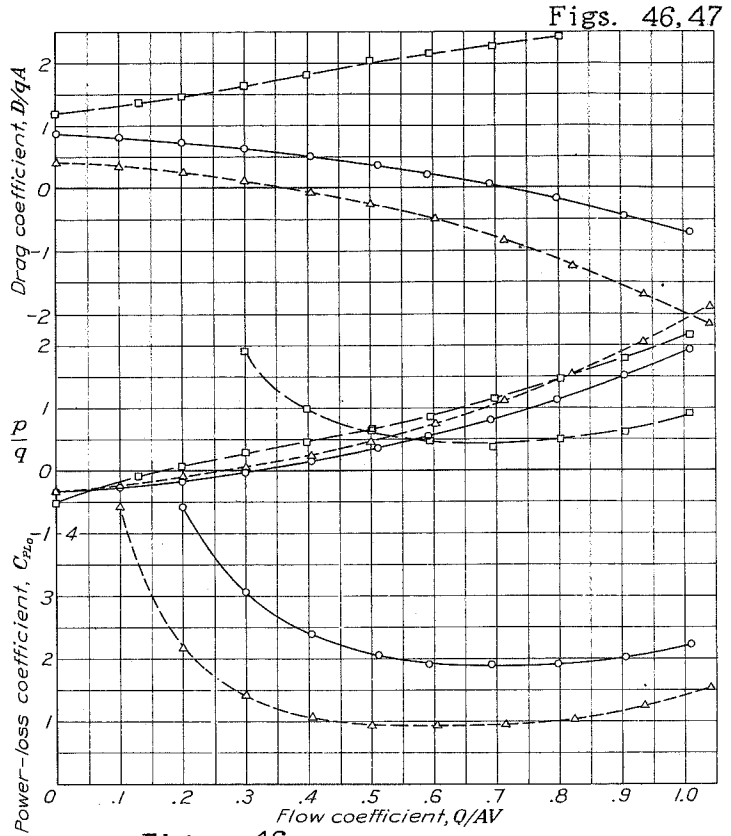
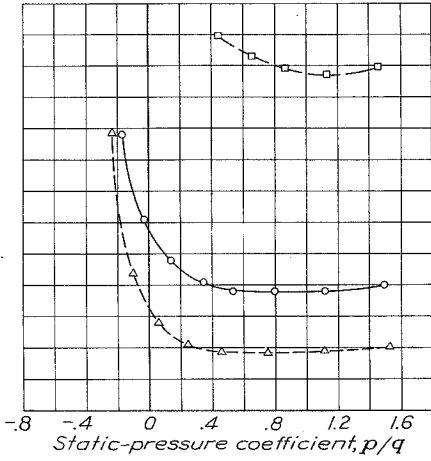
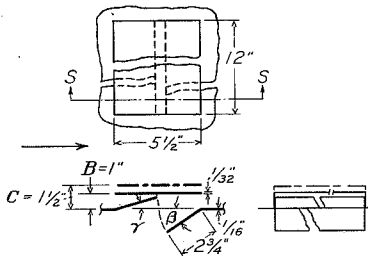


Figure 46



	A_1	$(\frac{A_1}{A_2})^2$	D_e	τ	β
	sq.ft.		tails		deg.
○	8SA-0-10	.0343	.000	B	0-10
△	8SA+10-0	.0343	.000	B	10 0
□	8SB+20+10	.0368	.000	C	20 10

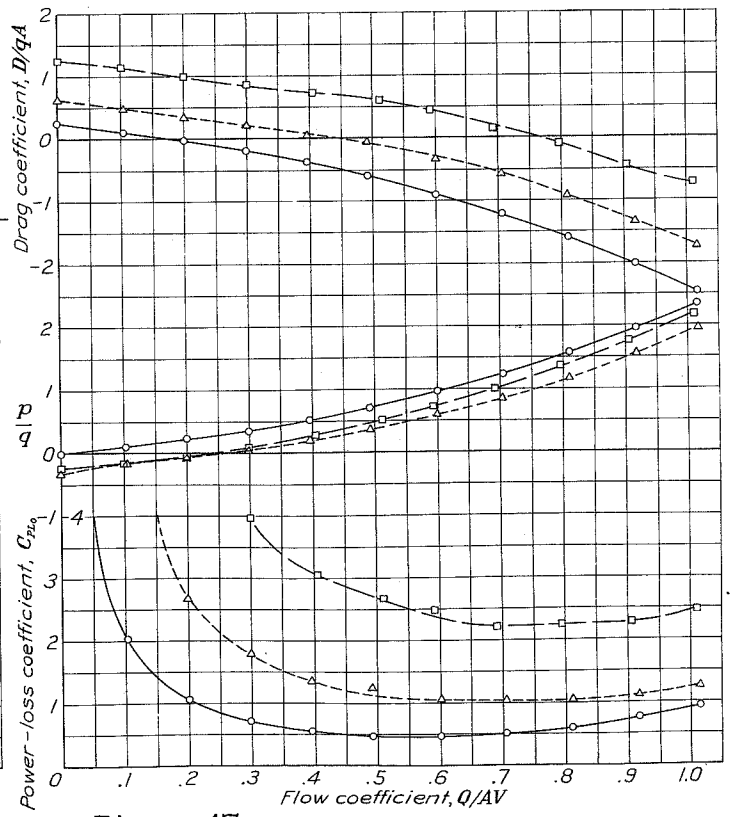
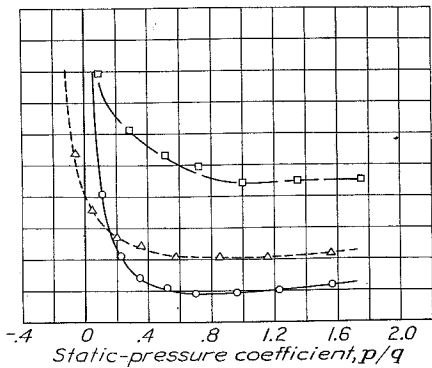
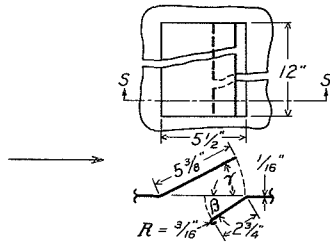


Figure 47



	$A, (A_d)^2$ sq. ft.	$\tau, \beta,$ tails deg.
○ — 10SA+10-10	.0656	.001 - 10-10
△ — 10SA+10-20	.0676	.001 - 10-20
□ — 10S +10-10	.0656	.001 R 10-10
▽ — 10S +10-20	.0676	.001 R 10-20
◇ — 10S +20-30	.1435	.007 R 20-30
⊠ — 10S +10-30	.0668	.001 R 10-30

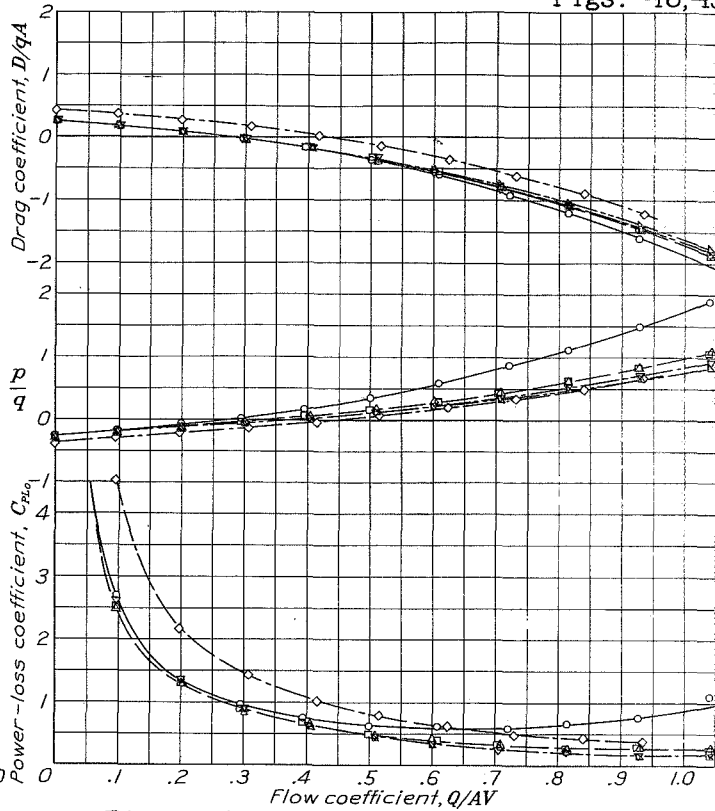
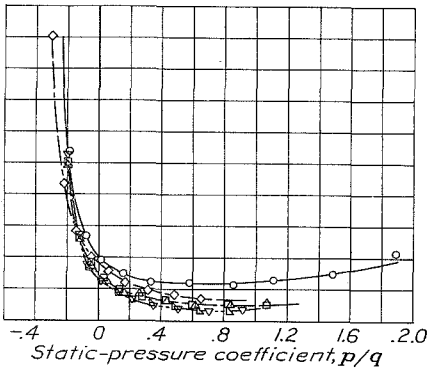
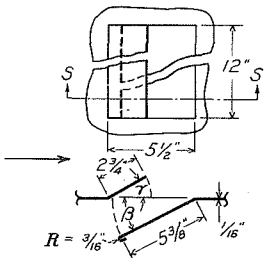


Figure 48



	$A, (A_d)^2$ sq. ft.	$\tau, \beta,$ degrees
○ — 9S+0-10	.0289	.000 0-10
△ — 9S+0-20	.0668	.001 0-20
□ — 9S+0-30	.1014	.003 0-30
▽ — 9S+10-20	.1039	.003 10-20
◇ — 9S+10-30	.1369	.006 10-30

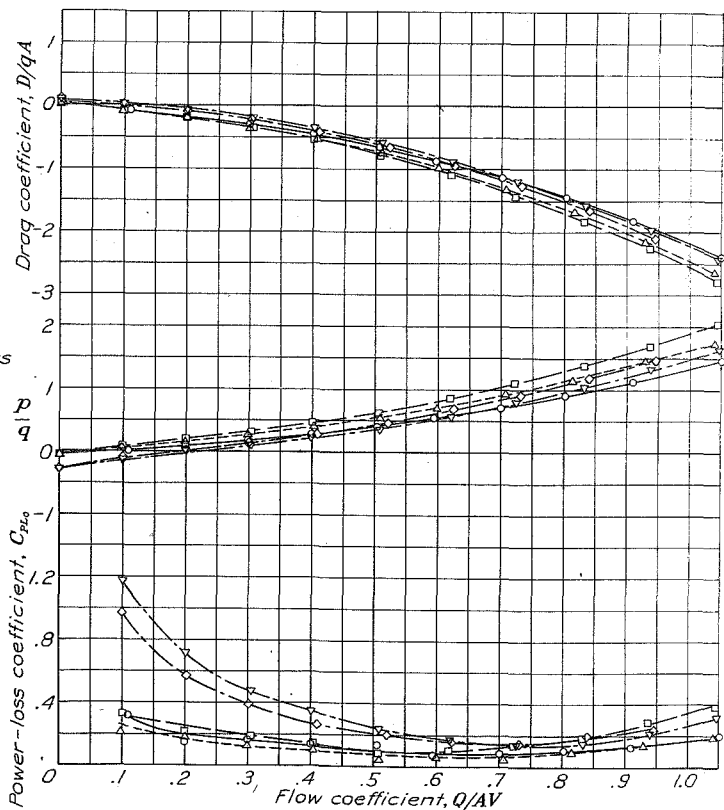
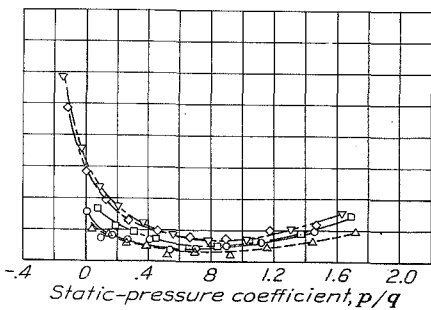
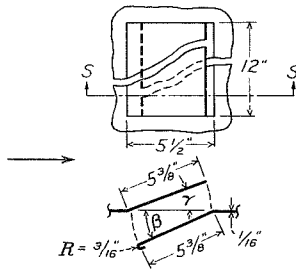


Figure 49

N.A.C.A.

Figs. 50, 51



	$A, (A_2)^2$ sq. ft.	$\gamma, \beta,$ degrees
○ ——— 11S+10-10	.0610	.001 10-10
△ ——— 11S+10-20	.0652	.001 10-20
□ ——— 11S+10-30	.0643	.001 10-30
▽ ——— 11S+20-30	.1369	.006 20-30

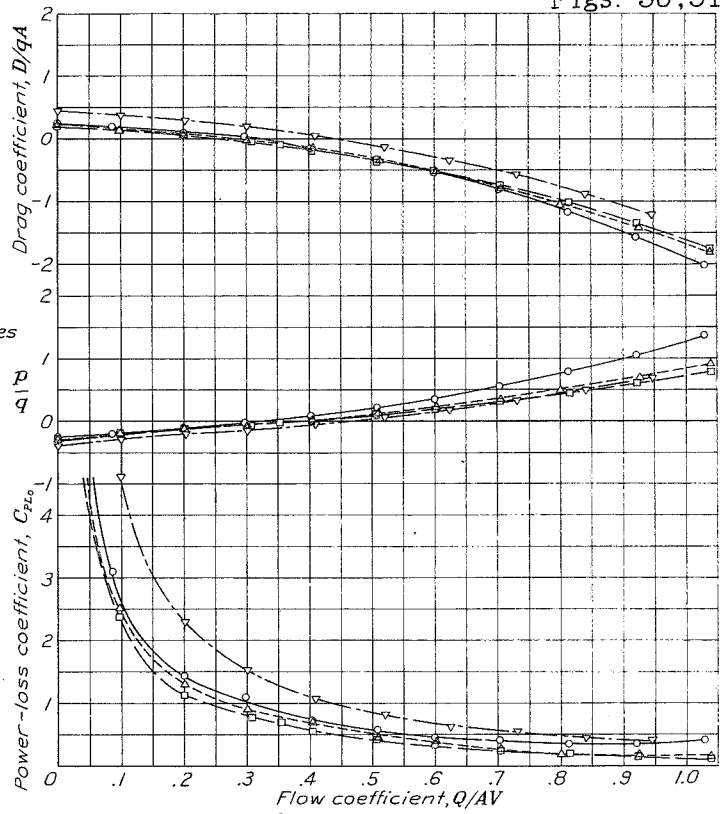
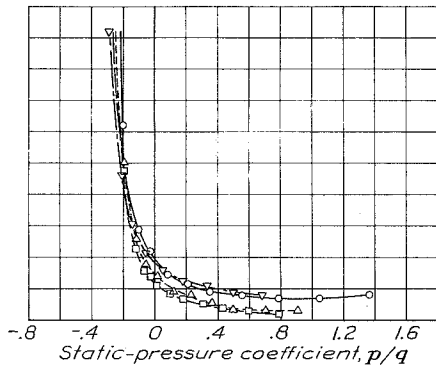
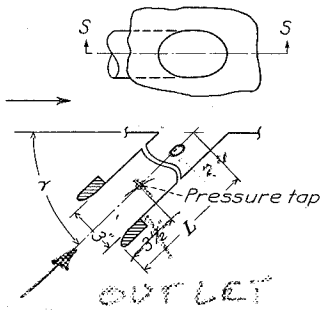


Figure 50



	$V, A, (A_2)^2$ m.p.h. sq. ft.	$L, \gamma,$ in. deg.
○ ——— 3S30-90	40 .0441 1.000	$16\frac{1}{2}$ 90
△ ——— 3S30-60	40 .0441 1.000	$13\frac{1}{2}$ 60
□ ——— 3S30-45	40 .0441 1.000	13 45
▽ ——— 3S30-90	80 .0441 1.000	$16\frac{1}{2}$ 90

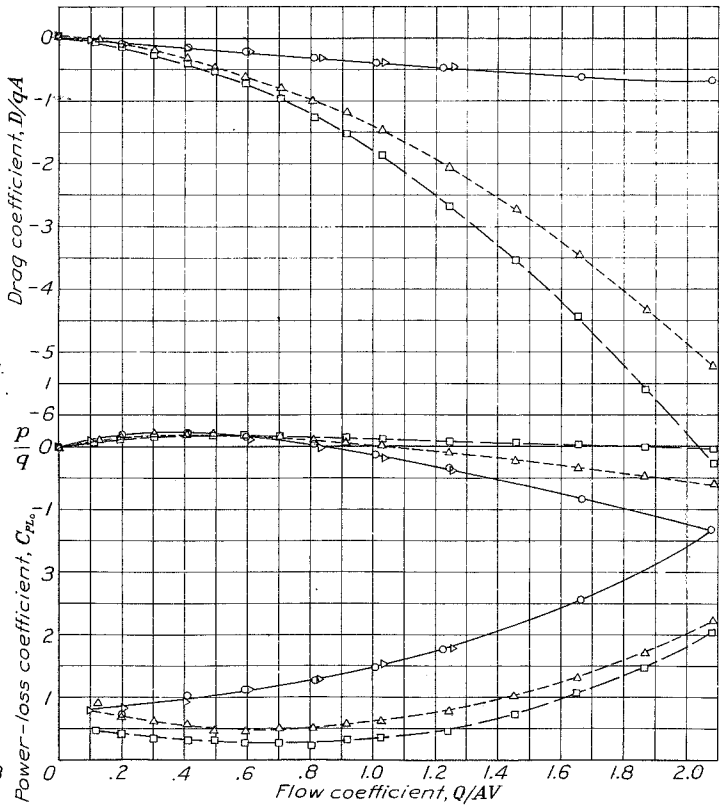
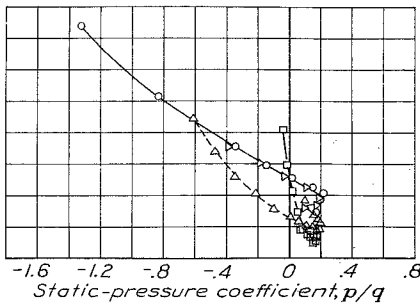
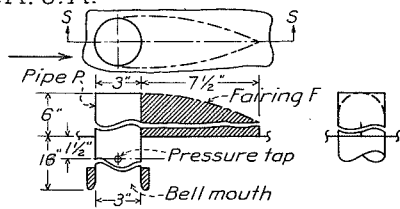


Figure 51

N.A.C.A.



	V	A	$(\frac{A}{A_0})^2$	De-
	m.p.h.	sq.ft.		tails
○	40	.0441	1.000	P
△	40	.0441	1.000	P&F
▽	80	.0441	1.000	P
◊	80	.0441	1.000	P&F

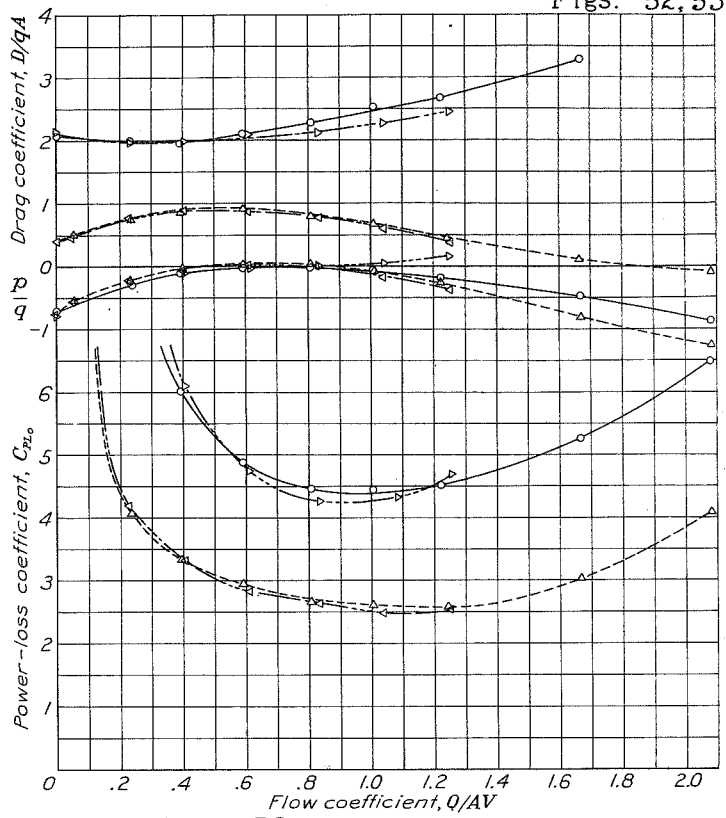
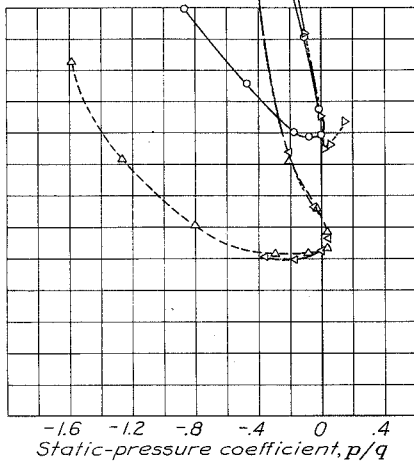
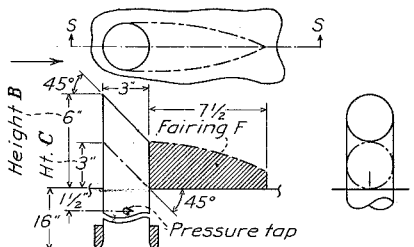


Figure 52



	V	A	$(\frac{A}{A_0})^2$	De-
	m.p.h.	sq.ft.		tails
○	40	.0441	1.000	B
△	40	.0441	1.000	B&F
◻	40	.0441	1.000	C
▽	80	.0441	1.000	B
◊	80	.0441	1.000	C

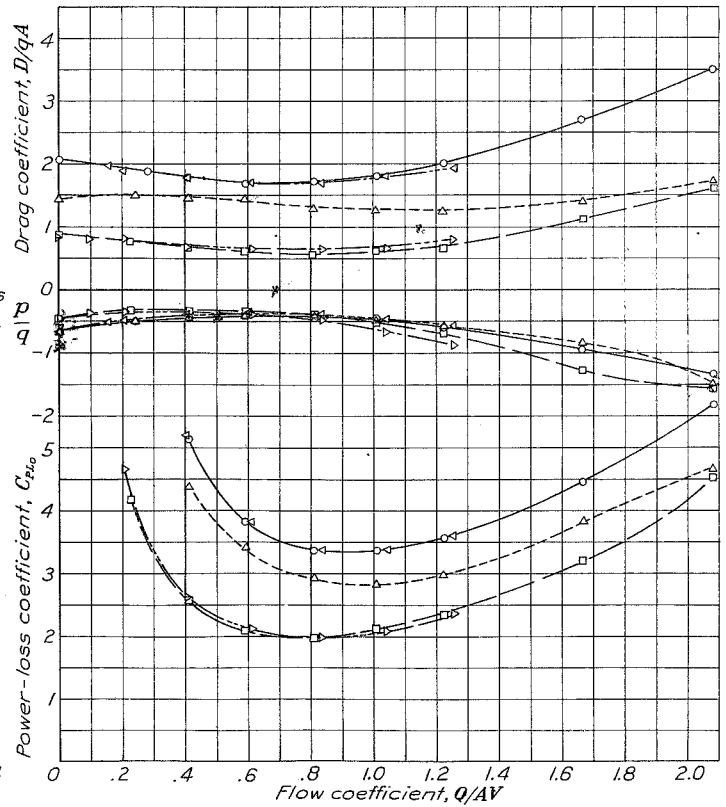
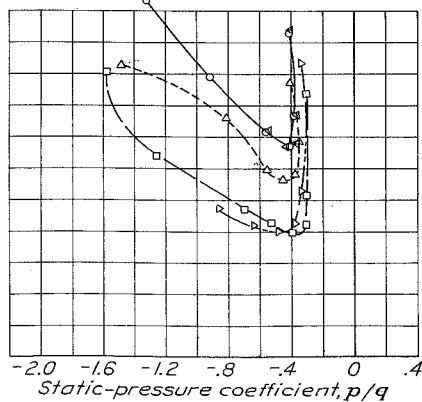
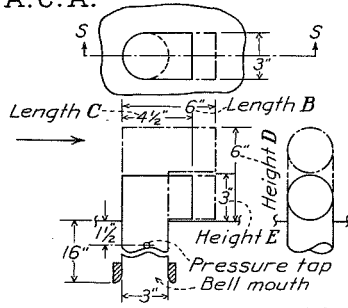
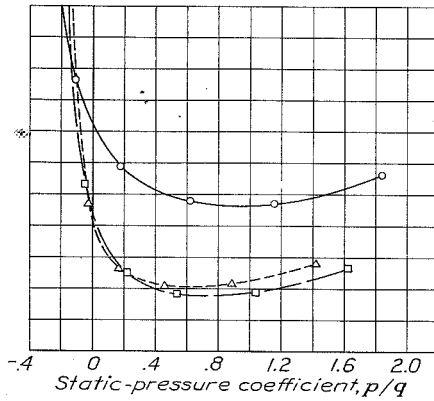


Figure 53

N.A.C.A.



	A.	($\frac{A}{A_0}$) ²	De-
○	2S366	.0441	1.000 B&D
△	2S336	.0441	1.000 B&E
□	2S3345	.0441	1.000 C&E



Figs. 54,55

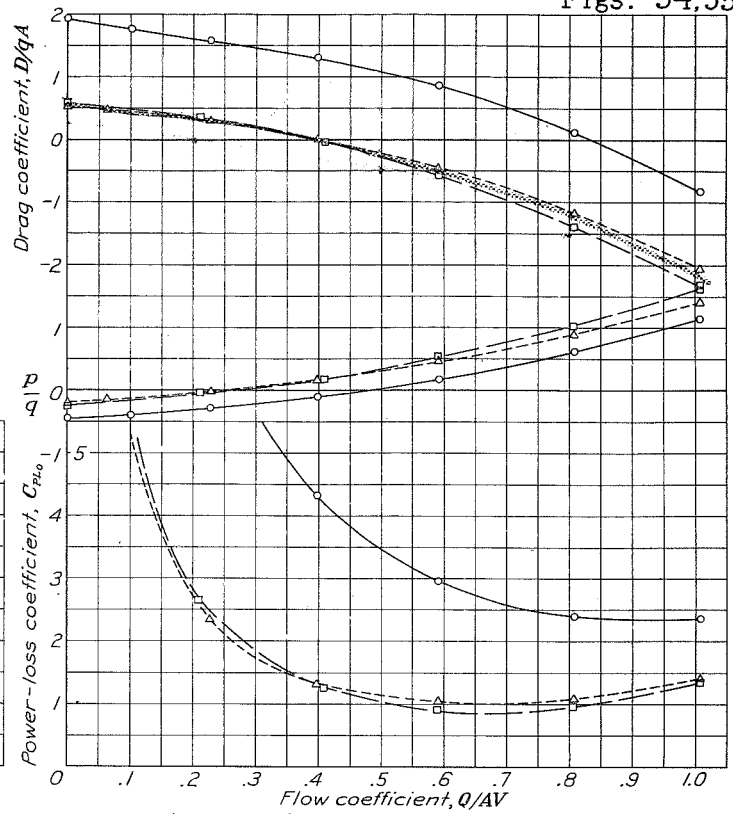
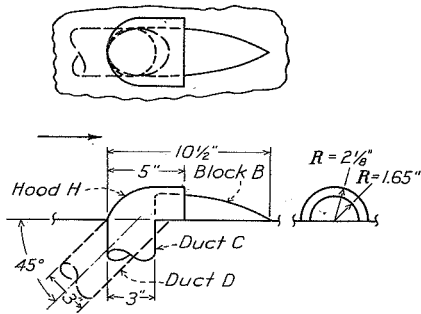


Figure 54



	A.	($\frac{A}{A_0}$) ²	De-
○	3S30-90	.0441	1.000 C
△	5S3-15-0P	.0441	1.000 C&H
□	3S30-45	.0441	1.000 D
▽	14S45-5	.0441	1.000 D&H
◇	12S5A	.0196	0.197 B,C&H

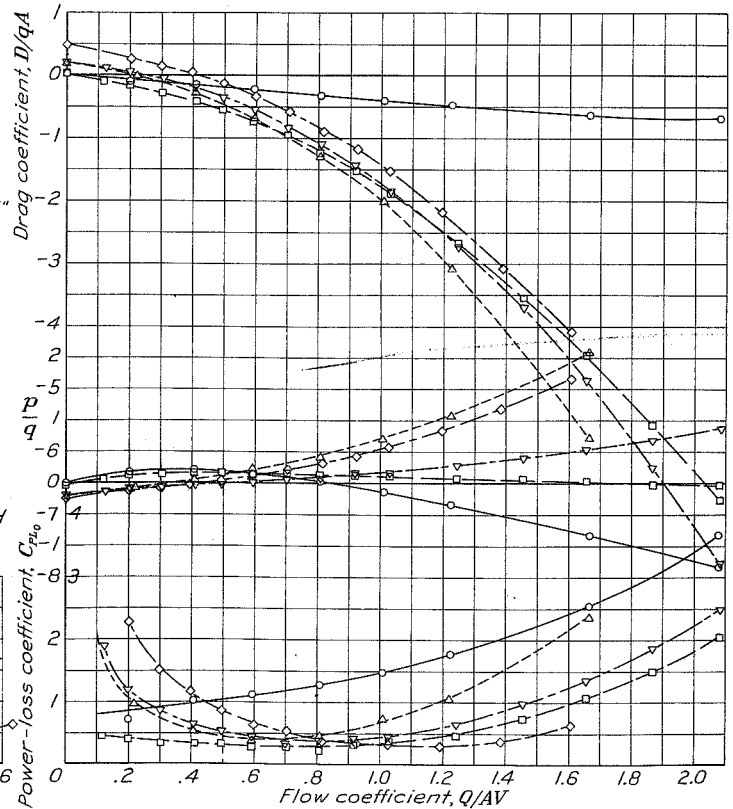
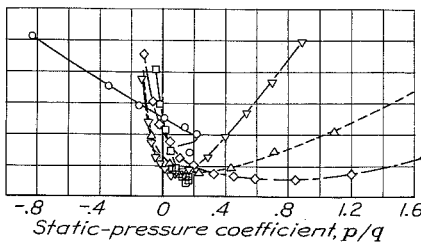
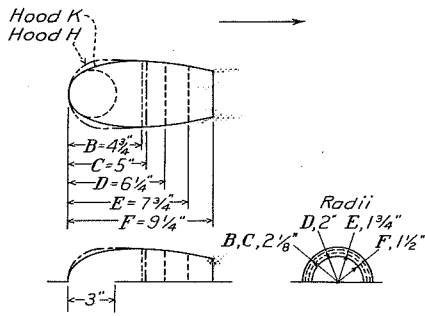


Figure 55

N.A.C.A.

Figs. 56,57



	V, m.p.h.	A, sq.ft.	(A/A ₀) ²	De- tails
○	5S3-1500	40	.0490	.001 H, C
△	13S-475	40	.0514	.001 K, B
□	13S-625	40	.0460	.001 K, D
▽	13S-775	40	.0365	.000 K, E
◇	13S-925	40	.0257	.000 K, F
△	5S3-1500	80	.0490	.001 H, C

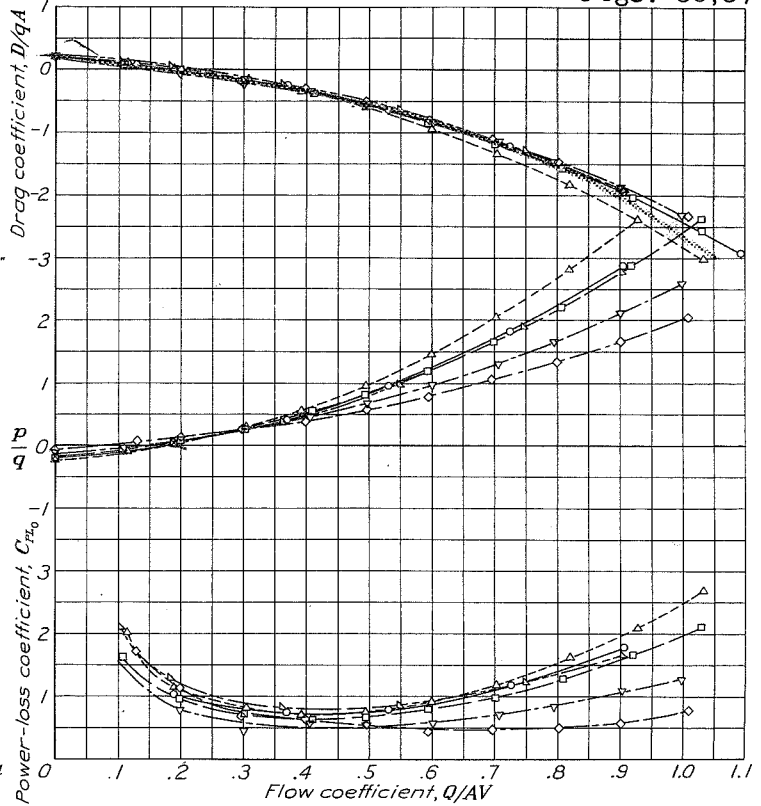
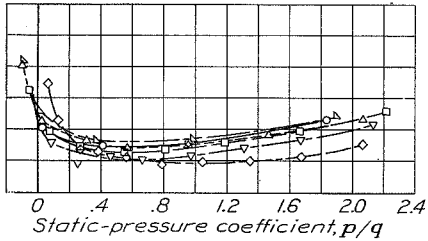
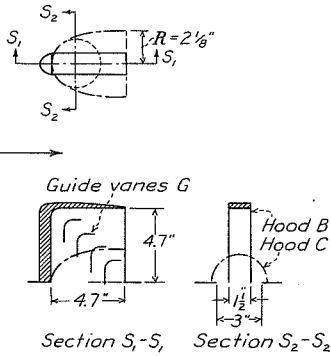


Figure 56



	A, sq.ft.	(A/A ₀) ²	De- tails
△	13S475	.0514	.001 C
○	15S	.0490	.001 B
□	15S-G	.0490	.001 B&G

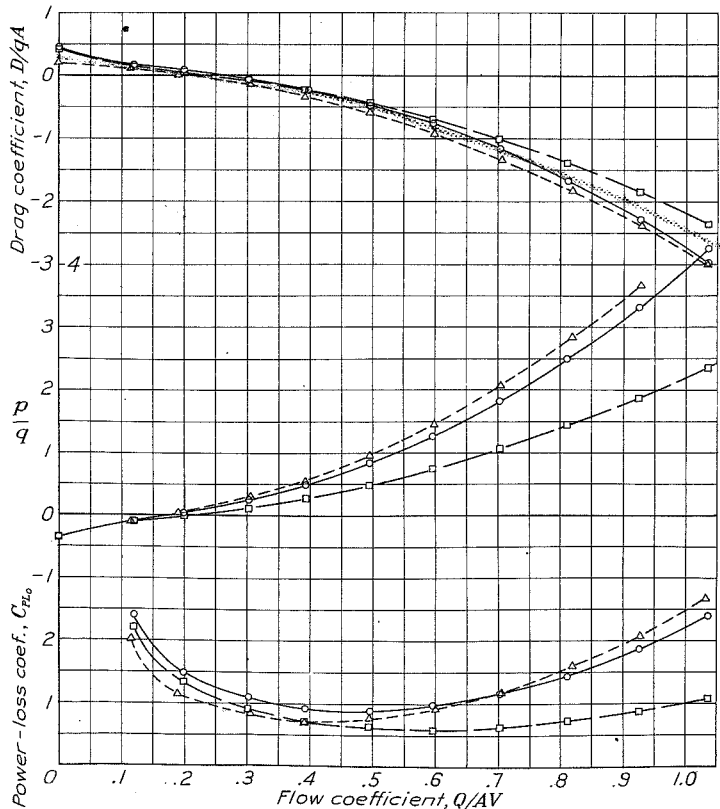
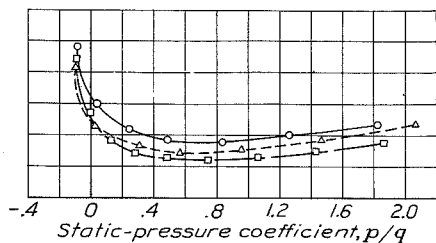
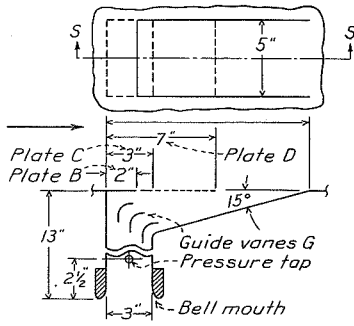


Figure 57



	A_1	$(\frac{A_1}{A_2})^2$	De-tails
○	16S15-3	.1042	1.000 B
□	16S15-3G	.1042	1.000 B&G
△	16S15-4G	.0590	.321 D&G
▽	16S15-5G	.0912	.764 C&G

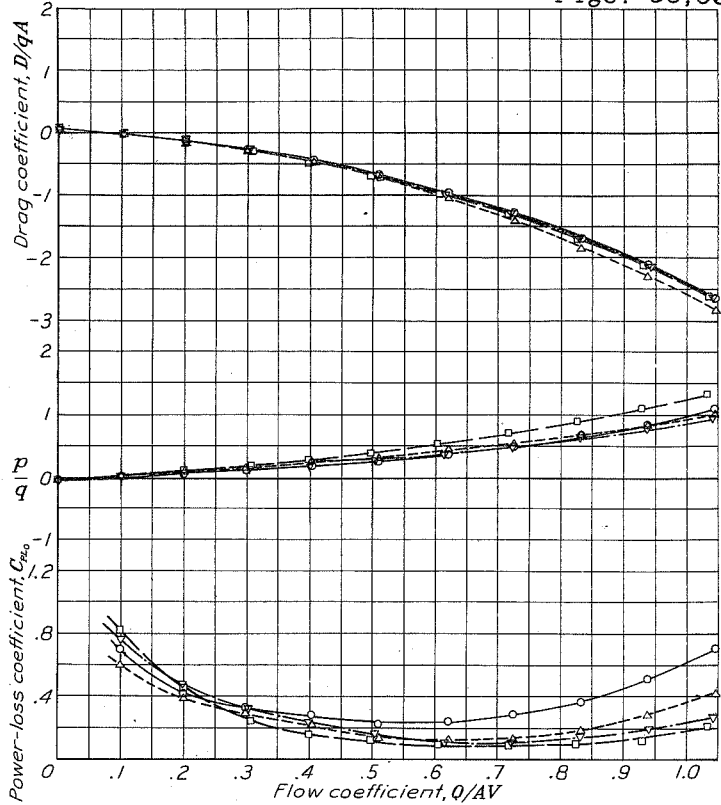
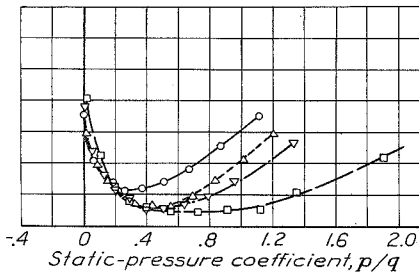
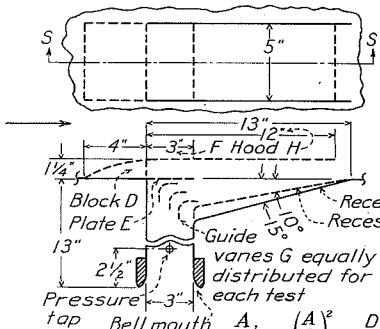


Figure 58



	A_1	$(\frac{A_1}{A_2})^2$	De-tails
○	18S10	.1042	1.000 B,D&F
□	18S10-G	.1042	1.000 B,D,F&G
△	17S10-G	.0542	.270 B,D,H&G
▽	16S15-5G	.0912	.764 C,E&G

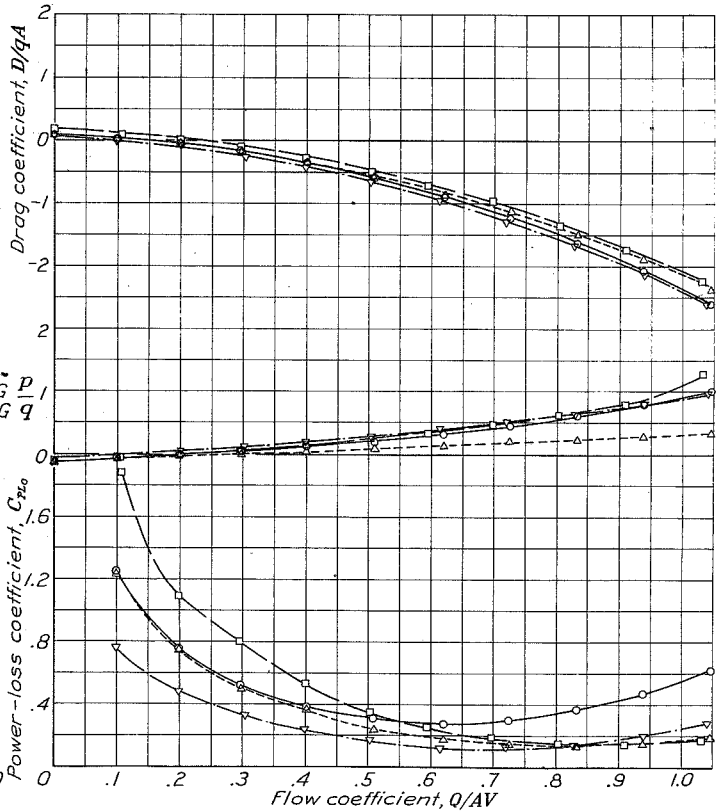
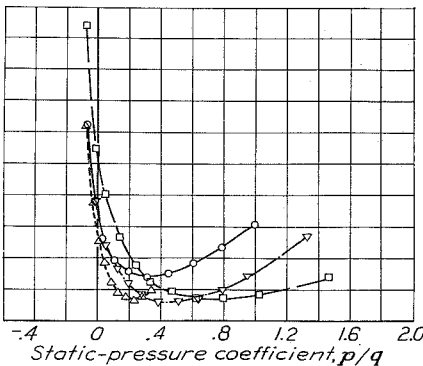


Figure 59

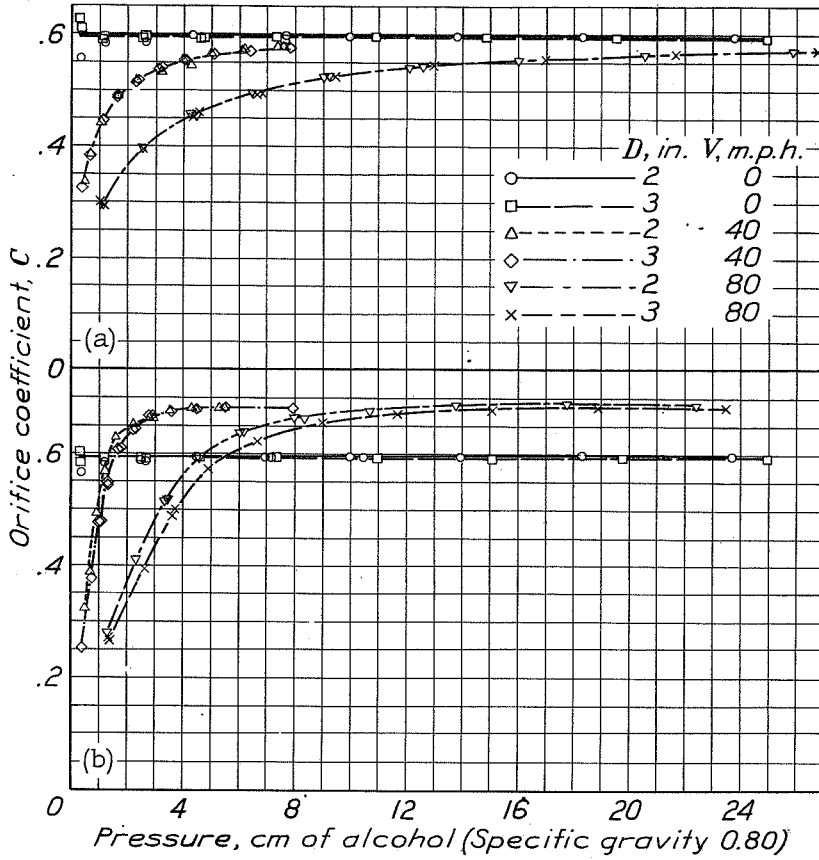


Figure 60

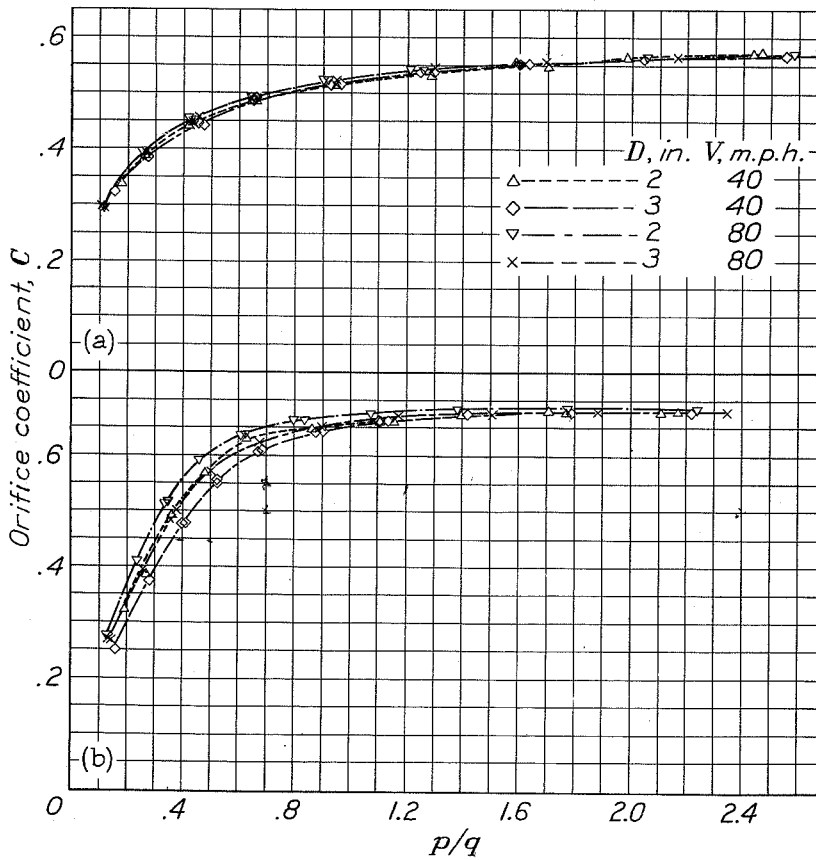


Figure 61

N.A.C.A.

Figs. 62,63

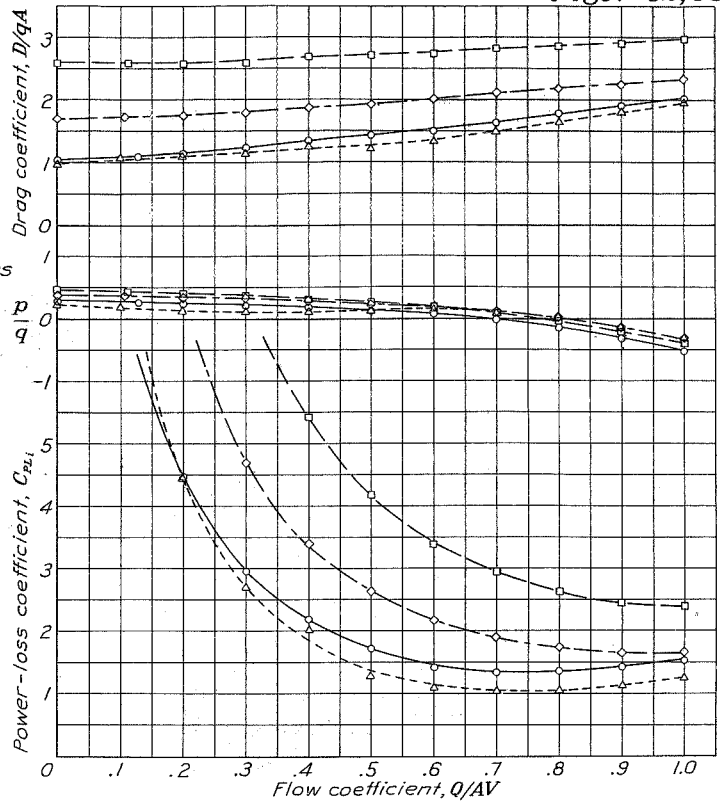
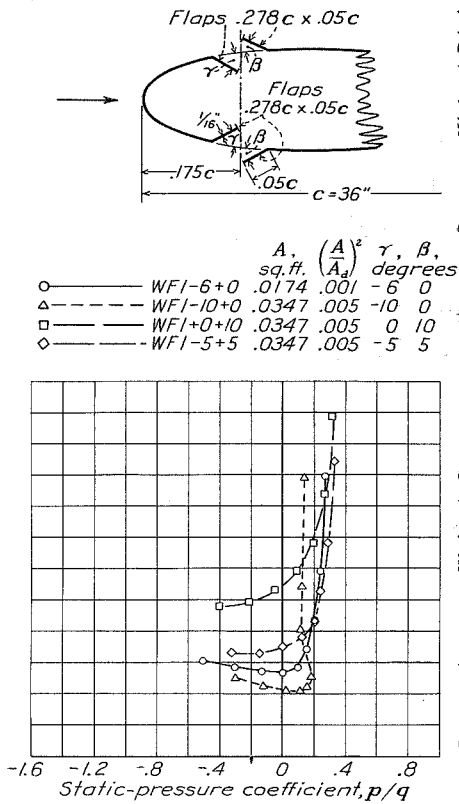


Figure 62

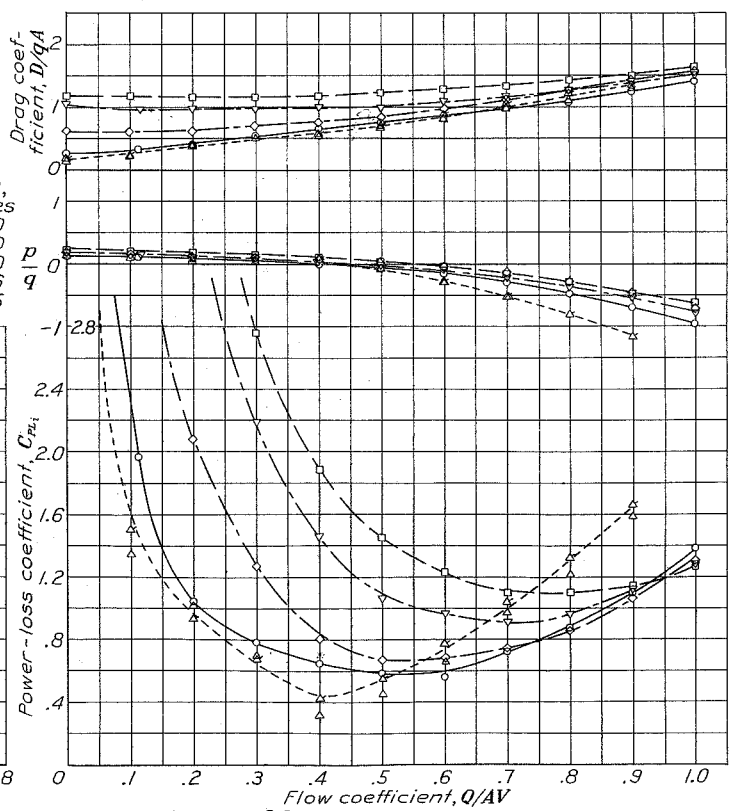
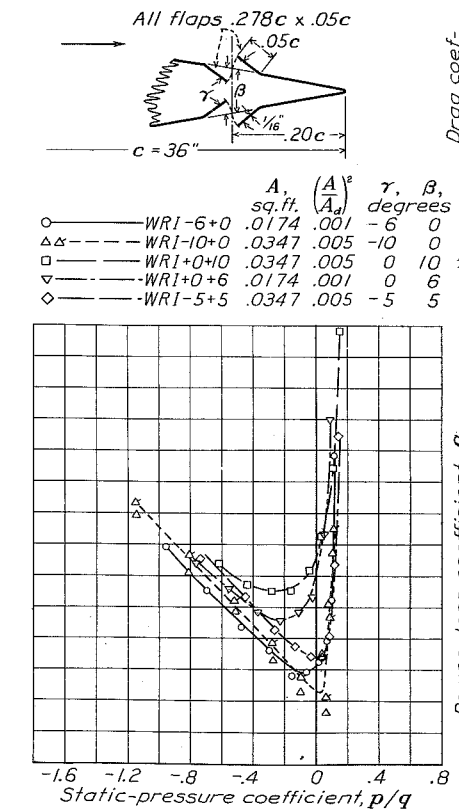
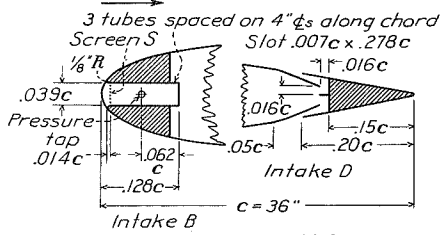


Figure 63



	A, sq.ft.	$(\frac{A}{A_d})^2$	Type	De-	
○	WNI	.0322	.004	B	-
△	WNI S	.0322	.004	B	-
□	WRI B	.0347	.005	D	-
▽	WRI A	See WREA, Figure 66			

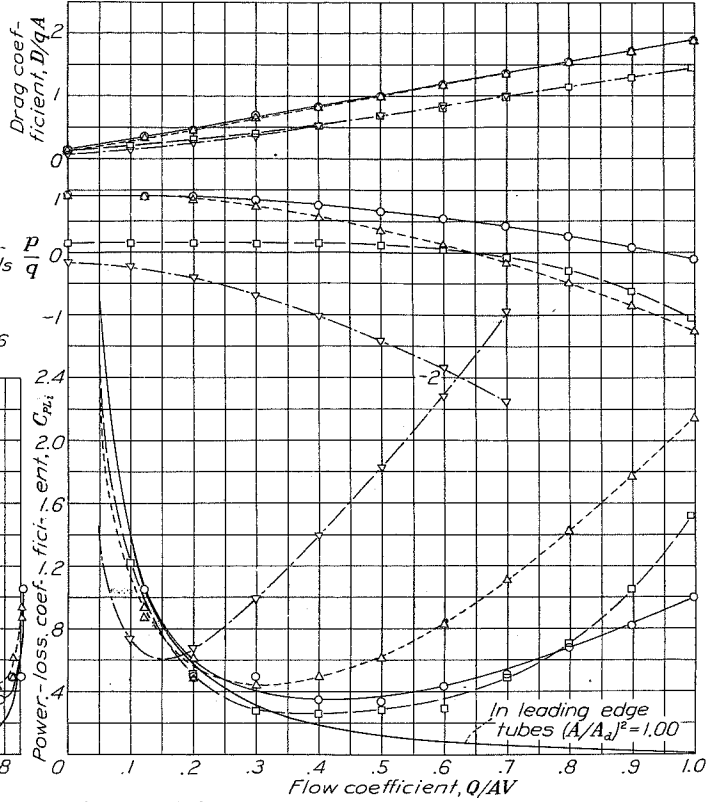
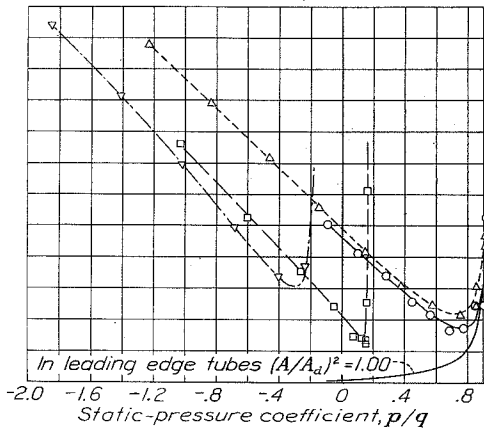
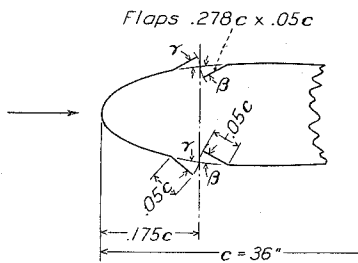


Figure 64



	A, sq.ft.	$(\frac{A}{A_d})^2$	τ degrees	β degrees
○	WFE+0-6	.0174	.001	0 -6
△	WFE+0-10	.0347	.005	0 -10
◇	WFE+5-5	.0347	.005	5 -5

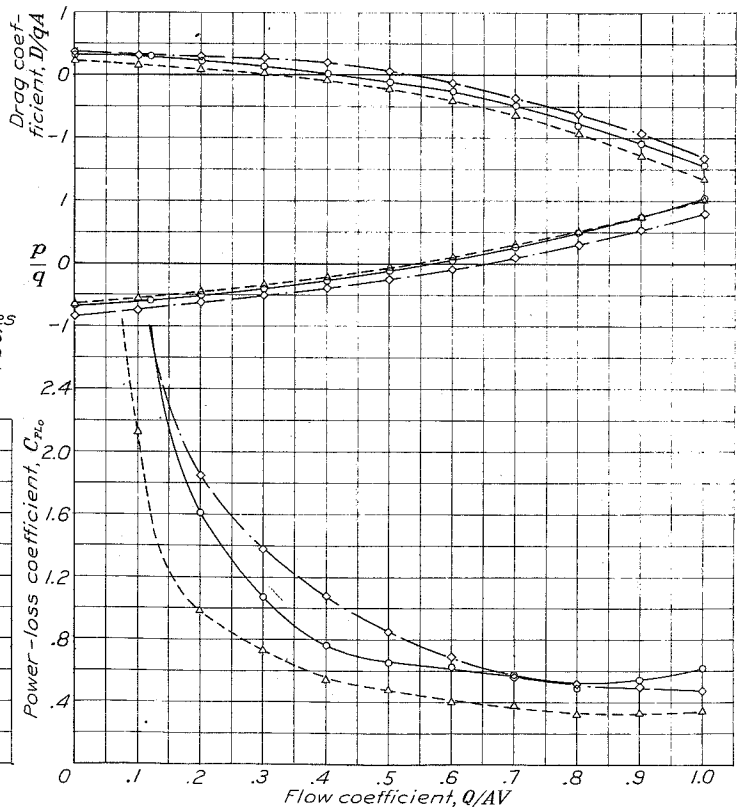
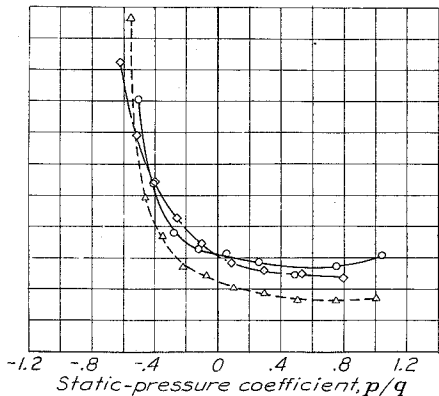
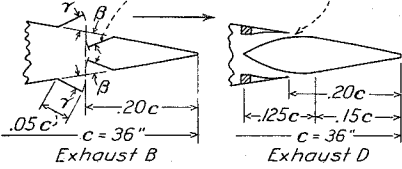


Figure 65

N.A.C.A.

All flaps .05c x .278c Slot .007c x .278c



	A, (A _d) ² sq.ft.	γ, β, Type degrees
○—WRE+0-6	.0174 .001	B 0 -6
△—WRE+0-10	.0347 .005	B 0 -10
◇—WRE+5-5	.0347 .005	B 5 -5
—WREA	.0347 .005	D - -

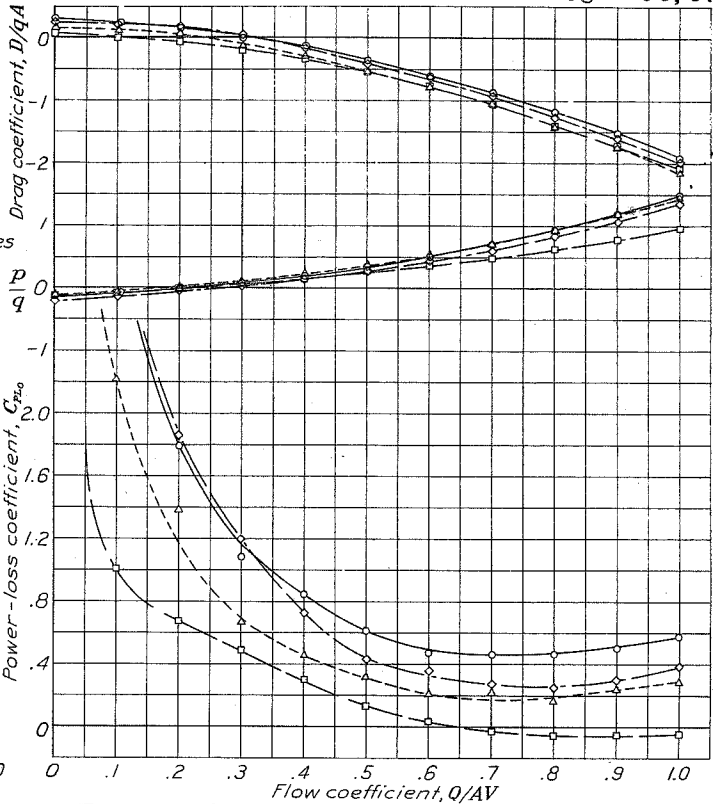
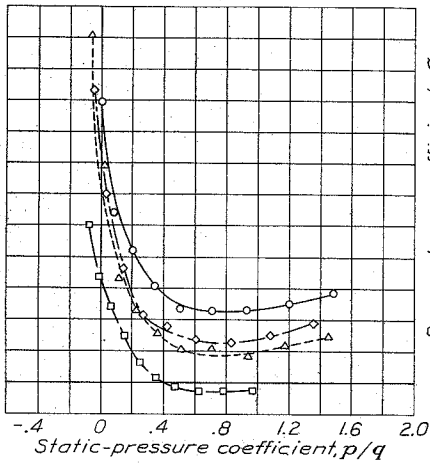


Figure 66

	Figures
— WNI	64
- - - WF1-10+0	62
— WR1-10+0	63
— 7P-10+0	14
- - - Theory, V _i /V = 1.0	69

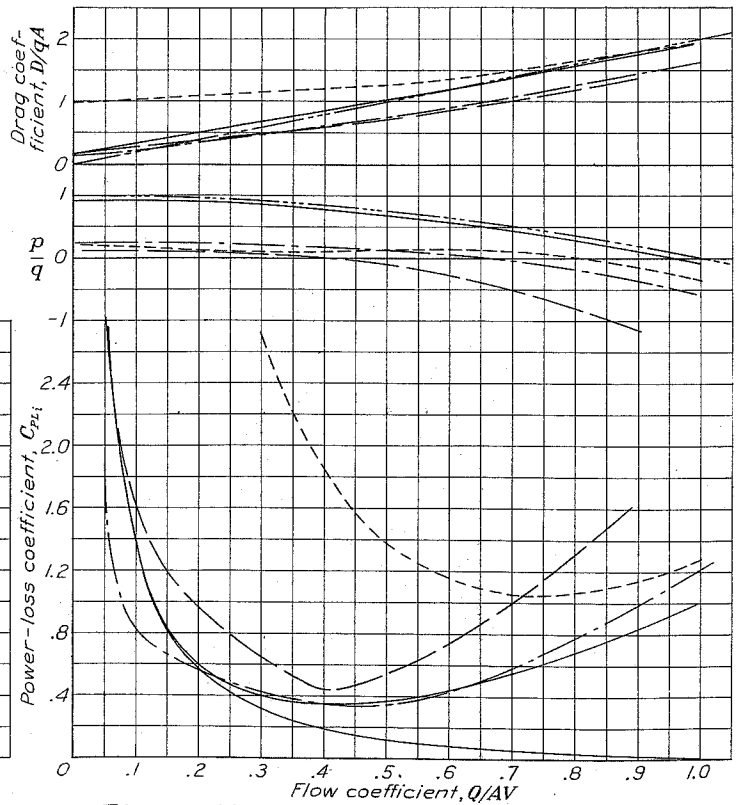
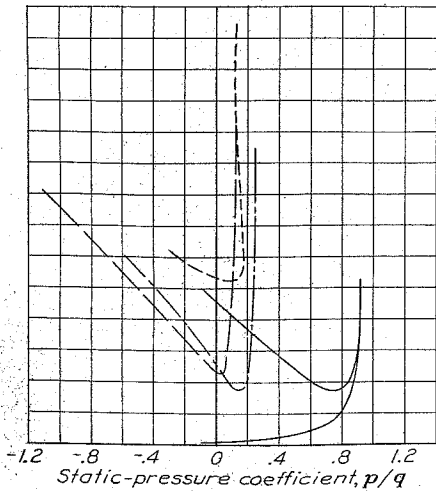


Figure 67

Figs. 66, 67

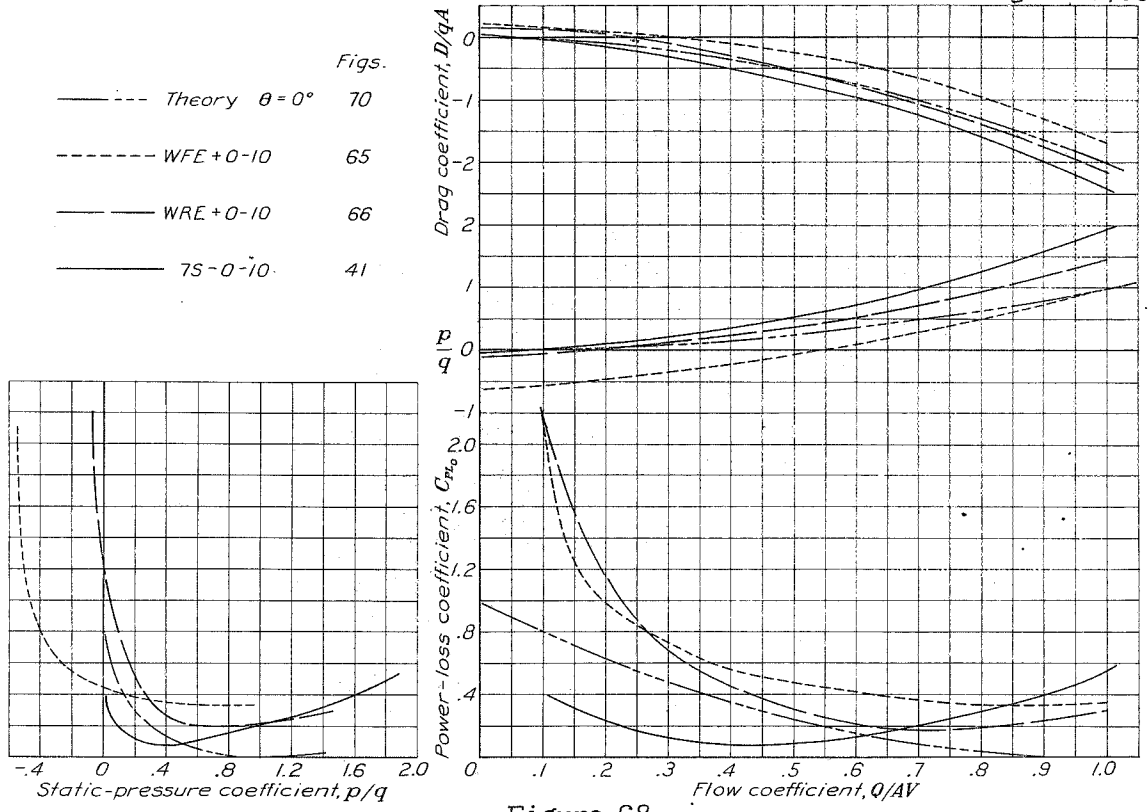


Figure 68

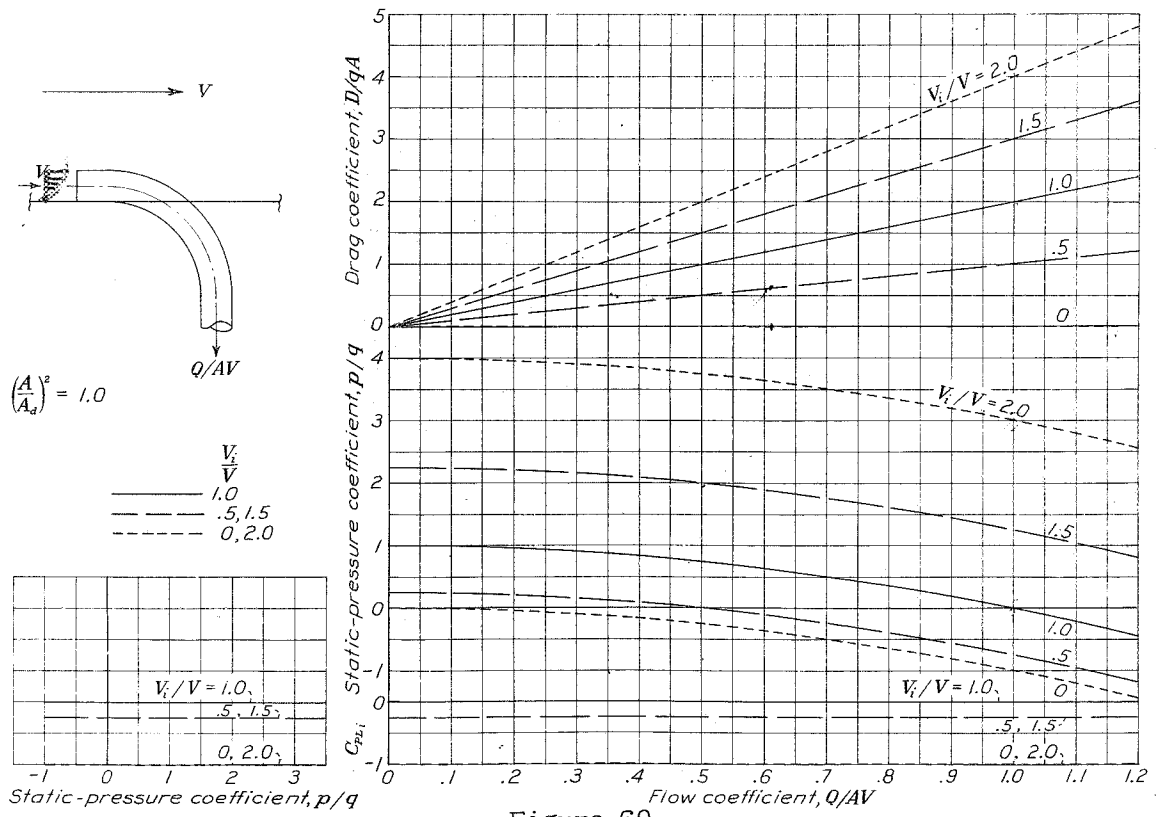


Figure 69

N.A.C.A.

Figs. 70,71

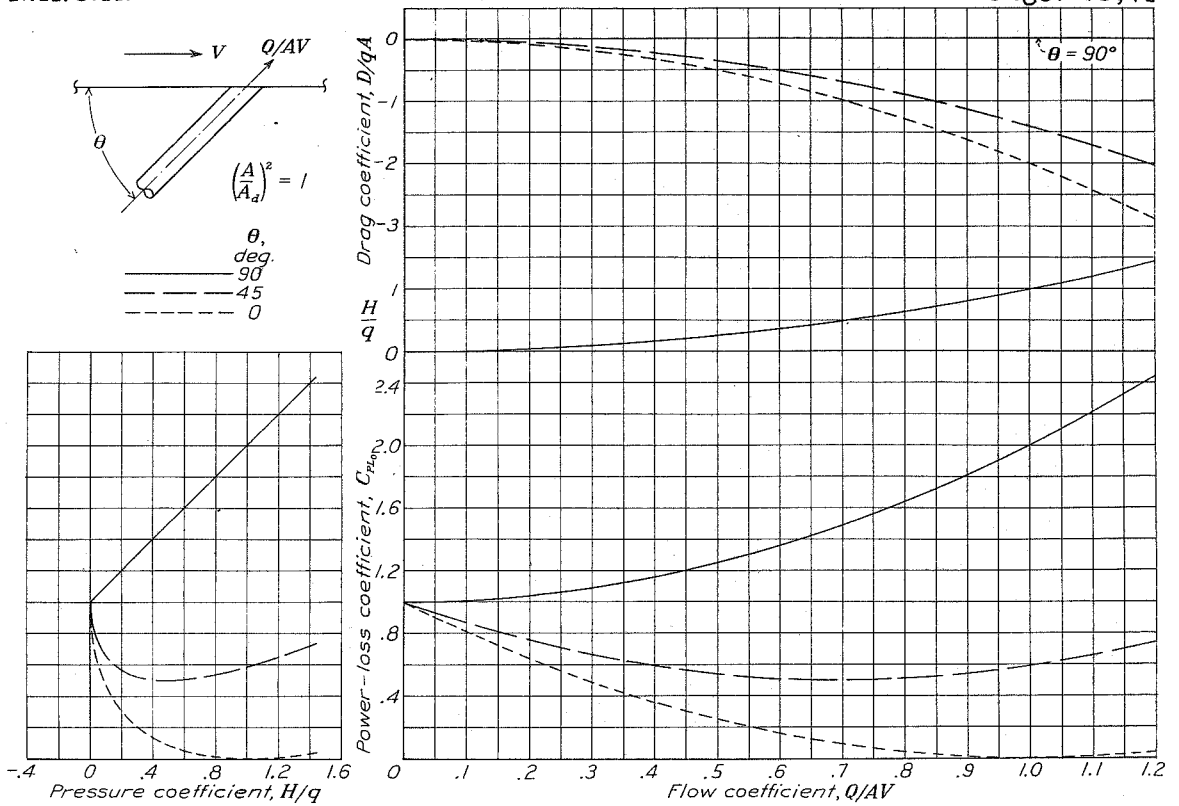


Figure 70.

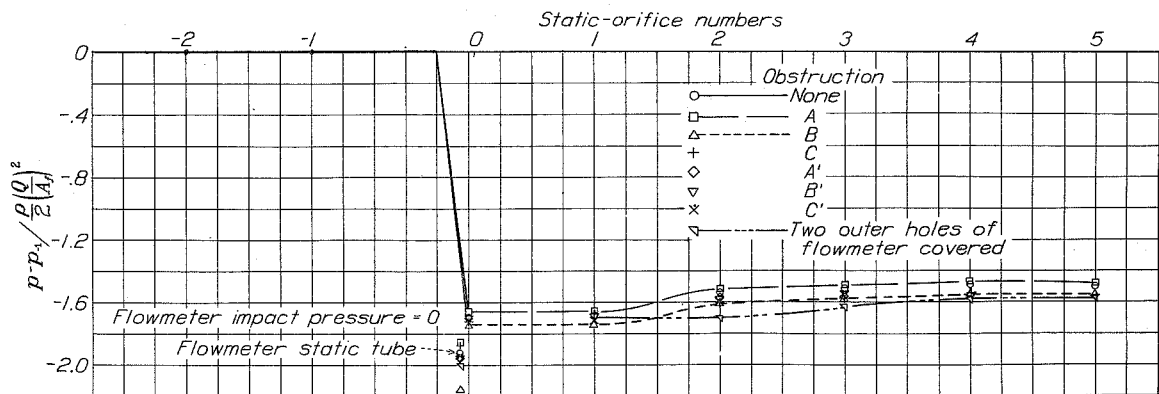
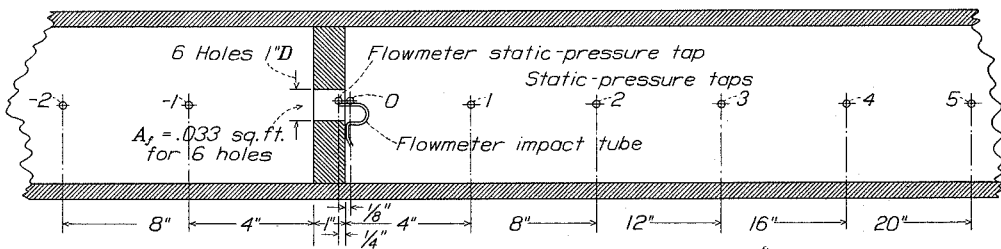


Figure 71

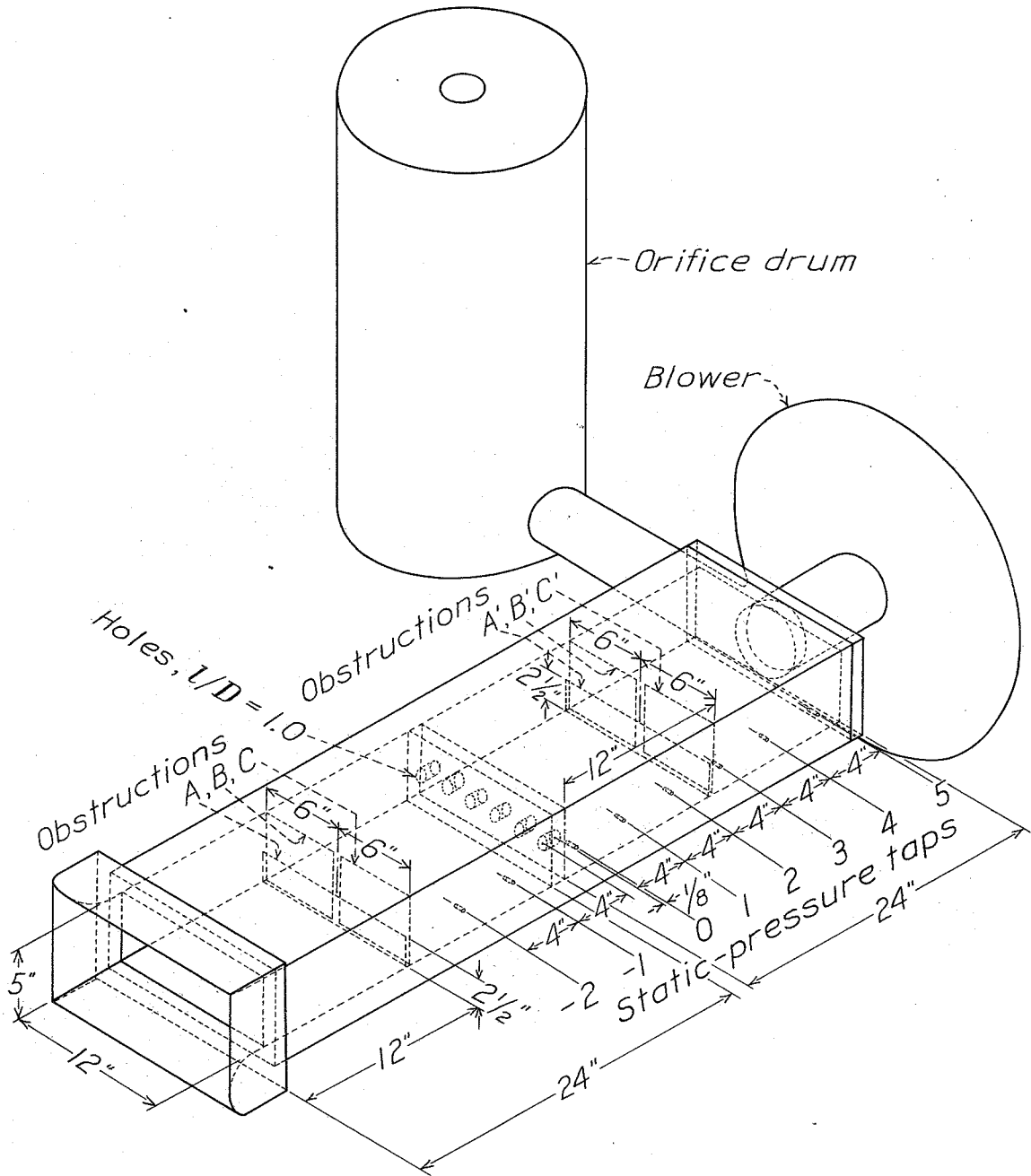


Figure 72.